(2)

FERRITE PHASE SHIFTERS USING STRESS INSENSITIVE MATERIALS

PHASE I

FINAL REPORT

PERIOD COVERED: JULY 1991 TO JULY 1992

CONTRACT NO. N00014-91-C-2202

CDRL A003

EMS JOB NO. 15638

PREPARED FOR:

NAVAL RESEARCH LABORATORY
4555 OVERLOOK AVENUE, S.W.
WASHINGTON, D.C. 20375-5000
DR. DENIS WEBB, COTR

PREPARED BY:

ELECTROMAGNETIC SCIENCES, INC.
P. O. BOX 7700
660 ENGINEERING DRIVE
TECHNOLOGY PARK / ATLANTA
NORCROSS, GA 30091-7700

JUNE 11, 1992

UNCLASSIFIED

ECURITY CLASSIFICATION OF THIS PAGE

REPORT DOCUMENTATION PAGE

1a. REPORT SECURITY CLASSIFICATION UNCLASSIFIED	1b. RESTRICTIVE MARKINGS
2a. SECURITY CLASSIFICATION AUTHORITY	3. DISTRIBUTION / AVAILABILITY OF REPORT UNLIMITED
2b. DECLASSIFICATION / DOWNGRADING SCHEDULE	
4. PERFORMING ORGANIZATION REPORT NUMBER(S) EMS Job No. 15638, CDRL A003	5. MONITORING ORGANIZATION REPORT NUMBER(S)
6a. NAME OF PERFORMING ORGANIZATION Electromagnetic Sciences, Inc 6b. OFFICE SYMBOL (If applicable)	7a. NAME OF MONITORING ORGANIZATION Naval Research Laboratory
6c. ADDRESS (City, State, and ZIP Code) P. O. Box 7700 Norcross, Georgia 30091-7700	7b. ADDRESS (City, State, and ZIP Code) 4555 Overlook Avenue, S.W. Washington, D.C. 20375-5000
8a. NAME OF FUNDING / SPONSORING ORGANIZATION 8b. OFFICE SYMBOL (If applicable)	9. PROCUREMENT INSTRUMENT IDENTIFICATION NUMBER Contract No. N00014-91-C-2202
8c. ADDRESS (City, State, and ZIP Code)	10. SOURCE OF FUNDING NUMBERS PROGRAM ELEMENT NO. / PROJECT NO. / TASK NO. / WORK UNIT ACCESSION NO.

11. TITLE (Include Security Classification)

Ferrite Phase Shifters Using Stress Insensitive Materials

12. PERSONAL AUTHOR(S)

Paul Cox, Gordon Harrison, Pete Rodrigue, Todd Vaughn

13a. TYPE OF REPORT	13b. TIME COVERED	14. DATE OF REPORT (Year, Month, Day)	15. PAGE COUNT
Final	FROM 7/91 TO 7/92	1992 June 11	132

16. SUPPLEMENTARY NOTATION

17. COSATI CODES			18. SUBJECT TERMS (Continue on reverse if necessary and identify by block number)
FIELD	GROUP	SUB-GROUP	Ferrite Phase Shifters, Stress Insensitive Materials

19. ABSTRACT (Continue on reverse if necessary and identify by block number)

This R&D program sponsored by the Naval Research Laboratory and being conducted by Electromagnetic Sciences, Inc., Norcross, Georgia, is focused toward achieving improved performance in microwave switching components via use of "stress insensitive" microwave ferrite materials for applications where stable hysteresis characteristics of the materials are critical to the RF performance. The program, therefore, primarily addresses how to relieve or improve the magnetostrictive characteristics of the materials with emphasis on the specific application and demonstration of these materials in microwave switching components, particularly ferrite toroidal phase shifters.

20. DISTRIBUTION / AVAILABILITY OF ABSTRACT	21. ABSTRACT SECURITY CLASSIFICATION
☒ UNCLASSIFIED/UNLIMITED ☐ SAME AS RPT. ☐ DTIC USERS	UNCLASSIFIED
22a. NAME OF RESPONSIBLE INDIVIDUAL	22b. TELEPHONE (Include Area Code) / 22c. OFFICE SYMBOL

D FORM 1473, 84 MAR 83 APR edition may be used until exhausted. All other editions are obsolete.

SECURITY CLASSIFICATION OF THIS PAGE

FERRITE PHASE SHIFTERS USING STRESS INSENSITIVE MATERIALS

PHASE I

FINAL REPORT

PERIOD COVERED: JULY 1991 TO JULY 1992

CONTRACT NO. N00014-91-C-2202

CDRL A003

EMS JOB NO. 15638

PREPARED FOR:

NAVAL RESEARCH LABORATORY
4555 OVERLOOK AVENUE, S.W.
WASHINGTON, D.C. 20375-5000
DR. DENIS WEBB, COTR

PREPARED BY:

ELECTROMAGNETIC SCIENCES, INC.
P. O. BOX 7700
660 ENGINEERING DRIVE
TECHNOLOGY PARK / ATLANTA
NORCROSS, GA 30091-7700

JUNE 11, 1992

TABLE OF CONTENTS

1.0 INTRODUCTION AND PROGRAM OBJECTIVES

1.1 INTRODUCTION

This R&D program sponsored by the Naval Research Laboratory and being conducted by Electromagnetic Sciences, Inc., Norcross, Georgia, is focused toward achieving improved performance in microwave switching components via use of "stress insensitive" microwave ferrite materials for applications where stable hysteresis characteristics of the materials are critical to the RF performance. The program therefore primarily addresses how to relieve or improve the magnetostrictive characteristics of the materials with emphasis on the specific application and demonstration of these materials in microwave switching components, particularly ferrite toroidal phase shifters.

1.2 PROGRAM OBJECTIVES

The overall technical objective of this program is to improve the performance of microwave switching components using stress insensitive ferrite materials. Ferrite compounds exhibiting minimum stress sensitive hysteresis properties will be "molecularly engineered" and processed into toroidal structures to demonstrate improved performance in high power, high accuracy microwave ferrite toroidal phase shifters.

The investigative program will include further analysis of the molecular and physical mechanisms which appear to influence and/or control the stress sensitive characteristics of the cubic ferromagnetic compounds of interest (emphasis will be focused on the ferromagnetic garnet compounds). The magnetostrictive characteristics will be related to the molecular crystalline structure and "molecular engineering" techniques will be utilized to minimize (compensate) the dominant magnetostrictive constants. The analysis will include the relative importance and magnitude of the magnetocrystalline anisotropy to magnetostrictive anisotropy. Compounds will be formulated based on these analyses and the material compositions prepared, processed and evaluated. Iteration of this cycle will be implemented where appropriate. The material properties measured will be

evaluated not only for stress insensitive hysteresis characteristics but also for acceptable microwave and magnetic properties supportive of toroidal phase shifter applications. A specific compound will be generated which is optimized for high power phase shifter application and demonstration in the X-band frequency region.

The goal of the investigative effort will be to demonstrate high power, high accuracy, stress insensitive dual toroid waveguide ferrite phase shifters over the 7 to 11 GHz frequency region with results applicable to structures covering the 6 to 18 GHz frequency region. A breadboard model of the X-band phaser will be fabricated to demonstrate performance advancements achieved. Stress sensitivity will be fully evaluated for phase states corresponding to minor hysteresis loop operation.

1.3 PROGRAM TECHNICAL TASKS (PHASE 1)

1.3.1 Selection of Baseline Test Vehicle

An existing X-band phase shifter will be selected for a test vehicle with the concurrence of the NRL COTR. The stress sensitivity of the RF performance of this phase shifter is to be characterized. Typical performance goals for this baseline phase shifter are as follows:

Frequency:	7 to 11 GHz
RF power (peak/average):	5 kW/300 watts
Temperature range:	-10 to 80 °C
Accuracy:	four bits

1.3.2 Analytical Phaser Model Studies

An analytical phaser model will be established and utilized to (a) predict performance with stress insensitive materials, and to (b) predict performance of composite ferrite toroid structures.

1.3.3 Materials Preparation and Characterization

One or more promising stress insensitive materials compositions will be prepared and the physical, magnetic and electrical properties of these compounds will be characterized. "Static" stress sensitivity tests with both near-saturated and minor loop operation will be conducted.

1.3.4 RF Evaluation

The most promising materials will be selected for RF evaluation. These materials will be characterized in an RF waveguide phaser structure as a function of frequency, temperature and RF power. The performance achieved will be compared with that of the baseline test vehicle.

This phase shifter test vehicle with driver will be provided to NRL for evaluation.

2.0 BACKGROUND DISCUSSION ON REMANENT STATE FERRITE PHASERS, REMANENT MAGNETIZATION AND MAGNETOSTRICTION

2.1 REMANENT STATE FERRITE PHASERS

Microwave ferrite digital phase shifters utilize ferrite toroidal structures and the hysteresis properties (square loop characteristics) of the ferrite for their operations.

The phase shifters are constructed in waveguide using either a single toroid or a dual toroid configuration. These structures are shown in Figures 2-1, 2-2, and 2-3.

The ferrite toroid fully fills the waveguide from top to bottom. The designs must include features that prevent any gaps at the top or bottom of the waveguide-ferrite interface. This generally requires that the ferrite toroid be captured in the structure with a slight "crush" from top to bottom. This is often implemented in a structure by a design approach referred to as a "soft" top. The top of the waveguide channel is either made from soft metal or is thin enough to flex slightly or both.

The insertion phase length of the structure is dependent on the remanent magnetization of the ferrite (see the hysteresis loop shown in Figure 2-4). The toroids are threaded with a switching wire as shown in Figures 2-2 and 2-3 and the insertion phase length is changed by switching the ferrite to different remanent states. This switching operation provides a controlled differential phase shift. A 360 degree differential phase shift is achieved by selecting the magnetization of the material and the length of the toroid used.

The remanent magnetization ($4\pi M_r$) and the saturated value ($4\pi M_s$) changes with temperature and the RF design and material are selected for operation over a specified temperature range. The RF power of operation is also an influence on the design and resultant performance.

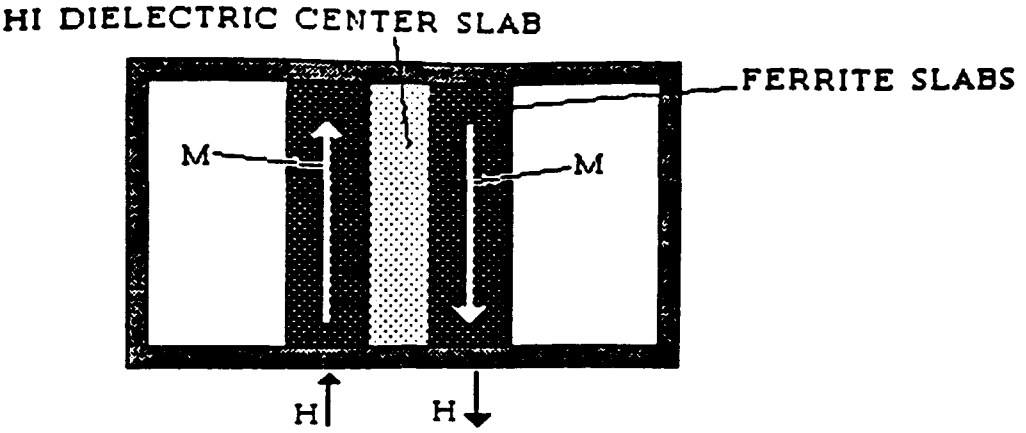

a. TWIN SLAB PHASE SHIFTER

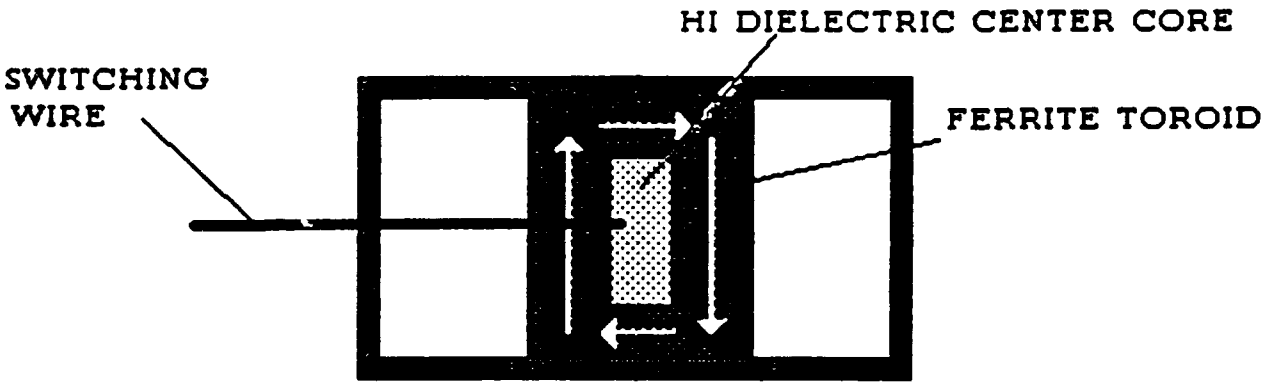

b. SINGLE TOROID PHASE SHIFTER

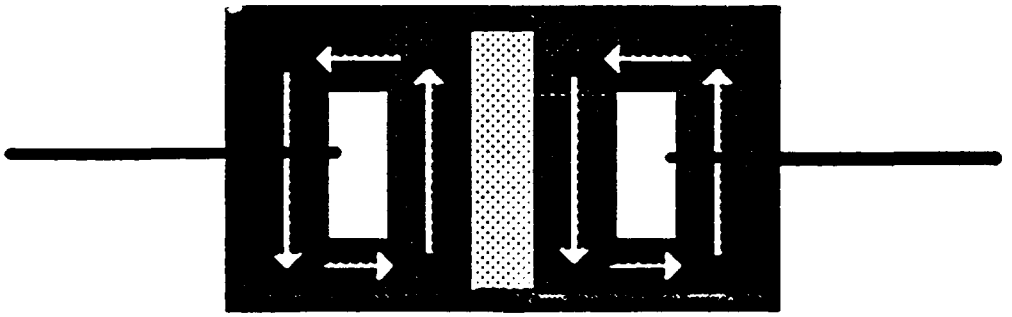

c. DUAL TOROID PHASE SHIFTER

FIGURE 2-1: Phase Shifter Configurations

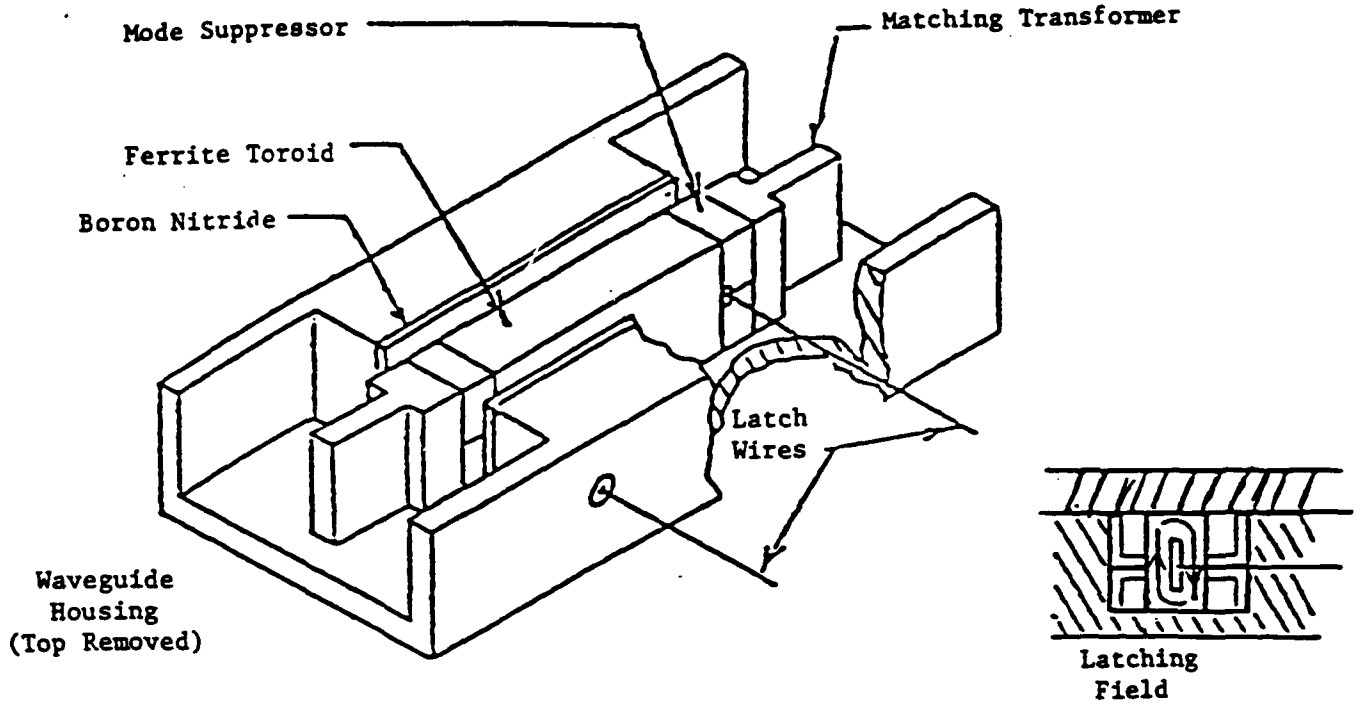

FIGURE 2-2: Single Toroid Design

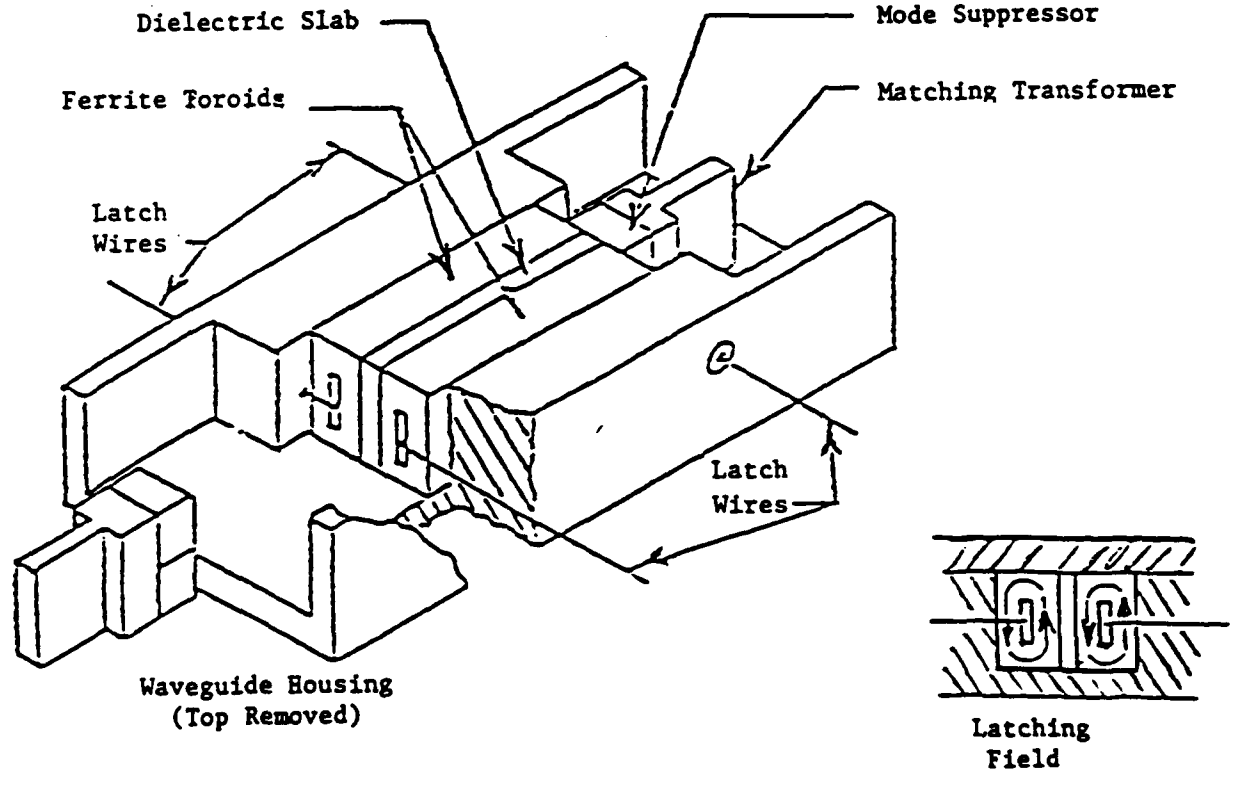

FIGURE 2-3: Dual Toroid Design

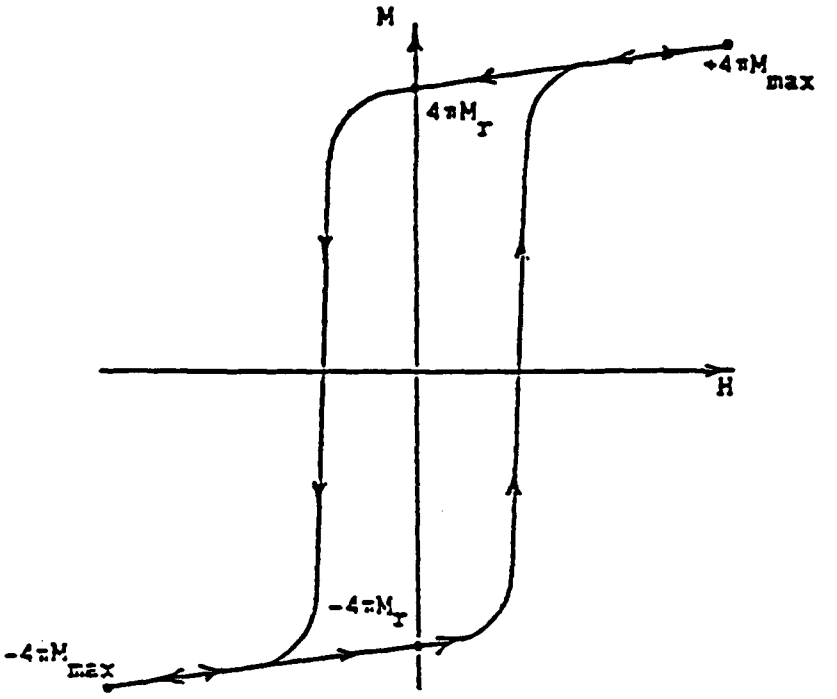

FIGURE 2-4: Typical Hysteresis Loop of a Latching Phase Shifter Operating With Major Loop Switching

One characteristic of the ferrite material that often has an impact on observed performance is "stress sensitivity" which is related to the magnetostrictive properties of the ferrite. Stress sensitivity, in this case, is evident by changes in the shape of the hysteresis curve and, in particular, the value of the remanent magnetization and thus phase shift, as a function of external or internal stress. The ferrite material, as implied previously, is captured in the waveguide structure with some controlled top to bottom "crush." The crush changes with temperature since the ferrite and metallic housing expand and contract at different rates. This creates not only a top to bottom stress but also a longitudinal stress. Similarly differential RF heating in the ferrite can generate some internal stress. If the hysteresis properties of the material are stress sensitive, such effects cause erratic phase changes that severely impact phase shifter performance; thus, materials with hysteresis properties (particularly the value of remanent magnetization) are desired that exhibit minimum sensitivity to stresses.

2.2 REMANENT MAGNETIZATION

The relative acceptability of a ferrite material for use in a digital phase shifter depends strongly on the materials' ratio of remanent magnetization to saturation magnetization, its coercive field, and time required for switching it from one remanent state to the other. In general, a "good" ferrite for digital phase shifter applications will have a high remanence ratio, a low coercive field, and a small switching time.

The remanence ratio is probably the single most important square loop property as far as microwave applications of ferrite toroids is concerned. Ideally, the remanent magnetization should equal the saturation magnetization, i.e., the remanence ratio R_r should be 1.0. This ideal situation is unlikely to be attained in practice. Remanence ratios of 0.6 to 0.7 are more normally encountered.

In a polycrystalline ferrite or garnet material, the magnetization in the individual crystallites will, due to crystalline anisotropy, prefer to be aligned along the easy (111) directions (body diagonals of the cubic

structure) of the crystallites. If magnetocrystalline anisotropy were the only factor influencing the magnetization in individual crystallites, the remanence ratio for a cubic material would be approximately 0.87. This result assumes that in the saturated state the magnetization in all crystals is parallel to the applied field and relaxes to the nearest easy direction, or body diagonal, when the field is removed. This ideal value is difficult to realize in practice because of unfavorable contributions from other anisotropies (stress anisotropy or magnetostriction and shape anisotropy). The existence in polycrystalline materials of pores or voids and corners in the material also gives rise to local demagnetizing fields which will lower the resultant remanence ratio (see Figure 2-5). Thus, magnetocrystalline anisotropy will tend to favor a high remanence ratio while porosity and other anisotropies tend to decrease remanence ratio. If the magnetocrystalline anisotropy is large compared to other anisotropies and demagnetizing fields arising at magnetic discontinuities in the materials, the remanence ratio can approach the theoretical limit of 0.87. Thus, highest remanence ratios will be realized in materials having low magnetostriction, low unfavorable internal stresses, and a dense, homogenous magnetic structure with a relatively high magnetocrystalline anisotropy (relatively high to other unfavorable anisotropies).

A unidirectional anisotropy favoring high remanence ratio can sometimes be built into a material by controlling its shape and internal stresses. Quenching, lattice deformation, applied pressure, etc., are techniques sometimes used.

In actual phase shifter applications, the ferrite materials are not driven into saturation with available drive fields. The hysteresis loop on which operation is based is then not the saturated loop, but rather minor hysteresis loops. This is particularly true with the "flux controlled" phase shifter where phase states are changed by switching a controlled amount of flux and thus changing the value of the resultant remanent magnetization.

The important (and measured) characteristics of toroidal ferrite materials are presented in Figure 2-6. The remanence ratio is the ratio of the remanent magnetization to the saturated magnetization ($4\pi M_r/4\pi M_s$).

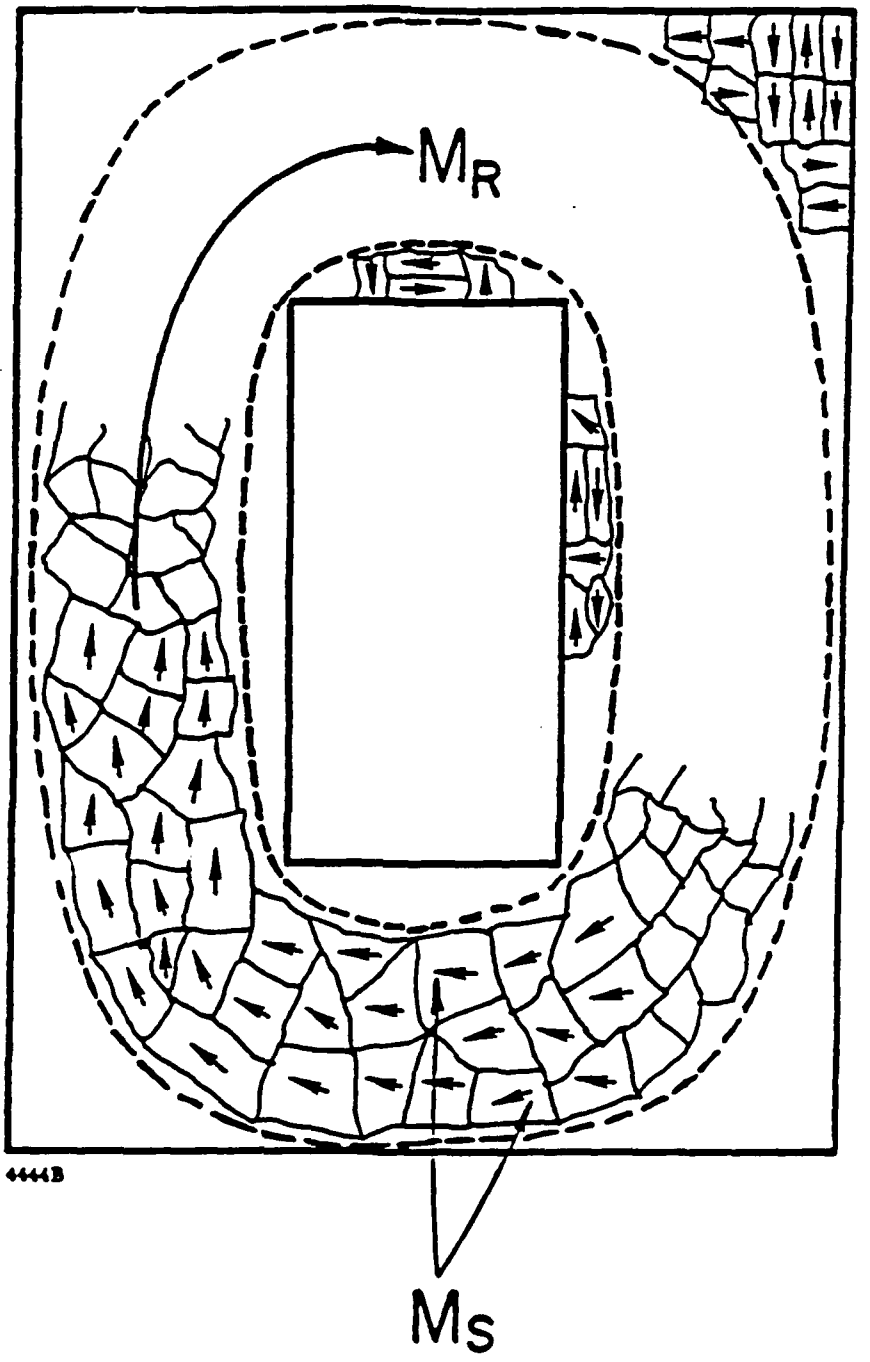

FIGURE 2-5: Possible Domain Configurations in Remanent Toroids

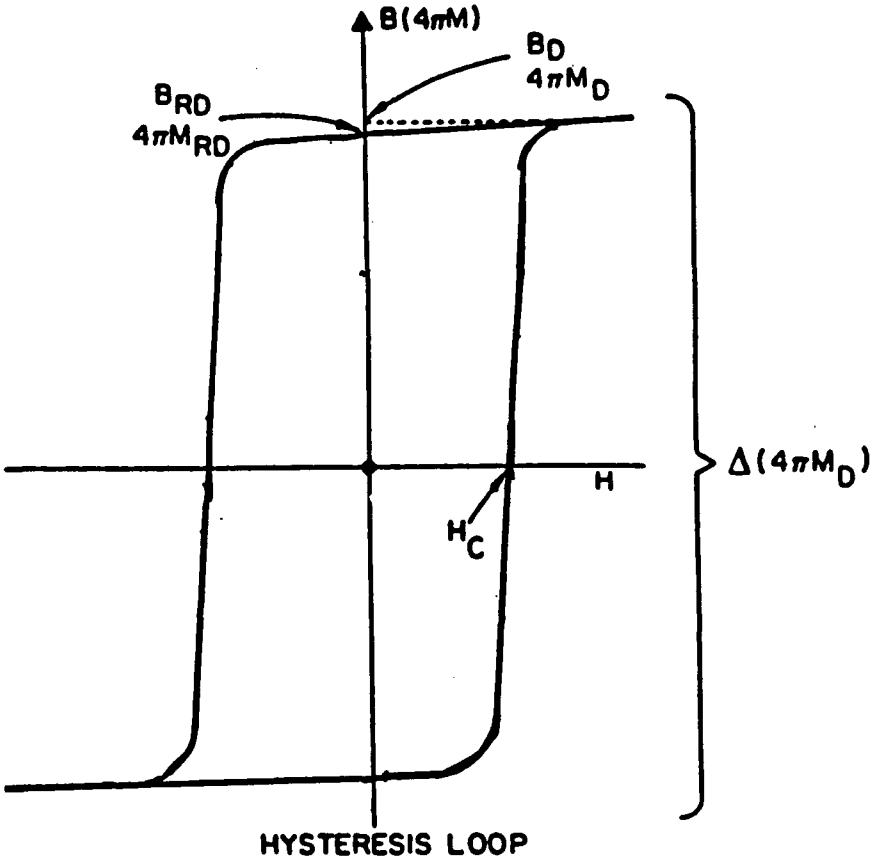

FIGURE 2-6: Hysteresis Curve of a Ferrite Toroidal Material Indicating Measured Characteristics

In Figure 2-6 ($4\pi M_D$), the drive magnetization is considerably less than $4\pi M_s$. The drive field for $4\pi M_D$ is typically five times the coercive field (H_C). The $4\pi M_{RD}$ is the remanent magnetization at the drive field used. At a drive field of $5H_C$, $4\pi M_{RD}$ is very nearly equal to the remanent magnetization. The squareness ratio (indicating the squareness of the hysteresis loop) is the ratio of $4\pi M_{RD}$ to $4\pi M_D$ or $4\pi M_{RD}/4\pi M_D$. If the material is stress sensitive, all of these measured parameters will change with stress.

To achieve a desired square hysteresis loop, the material should possess a dense homogenous magnetic structure, a high magnetocrystalline anisotropy and low magnetostriction and unfavorable internal stresses. A remanence ratio as high as possible and low H_C are desired with a uniform microstructure (uniform modest grain size of 10 to 30 microns).

2.1.3 Magnetostriction

Theory

Magnetostriction describes the experimental fact that magnetic materials will become deformed (change their physical length) when they are magnetized. The deformation is measured along the direction of magnetization. Magnetostrictive constants are measured along crystalline axes. In cubic materials this is along the 111 (body diagonal) and 100 (cube edge) direction. Chickazumi states that as the magnetization goes from 0 to M_s, the length of the sample will change by:

$$\frac{\Delta l}{l} = \frac{3}{2}\lambda_{100}\left(\alpha_1^2\beta_1^2 + \alpha_2^2\beta_2^2 + \alpha_3^2\beta_3^2 - \frac{1}{3}\right)$$

$$+ 3\lambda_{111}\left(\alpha_1\alpha_2\beta_1\beta_2 + \alpha_2\alpha_3\beta_2\beta_3 + \alpha_3\alpha_1\beta_3\beta_1\right),$$

where $\Delta l/l$ is the fractional change in length, the α_i's are direction cosines between M and the x, y, and z crystal axes, and the β's are the direction cosines between the measured deformation and the x, y, and z crystal axes.

λ_{100} is the magnetostrictive constant along the 100 direction and λ_{111} is the magnetostrictive constant along the 111 direction.

For example, if the material becomes saturated along the cube edge, [100], of a single crystal and the deformation is measured along this same direction, then $\alpha_1 = \beta_1 = 1$ and all others = 0 so that:

$$\left.\frac{\Delta l}{l}\right]_{100} = \frac{3}{2}\lambda_{100}\left(1 - \frac{1}{3}\right) = \lambda_{100}.$$

If the material were saturated along the body diagonal, [111], of a single crystal and the deformation measured along this same direction, then each α and β become $1/\sqrt{3}$ so that:

$$\left.\frac{\Delta l}{l}\right]_{100} = 3\lambda_{111}\left(\frac{1}{3}\right) = \lambda_{111}.$$

For a polycrystalline material the random alignment of crystallites requires that an average be taken over various directions. When this is done (under the assumption that $\beta_i = \alpha_i$), the effective magnetostrictive constant for a polycrystalline material is found to be:

$$\lambda_s = \frac{2}{5}\lambda_{100} + \frac{3}{5}\lambda_{111},$$

where the deformation is measured along the direction of M. Then a polycrystalline material with $\lambda_{100} = -1.5\lambda_{111}$ would show no deformation along the direction of applied field as it is brought from a demagnetized state to saturation. Internally some crystallites are elongated and others shortened, but the net effect is compensated.

If a material possesses a negative $\lambda\left(\lambda = \frac{\Delta l}{l}\right)$, then the material contracts in the direction of magnetization. (Corollary) Physically compressing the material would cause the magnetization to more favorably align in the direction of the compression. Physically stretching the material would cause the magnetization to become less aligned with the direction of the stretching.

If a material possesses a positive $\lambda\left(\lambda = \frac{\Delta l}{l}\right)$, then the material elongates in the direction of magnetization. (Corollary) Physically stretching the material in this direction would cause the magnetization to favorably align in the stretching direction. Physically compressing the material would cause the magnetization to become less aligned with the direction of the compression.

Gerald Dionne at MIT Lincoln Labs has studied magnetostrictive effects on remanence extensively. These studies have sought answers to two questions:

1) What effect does magnetostriction have on remanence ratios of ferrites (under no external stress)?

2) How does magnetostriction influence the effects of externally or internally applied stress on remanent magnetization?

The answer to question #2 is needed in order to make stress insensitive phase shifters. Dionne's paper (IEEE Trans on MAG, September 1971) treats this problem for stress applied both parallel and perpendicular to the magnetization, and the paragraphs below summarize his findings.

In each grain the direction of magnetization (in the absence of an applied field) is determined by the combined effects of magnetocrystalline anisotropy (K_1) and magnetostriction (λ_{100}, λ_{111}). The magnetostrictive contribution will depend directly on the mechanical stress (σ) that is applied to that grain. The combined anisotropy stress energy is given by:

$$E_{K\sigma} = K_1 \left(\alpha_1^2\alpha_2^2 + \alpha_2^2\alpha_3^2 + \alpha_3^2\alpha_1^2\right)$$

$$+ \frac{3}{2}\sigma\lambda_{100}\left(\alpha_1^2\beta_1^2 + \alpha_2^2\beta_2^2 + \alpha_3^2\beta_3^2\right)$$

$$+ 3\sigma\lambda_{111}\left(\alpha_1\alpha_2\beta_1\beta_2+\alpha_2\alpha_3\beta_2\beta_3+\alpha_3\alpha_1\beta_3\beta_1\right),$$

where

K_1 is the first order anisotropy constant in units of energy/volume,

λ_{100}, λ_{111} are the magnetostriction coefficients,

σ is the mechanical stress in units of energy/volume,

the α_i's and β_i's are the direction cosines as defined previously.

For a given set of K_1, λ_{100}, λ_{111}, and σ, some direction for M will result in a minimum energy, $E_{K\sigma}$. This direction will be the "easy" direction. Note that when $\sigma \neq 0$, the "easy" direction is determined by the <u>combined</u> effects of K_1, λ_{100}, and λ_{111}. (If $\sigma = 0$, the usual "easy" directions due to anisotropy alone prevail.) Thus the applied stress, σ, can cause a rotation of M within each grain.

The remanence ratio, R, is the cosine of the angle between the easy direction of that grain and the applied field or average, macroscopic, magnetization. For a polycrystalline material the remanence ratio is the average of this cosine over all individual grains. Of particular interest is the sensitivity of remanence ratio to stress, or

$$\frac{\delta R}{\delta \sigma} = \text{stress sensitivity of remanence ratio.}$$

The results of stress sensitivity (as reported by Dionne) for several particular cases are given below. (Dionne simulated a polycrystalline material by considering only the principal symmetry axes <100>, <110>, <111>, and weighted them by their frequency of occurrence 3, 6, and 4, respectively. This model represents somewhat of an approximation, and therefore the resultant numbers cannot be considered to be precise.)

A) Stress applied parallel to M

a) For $K_1 < 0$ (all useful ferrites and garnets):

$$\frac{\delta R}{\delta \sigma}|| = 0.34 \frac{\lambda_{100}}{K_1} + 0.14 \frac{\lambda_{111}}{K_1} .$$

There will be no sensitivity to stress for $\lambda_{100} = -0.4\lambda_{111}$, or $\lambda_{100} = \lambda_{111} = 0$ or if $|K_1| >> \sigma\lambda_s$. Further, λ_{100} would appear to be more important than λ_{111}.

b) For $K_1 > 0$ (no practical ferrites or garnets);

$$\frac{\delta R}{\delta \sigma}|| = -0.44 \frac{\lambda_{111}}{K_1} .$$

No stress sensitivity for $\lambda_{111} = 0$ or $|K_1| >> \sigma\lambda_{111}$.

B) Stress applied perpendicular to M

a1) For $K_1 < 0$ and $\lambda_{111} < 0$ (most garnets and nickel ferrites)

$$\frac{\delta R^{\perp}}{\delta \sigma} = -0.13 \frac{\lambda_{100}}{K_1} \quad -0.15 \frac{\lambda_{111}}{K_1} .$$

No stress sensitivity if $\lambda_{100} \simeq -\lambda_{111}$ or $\lambda_{100} = \lambda_{111} = 0$ or $|K_1| >> \sigma\lambda_s$.
Both λ's are equally important.

a2) For $K_1 < 0$ and $\lambda_{111} > 0$ (lithium ferrites and MgMn ferrites)

$$\frac{\delta R^{\perp}}{\delta \sigma} = -0.13 \frac{\lambda_{100}}{K_1} \quad -0.05 \frac{\lambda_{111}}{K_1} .$$

No stress sensitivity if $\lambda_{100} = -0.38\ \lambda_{111}$, or $\lambda_{100} = \lambda_{111} = 0$ or $|K_1| >> \sigma\lambda_s$.

In this case λ_{100} is the dominant term.

b) For $K_1 > 0$ (No practical ferrites)

$$\frac{\delta R^{\perp}}{\delta \sigma} = 0.56 \frac{\lambda_{111}}{K_1} \qquad \text{for } \lambda_{111} < 0$$

$$\frac{\delta R^{\perp}}{\delta \sigma} = 0.46 \frac{\lambda_{111}}{K_1} \qquad \text{for } \lambda_{111} > 0$$

No stress sensitivity for $\lambda_{111} = 0$ in either case.

Note: Materials would be stress insensitive when $K_1 > 0$ and $\lambda_{111} = 0$, for stress applied both parallel and perpendicular to M.

In accordance with this theory, to get insensitivity to stress in both the parallel and perpendicular cases would require a material with

$K_1 < 0$, $\lambda_{111} > 0$

and with

$\lambda_{100} = -.4\lambda_{111}$.

"Molecular engineering" techniques can be used to alter the magnetostrictive constants. For example, within a particular class of materials, a compound with a positive λ_{111} can be mixed (reacted) with a compound of negative λ_{111} to generate a resultant compound (solid solution of the two compositions) with a weighted average of these two values of magnetostriction. In this case a compound with zero value for λ_{111} could be formulated.

As an example, consider a solid solution of yttrium-iron garnet (YIG) and gadolinium-iron garnet (GdIG) such as

$Y_{2.6}Gd_{0.4}Fe_5O_{12}$ or [YIG (13.3%Gd)].

This compound is a mixture of

86 2/3% YIG and 13 1/3% GdIG.

The measured magnetostrictive constants of YIG and GdIG are as follows;

	λ_{100}	λ_{111}	λ_s
YIG	$-1.3X10^{-6}$	$-2.7X10^{-6}$	$-2.5X10^{-6}$
GdIG	$0x10^{-6}$	$-3.1X10^{-6}$	$-1.86x10^{-6}$
YIG (13.3%Gd)*	$-1.13x10^{-6}$*	$-2.75x10^{-6}$*	-2.1x10-6*

*Values computed from weighted average for the solid solution of the two compositions.

Dionne reported that the substitution of Mn^{+3} for Fe^{+3} in the garnet structure produces a change in the magnetostrictive constants as follows:

Change in magnetostrictive constant in garnet based on one Mn^{+3} ion per formula unit:

	λ_{100}	λ_{111}	λ_s
Mn^{+3}	$+67.3\times10^{-6}$	$+14.6\times10^{-6}$	$+35.7\times10^{-6}$

Therefore substituting the appropriate amount of Mn^{+3} into the YIG (13.3%Gd) compound can alter the magnetostrictive constant accordingly. Suppose that it is desired that λ_{100} be zero via Mn^{+3} substitution; the amount of Mn^{+3} would be 0.017 Mn^{+3} ions per formula unit [(1.13/67.3) = 0.0168].

Further considerations of the various substitutions are as follows:

Mn^{+3} Ions/Formula Unit	λ_{100}	λ_{111}	λ_s
0.0168 ($\lambda_{100} = 0$)	0	-2.5×10^{-6}	-1.5×10^{-6}
0.188 ($\lambda_{111} = 0$)	$+11.52\times10^{-6}$	0	$+4.61\times10^{-6}$
0.059 ($\lambda_s = 0$)	$+2.84\times10^{-6}$	-1.89×10^{-6}	0
0.047 ($\lambda_{100} \sim -\lambda_{111}$)	$+2.06\times10^{-6}$	-2.06×10^{-6}	-0.4×10^{-6}

The above illustrates the use of molecular engineering to alter magnetostrictive characteristics; however it should be noted that the substitution of Mn^{+3} produces no compositions with zero magnetostriction ($\lambda_{100} = \lambda_{111} = \lambda_s = 0$) or $\lambda_{111} > 0$ and $\lambda_{100} = -0.4\ \lambda_{111}$.

Experimental Studies (Selected Data Summary)

Dr. S. Iida measured the magnetostrictive constants for various rare earth garnets in the early 1960's while he was at Bell Labs. His data are presented in Table 2-1.

In the cubic garnet lattice and under remanent magnetization conditions, the magnetic moments are aligned (without other stresses) with a 111 direction; therefore with the magnetic moment aligned in the 111 direction, it would appear that λ_{100} is less important than λ_{111} and λ_s. While this may be a bad assumption based on Dionne's work, examination of Dr. Iida's data suggests that a solid solution of YIG and TbIG could provide a compound with $\lambda_{111} = 0$ at 25°C. Figure 2-7 shows the variation of λ_{111} with terbium content in YIG. $\lambda_{111} \sim 0$ for a compound composed of a solid solution of 16.7% TbIG and 83.3% YIG.

A series of compositions were prepared with Tb content as a compositional variable at 5 different firing temperatures. Measured data on these compositions are presented in Figures 2-8(a) and 2-8(b). Data from Technical Report, "Advanced Ferrimagnetic Materials Applied to Digital Phase Shifters," RADC Contract No. AF30(602)3490, conducted by Sperry Microwave Electronics Company, August, 1965. These data clearly indicate improved square loop properties and minimized stress sensitivity for the composition expected to provide $\lambda_{111} \sim 0$. While the magnetostriction is greatly reduced with terbium substitution, the microwave properties, particularly linewidth, are not acceptable to support applications.

Russ West of Trans Tech Inc. and Dionne have reported the results of studies of magnetostrictive constants for Mn^{+3} doped YIG. Measured magnetostrictive constant data taken on single crystals of YIG (doped with Mn) are presented in Figure 2-9. Using these values of λ_{100} and λ_{111}, the theory predicts

$$\frac{\delta R^{||}}{\delta \sigma} = 0 \text{ for } x = 0.05, \text{ and } \frac{\delta R^{\perp}}{\delta \sigma} = 0 \text{ for } x = 0.07.$$

TABLE 2-1

Magnetostrictive Constants For Various Rare Earth Garnets
(Data obtained by Private Communication, Dr. S. Iida, University of Tokyo, Tokyo, Japan)

		78°K	196°K	298°K(25°C)
YIG	λ_{100}	-1.0×10^{6}	-1.1×10^{6}	-1.4×10^{6}
	λ_{111}	-3.6×10^{6}	-3.9×10^{6}	-2.4×10^{6}
SmIG	λ_{100}	$+159 \times 10^{6}$	$+49 \times 10^{6}$	$+21 \times 10^{6}$
	λ_{111}	-183×10^{6}	-28.1×10^{6}	-8.5×10^{6}
EuIG	λ_{100}	$+86 \times 10^{6}$	$+51 \times 10^{6}$	$+21 \times 10^{6}$
	λ_{111}	$+9.7 \times 10^{6}$	$+5.3 \times 10^{6}$	$+1.8 \times 10^{6}$
GdIG	λ_{100}	$+4.0 \times 10^{6}$	$+1.7 \times 10^{6}$	0×10^{6}
	λ_{111}	-5.1×10^{6}	-4.5×10^{6}	-3.1×10^{6}
TbIG	λ_{100}	$+67 \times 10^{6}$	-10.3×10^{6}	-3.3×10^{6}
	λ_{111}	$+560 \times 10^{6}$	$+65 \times 10^{6}$	$+12 \times 10^{6}$
DyIG	λ_{100}	-254×10^{6}	-46.6×10^{6}	-12.5×10^{6}
	λ_{111}	-145×10^{6}	-21.6×10^{6}	-5.9×10^{6}
HoIG	λ_{100}	-82.2×10^{6}	-10.6×10^{6}	-3.4×10^{6}
	λ_{111}	-56.3×10^{6}	-7.4×10^{6}	-4.0×10^{6}
ErIG	λ_{100}	$+10.7 \times 10^{6}$	$+4.1 \times 10^{6}$	$+2.0 \times 10^{6}$
	λ_{111}	-19.4×10^{6}	-8.8×10^{6}	-4.9×10^{6}
PmIG	λ_{100}	$+25.0 \times 10^{6}$	$+4.9 \times 10^{6}$	$+1.4 \times 10^{6}$
	λ_{111}	-31.2×10^{6}	-11.3×10^{6}	-5.2×10^{6}
YbIG	λ_{100}	$+18.3 \times 10^{6}$	$+5.0 \times 10^{6}$	$+1.1 \times 10^{6}$
	λ_{111}	-14.4×10^{6}	-7.1×10^{6}	-4.5×10^{6}

NOTE: Powers of 10 should be 10^{-6}.

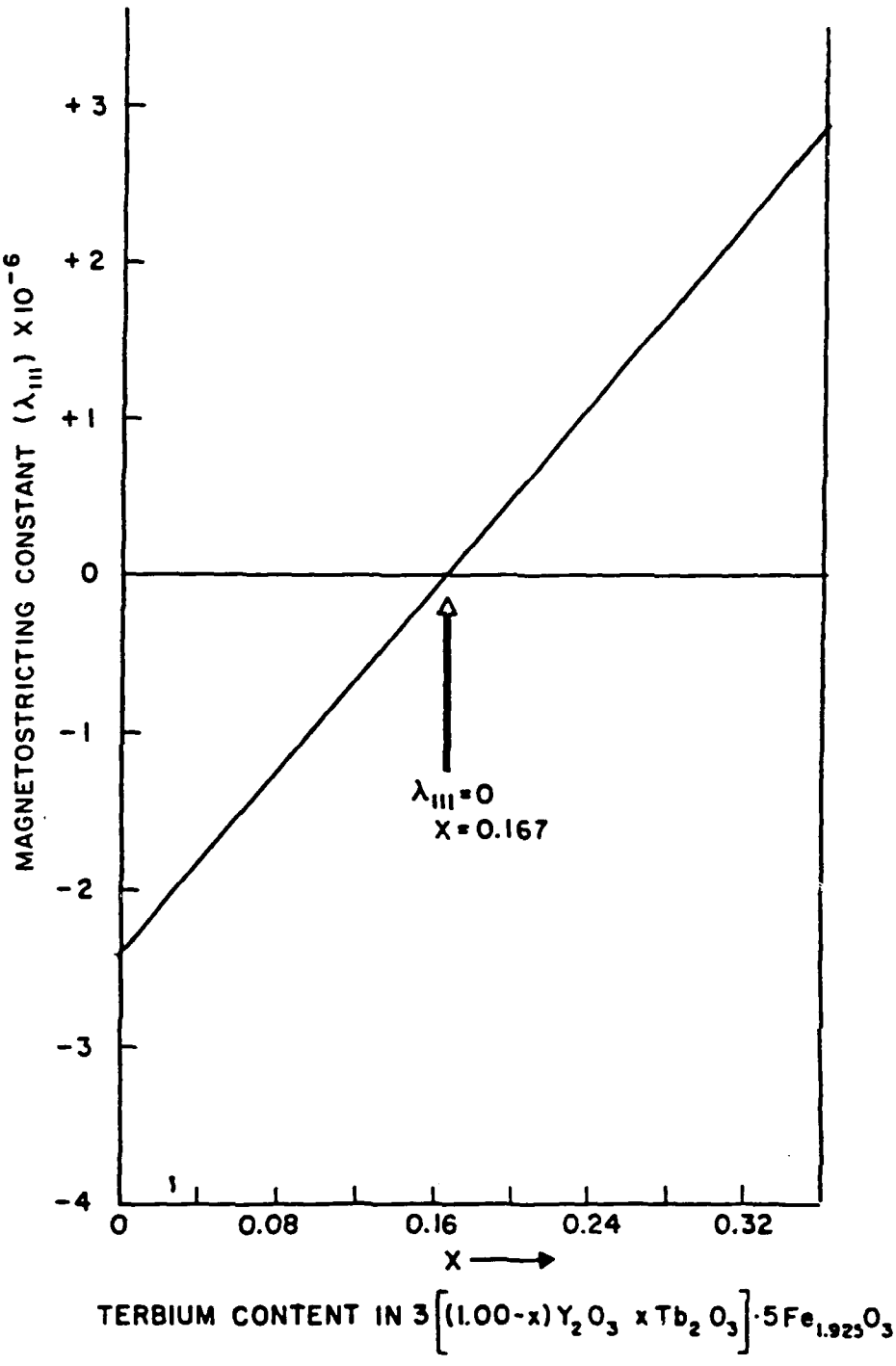

FIGURE 2-7: Magnetostrictive Constant (λ_{111}) as a Function of Terbium Content in YIG-TbIG

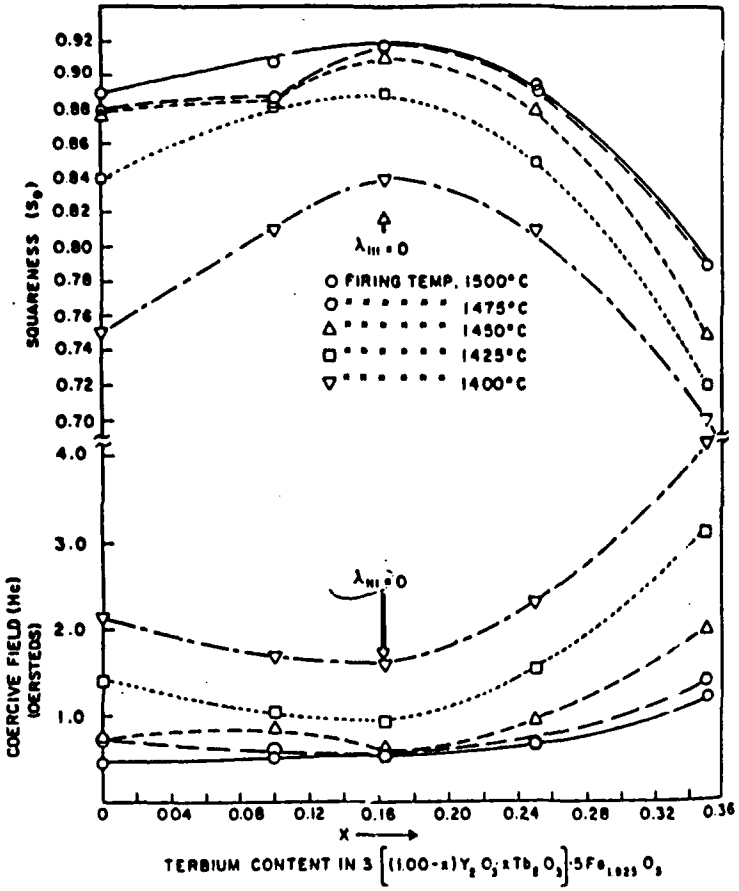

FIGURE 2-8(a): Squareness and Coercive Field for Various Firing Temperatures versus Terbium Content in Yttrium-Terbium iron garnet

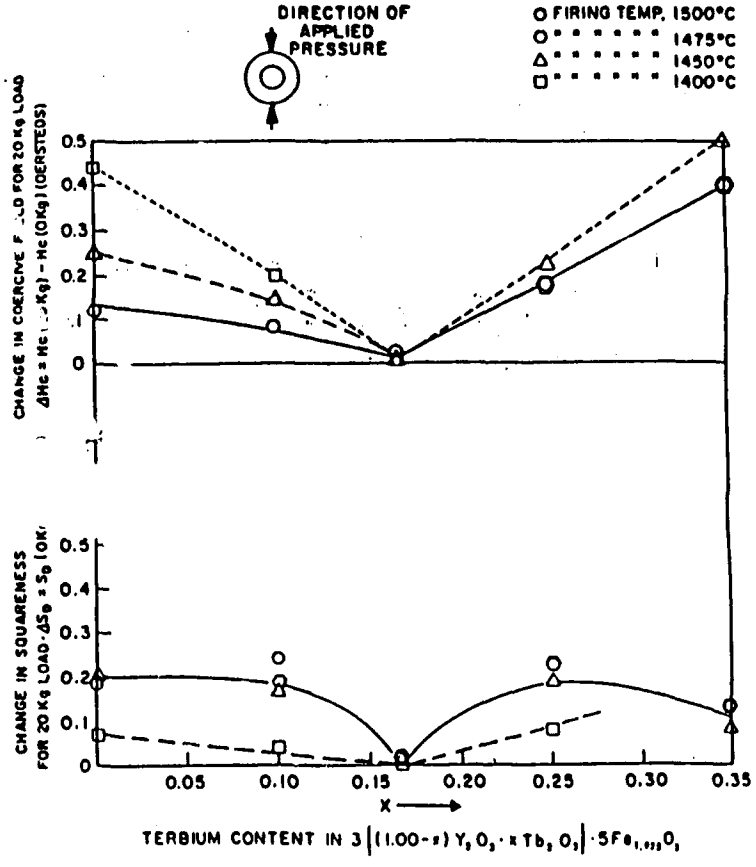

FIGURE 2-8(b): Change in Squareness and Coercive Field for an Applied Pressure of 20kg as a Function of Terbium Content in Yttrium-Terbium iron garnet

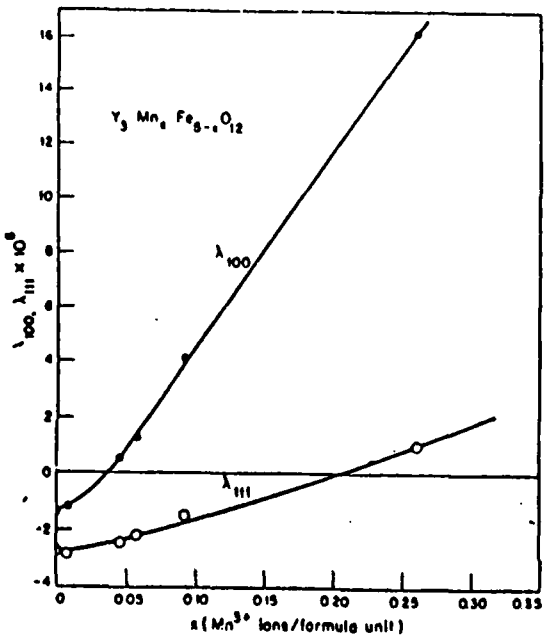

FIGURE 2-9: Room Temperature Magnetostriction Constants λ_{100} and λ_{111} for Family $Y_3Mn_xFe_{5-x}O_{12}$ (After Dionne)

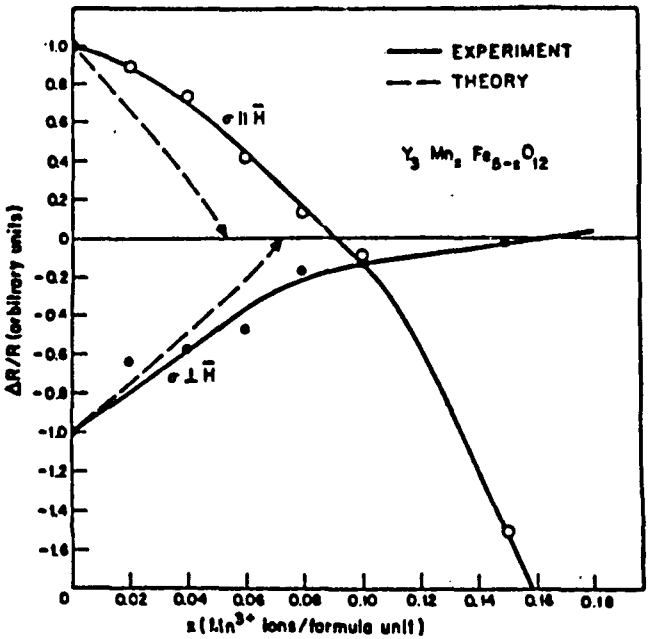

FIGURE 2-10: Fractional Change in Remanence Ratio as a Function of Mn^{3+} Content for Compressive Stress Both Parallel and Perpendicular to Magnetic Field (After Dionne)

Experimental measurements presented in Figure 2-10 indicate insensitivity at $x = 0.09$ and $x = 0.16$, for $R_{||}$ and $R_{\perp}$ respectively. Qualitatively, the agreement is pretty good, i.e., a higher manganese content for $R_{\perp}$ correction than for $R_{||}$ correction, and the orders of magnitude are O.K. But detailed, quantitative agreement is missing; experimentally it takes about twice the Mn predicted theoretically.

Mn substituted in the amount of 0.09 per formula unit is utilized commercially for most garnet materials. This substitution level is a result of the data in Figure 2-10. The materials are improved but still exhibit considerable stress sensitivity.

It should be noted that Dionne's theory is built around a Mn^{+3} ion in the garnet structure which is substituted for Fe^{+3}. However, the carbonate ($Mn^{+2}CO_3$) or oxide ($Mn^{+4}O_2$) used as a raw material provides Mn as a +2 or +4 ion. Mn^{+3} is not available in stable form as a free oxide such as Mn_2O_3. Therefore appropriate and controlled solid state chemical reactions must take place to convert the Mn in the above carbonate or oxide compound to the Mn^{+3} state. Some of the chemical reactions of importance are as follows:

$$Mn^{+2}CO_3 \longrightarrow Mn^{+2}O + CO_2$$

$$2Mn^{+2}CO_3 \longrightarrow Mn_2{}^{+3}O_3 + CO + CO_2$$

$$4Mn^{+4}O_2{}^{--} \xrightarrow{535°C} 2Mn_2{}^{+3}O_3 + O_2$$

From these reactions it is evident that Mn could exist as a +2, +3, or +4 ion and therefore one cannot be certain that the desired +3 state is totally achieved. Large substitutions (0.2) of Mn appears to alter the measured properties of the compound to suspect second phase formation.

Nonetheless, Mn, even with these uncertainties is presently the substitution most often used to reduce stress sensitivity in garnets and spinels.

Figure 2-11 presents data on the variations of the magnetostrictive constants of lithium ferrite (spinel) with Mn^{+3} concentration. In this magnetic

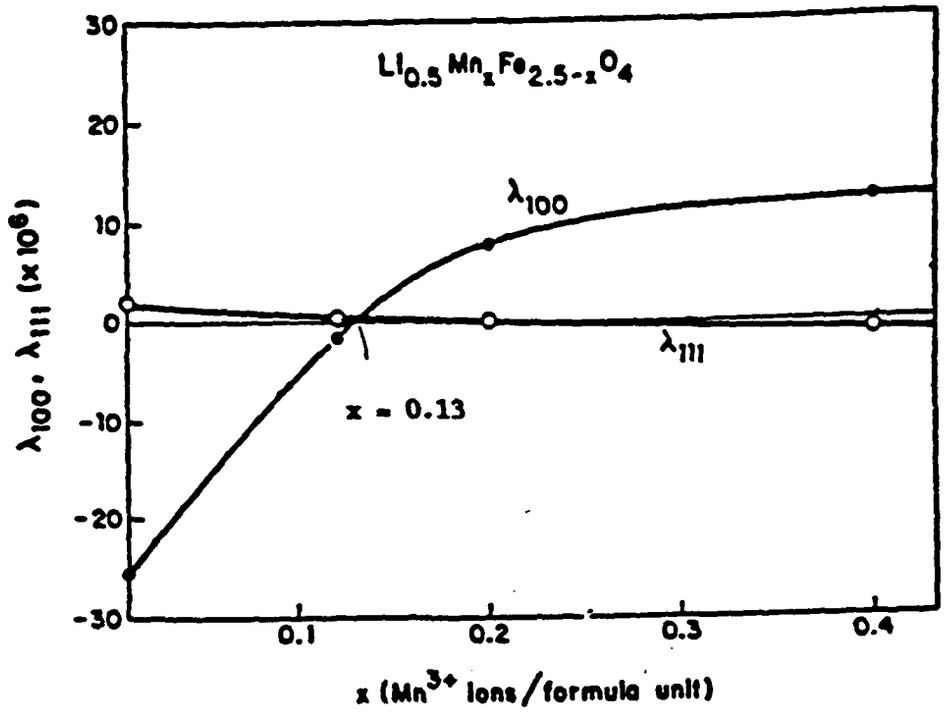

FIGURE 2-11: Variation in the Room-Temperature Magnetostriction Constants of Lithium Ferrite with Mn^{3+} Concentration (After Van Hook and Dionne)

compound, a Mn^{+3} concentration of 0.13 Mn^{+3} ions per formula unit appears to be ideal to adjust the magnitudes of both λ_{100} and λ_{111} to near zero values. This is a unique and valuable situation for these widely used spinels.

Dionne's work points out some interesting facts about the influence of small quantities of Mn^{+3}, Co^{+2}, and Fe^{+2} ions on magnetostriction. His June 1979 "Journal of Applied Physics" paper offers an explanation for the occurrence of these effects. The explanation is based on the effects of crystalline electric fields on energy levels of these ions, all of which are non-S-state and therefore have spin orbital coupling.

Mn^{+3} ions produce large positive changes in magnetostriction when they occur in octahedral sites of either spinels or garnets. Divalent manganese (Mn^{+2}) is an S-state ion and would not show such an effect. Manganese doping does not appear to strongly affect magnetocrystalline anisotropy.

Co^{+2} ions on octahedral sites appear to produce large negative changes in λ_{100} and negligible changes in λ_{111}. (See Dionne, "Journal of Applied Physics", Vol 50, No. 6, June 1979.)

Fe^{+2} ions produce large positive changes in λ_{111} and negligible changes in λ_{100}.

Since the occurrence of Fe^{+2} in either spinels or garnets is disastrous for dielectric loss tangents, divalent Fe cannot be considered to improve magnetostrictive characteristics.

The magnetostrictive effects of cobalt are of some interest since substitution of cobalt would also increase when the spin wave linewidth (ΔH_K) when this is desired for high power considerations. Manganese additions seem to provide control of magnetostriction with minimal side effects.

For reference purposes, Table 2-2 lists the magnetostrictive constants and anisotropy fields for many garnet and spinel compounds. The garnet compounds (YIG and hybrid YIG materials) exhibit prominent magnetostrictive (or stress sensitive) characteristics. Since these compounds are otherwise extremely valuable and important to phase shifter applications, reducing and controlling the stress sensitivity of these materials would be a major technical advancement.

Many of the spinel compounds are stress insensitive particularly the MgMn ferrites.

It is noted however from the data in Table 2-2 that the magnetostrictive constants of these spinels are often much larger than the garnet materials. Why then are the spinels less stress sensitive and is it really desirable and necessary to dope the magnetostrictive constants to zero?

It was previously pointed out that the combined anisotropy (K_1) and stress (σ) energy collectively act on the magnetic moments in the materials. If the anisotropy energy (field) is much larger than the stress (magnetostrictive) energy, then the materials would exhibit low stress sensitivity regardless of the value of the magnetostrictive constants. This is believed to be the situation in spinels (anisotropy energy, K_1 is much larger than stress energy, $\sigma\lambda_{100}$ or $\sigma\lambda_{111}$).

The anisotropy field in garnets is much lower than that of the spinels and thus stress energy is more evident and sometimes dominant. The following table (Table 2-3) lists values to compare these anisotropies in YIG with lithium ferrite and MgMn ferrite. In this table, a 400 kg weight on one cm^2 is used as a stress. This corresponds to approximately 137 psi or a σ of 3.92×10^7 joules/M^3. It is noted that the ratio of K_1 to $\sigma\lambda_s$ is much lower for YIG than the spinels.

These numbers reinforce the idea that magnetocrystalline anisotropy (K_1) overrides the effects of magnetostriction in some materials. Most spinels have

TABLE 2-2

Reported Magnetostrictive Constants and Anisotropy Fields for Some Garnet and Spinel Compounds at 25°C

Garnets	λ_{100} (10^{-6})	λ_{111} (10^{-6})	λ_s (10^{-6})	K_1 ergs/cm^3 (10^3)	$\frac{K_1}{M}$ (oe)	Ref
$Y_3Fe_5O_{12}$ (YIG)	-1.3	-2.7	-2.1	-6.0	-43.0	1
$Y_3Fe_{4.74}Mn_{0.26}O_{12}$	+16.2	+1.1	+7.1	-	-	1
$Y_3Fe_{4.36}Ga_{0.64}O_{12}$	-1.4	-1.7	-	-	-	2
$Gd_3Fe_5O_{12}$	-	-3.1	-1.9	-7.0	-	3
$Dy_3Fe_5O_{12}$	-12.5	-5.9	-8.5	-10.0	-	3
EuIG	+21.0	+1.8	+9.5	-3.0	-350.0	3
TbIG	-3.3	+12.0	+5.9	-10.0	-	3
$Yb_3Fe_5O_{12}$	+1.1	-4.5	-	-7.0	-41.5	3
$Er_3Fe_5O_{12}$	+2.0	-4.9	-	-7.0	-100.0	3
50%YIG·50%GdIG	-0.65	-2.9	-2.0	-	-	
Mn^{+3} Substitution	+69.0	+14.0	+36.0			
Spinels						
$NiFe_2O_4$	-45.9	-21.6	-31.0	-63.0	-200.0	4
$MgFe_2O_4$	-11.1	+2.3	-3.0	-25.0	-226.0	5
$MnFe_2O_4$	-26.0	+4.5	-7.7	-29.0	-53.0	6
$Li_{0.5}Fe_{2.5}O_4$	-25.6	+2.3	-8.9	-90.0	-	7
$Ni_{0.65}Zn_{0.35}Fe_2O_4$	-33.7	-13.2	-21.4	-25.0	-	8
80%Li·20%ZnFe	-22.4	+4.5	-6.3	-	-	
36%Li·64%ZnFe	-11.1	+2.3	-3.1	-	-	
Mn^{+3}Substitution in Spinels	+215.0	-10.0	+80.0	-	-	
Fe_3O_4	-20.0	+78.0	+39.0	-	-230.0	
$CoFe_2O_4$	-730.0	+130.0	-214.0	-	-	

TABLE 2-2 (Continued)

Reported Magnetostrictive Constants and Anisotropy Fields for Some Garnet and Spinel Compounds at 25°C

Garnets	λ_{100} (10^{-6})	λ_{111} (10^{-6})	λ_s (10^{-6})	K_1 ergs/cm^3	$\frac{K_1}{M}$ (oe)	Ref
$Co_{0.8}Fe_{2.2}O_4$	-590.0	+120.0	-164.0	-	-	
$Co_{0.3}Zn_{0.2}Fe_{2.2}O_4$	-210.0	+110.0	-18.0	-	-	
$Co_{0.3}Mn_{0.4}Fe_{2.0}O_4$	-200.0	+65.0	-41.0	-	-	
$Mn_{0.98}Fe_{1.86}O_4$	-35.0	1.0	-14.6	-	-	
$Mn_{0.6}Zn_{0.1}Fe_{2.1}O_4$	-14.0	+14.0	+2.8	-	-	
$Ni_{0.8}Fe_{2.2}O_4$	-36.0	-4.0	-16.8	-	-	
$Ni_{0.3}Zn_{0.45}Fe_{2.25}O_4$	-15.0	+11.0	+0.6	-	-	
$Mn_{0.1}Fe_{2.9}O_4$	-16.0	+75.0	+38.6	-	-	
Mn0.6Fe2.4O4	-5.0	+45.0	+25.0	-	-	
$Mn_{0.96}Fe_{2.05}O_4$	-22.0	+5.0	-5.8	-	-	
MgMnFe	-10.0	+2.4	-2.6	-	-	

References

1. G.F. Dionne, IEEE Trans Mag. 7, p.715 (1971)
2. G.F. Dionne, J. Appl. Phys., 40, p.4486 (1969)
3. S. Iida (See Table 2-1)
4. E.W. Lee, Repts. Proj. Phys. XVIII, 184, (1955)
5. A.B. Smith and R.V. Jones, J. Appl. Phys. 37, p.1001 (1966)
6. Migata and Funatogawa
7. H.J. Van Hook and G.F. Dionne, AIP Conf. Proc. 24, p.487 (1975)
8. G.F. Dionne, Lincoln Lab TR-737, Nov. 1985

TABLE 2-3

Material	K_1 (J/m^3)	λ_{100}	λ_{111}	λ_s	$\lvert\lambda s\ \sigma\rvert$ ($\sigma=3.92\times10^7 J/M^3$)	$\frac{K_1}{\lambda_s \sigma}$
YIG	~600	-1.3×10^{-6}	-2.7×10^{-6}	-2.1X10-6	~80	~7.5
Li-Fe	~9000	-26.0×10^{-6}	$+2.3\times10^{-6}$	-8.9X10-6	~350	~26
MgMn-Fe	~2000	-10×10^{-6}	2.4×10^{-6}	-2.6×10^{-6}	~100	~20

large anisotropy as evidenced by their relatively broad linewidths. In these situations little is gained by reducing the magnitudes of magnetostrictive constants. However, if techniques are available to molecular engineer λ_{111} and λ_{100} to near 0, such low values would provide stress insensitive ferrimagnetic materials and perhaps improve the hysteresis characteristics toward higher values of remanent magnetization (hysteresis loops would be more square).

Summary

The hysteresis properties of the garnet compounds exhibit considerably more stress sensitivity than do the ferrite spinels. This is believed to be due to the dominance of magnetocrystalline anisotropy energy over magnetostrictive energy in the spinels. The garnet compounds have smaller anisotropy energy and thus these materials more readily exhibit sensitivity to stress.

Ferrimagnetic compounds and associated substitutions have been identified with a wide range of magnetostrictive constants.

In the microwave cubic compounds (both garnets and spinels) when the magnetic moments are "latched" to the remanent state of magnetization, the magnetic moments relax to the closest 111 (body diagonal) crystallographic direction. Since the magnetic moments are more likely to be aligned with these crystallographic directions, this would suggest the magnetostrictive characteristics in this direction (λ_{111}) would be most important and molecular engineering techniques should be utilized to adjust $\lambda_{111} \sim 0$. In YIG (according to the data of Dionne presented in Figure 2-9) this requires a Mn^{+3} ion per formula unit of 0.2. (This assumes that the Mn substituted into the garnets as Mn^{+2} or Mn^{+4} ions is reacted to reach the Mn^{+3} desired state.)

Dionne's model for the stress sensitivity of remanance ratio however indicates that achieving compounds with $\lambda_{111} = 0$ is not sufficient to reach stress insensitive characteristics. In fact, his model indicates that λ_{100} is more important in some cases thans λ_{111}. His model predicts stress insensitivity in YIG would be achieved for Mn^{+3} content in the range of 0.05 to 0.07. For these values, neither λ_{100} nor λ_{111} are zero. He observed experimentally however

that YIG with higher values of Mn^{+3} (near 0.09) appreared to exhibit less stress sensitivity. Others have reported that higher Mn substitutions (0.15 to 0.18) in hybrid YIG compounds appear to further reduce the stress sensitivity of these materials; however difficulty is encountered in achieving good single phase compounds with these higher levels of Mn. The improvements observed therefore may be due to altering other properties (such as magnetocrystalline anisotropy and microstructure) rather than magnetostriction.

In a phase shifter, stresses due to heating and cooling the structure will most likely not be along the direction of the remanent magnetization, thus the potential importance in this situation of λ_{100} rather than λ_{111}. It would appear that to totally compensate magnetostrictive effects that both λ_{100} and λ_{111} should possess values as close to zero as possible.

3.0 PROGRAM PLAN

3.1 BASELINE TEST VEHICLE

An existing X-band dual toroid test structure (see Figure 2-1(c) and Figure 2-3) was selected as the baseline test vehicle.

This structure had previously been developed for utilization as a phase shifter in an earlier NRL program. The garnet material used in this baseline phaser was Trans Tech G-1002 with a 0.09 Mn substitution. This structure uses a "drum" top to capture the ferrite material. RF input and output ports are double ridged waveguide.

Excellent room temperature RF performance was achieved in this structure. However, Figure 3-1 illustrates the typical differential phase shift observed as a function of temperature. A phase hysteresis is observed with over 10° change between increasing temperature and decreasing temperature. In this material a clockwise hysteresis response is observed. This hysteresis response is due to the material possessing stress sensitive characteristics and the stress being experienced is due to the difference in the differential expansion characteristics of metallic housing and garnet material. The elimination of this effect is the prime thrust of the program.

This undesirable characteristic is very detrimental to differential phase shift type RF switches. Here, the RF phaser structure is similar but the phasers are utilized in a differential phase bridge configured as a switch. The structure utilizes magic tees as the input and output terminals with a phase shifter in each arm as shown schematically in Figure 3-2.

LOWBAND TEMPERATURE HYSTERESIS WITH TRANSTECH MATERIAL

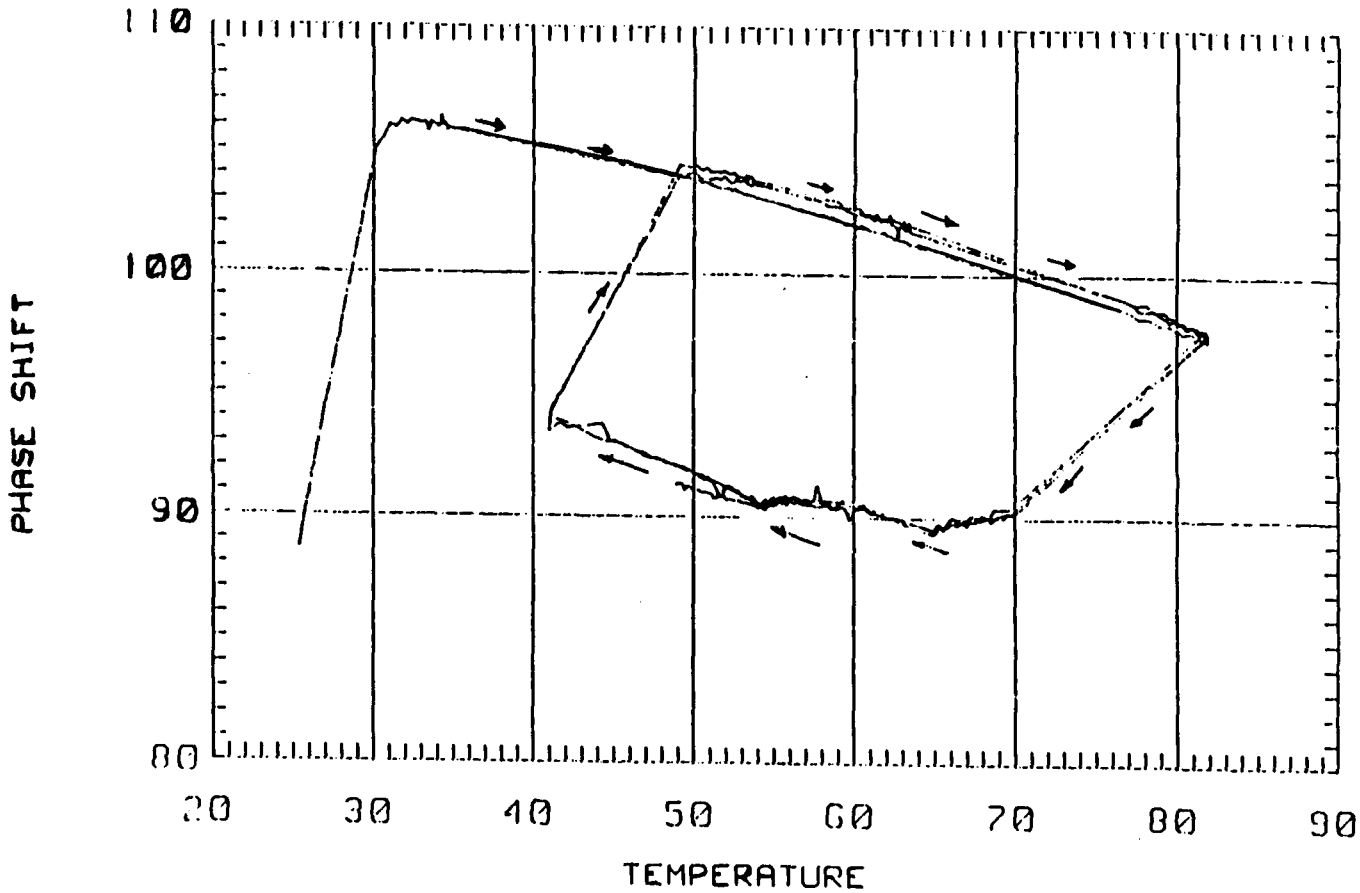

TT G1002 (0.09 Mn)

Figure 3-1

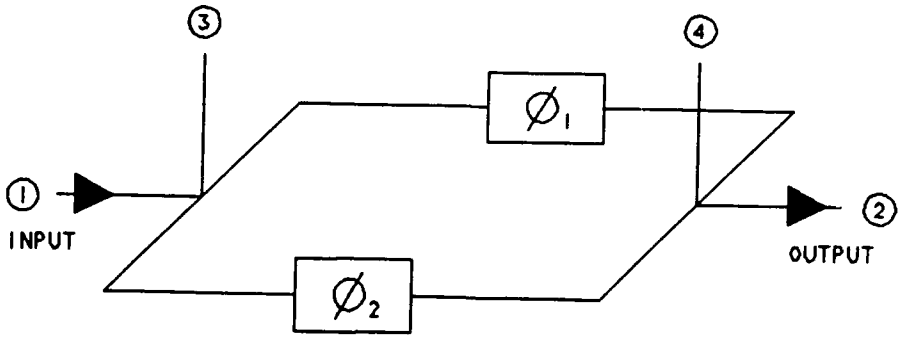

Figure 3-2

For operation, 180° degrees of differential phase shift is required. Often 90° phasers are used with a "designed in" 90° offset. Figure 3-3 presents the total available relative insertion phase shift in each channel with the 90° offset between channels. Note the hysteresis with temperature observed in each phase state (long and short) of the phasers. The short states exhibit clockwise hysteresis and the long states exhibit counterclockwise hysteresis. This hysteresis effect is further noted in Figure 3-4 which plots the phase difference (90° desired) between the short and long state for each channel. In channel B a phase hysteresis with temperature of nearly 20° was observed. Channel A is much better with about 8° of hysteresis. This type performance related to stress sensitivity of the material is extremely detrimental to the desired and required RF performance of high power switches.

These data illustrate the problems arising from stress sensitive materials and associated RF structures. This is the problem the technical effort is trying to solve, improve and/or correct.

3.2 FERRITE MATERIAL STRESSES IN WAVEGUIDE PHASER STRUCTURES

The various potential stresses that a ferrite toroid may experience in a waveguide phaser structure are illustrated in Figure 3-5. Some of the

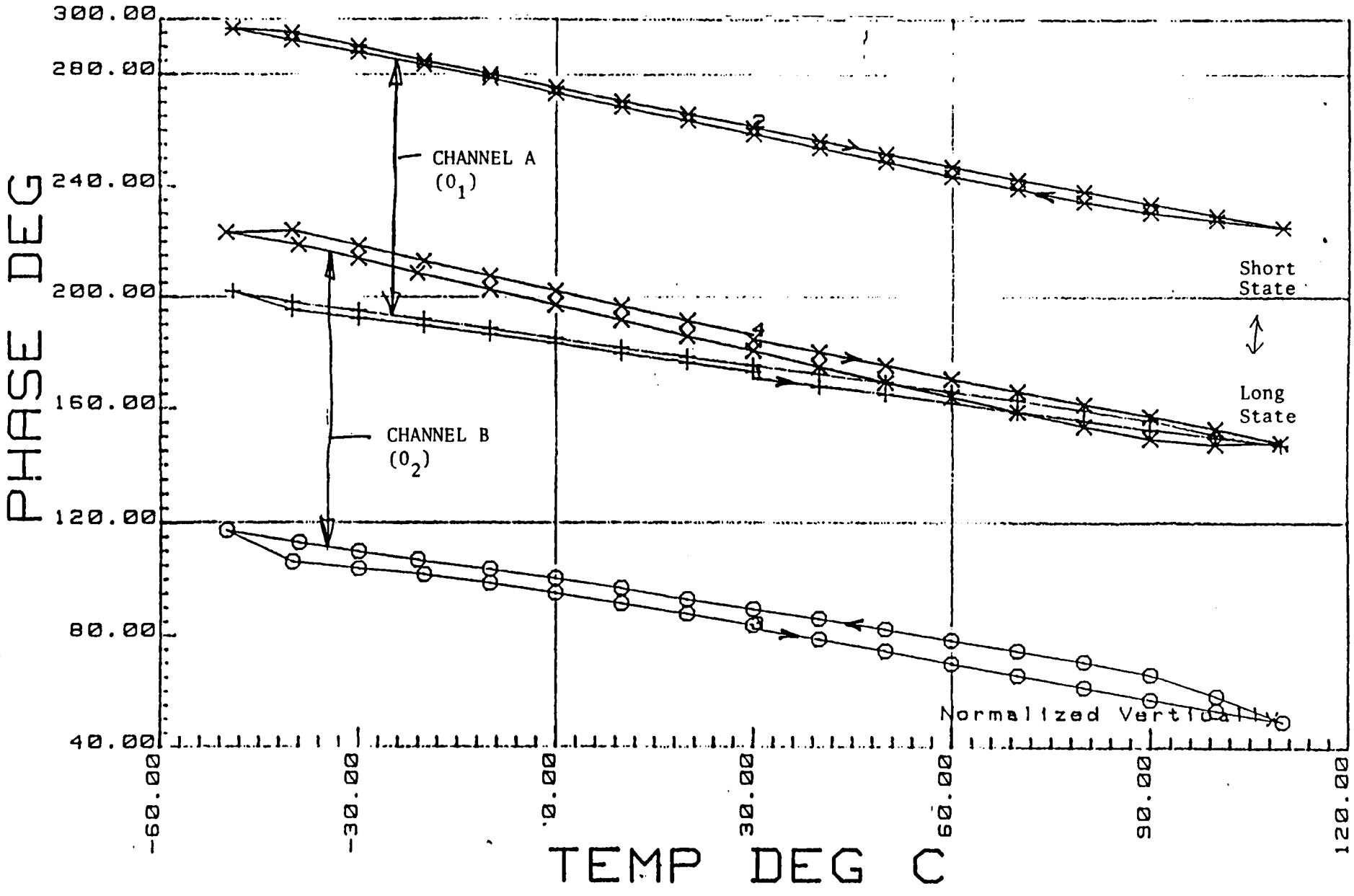

FIGURE 3-3

* Total available phase shift in each channel of switch schematic shown in Figure 3-2 with "designed in" 90° off set.

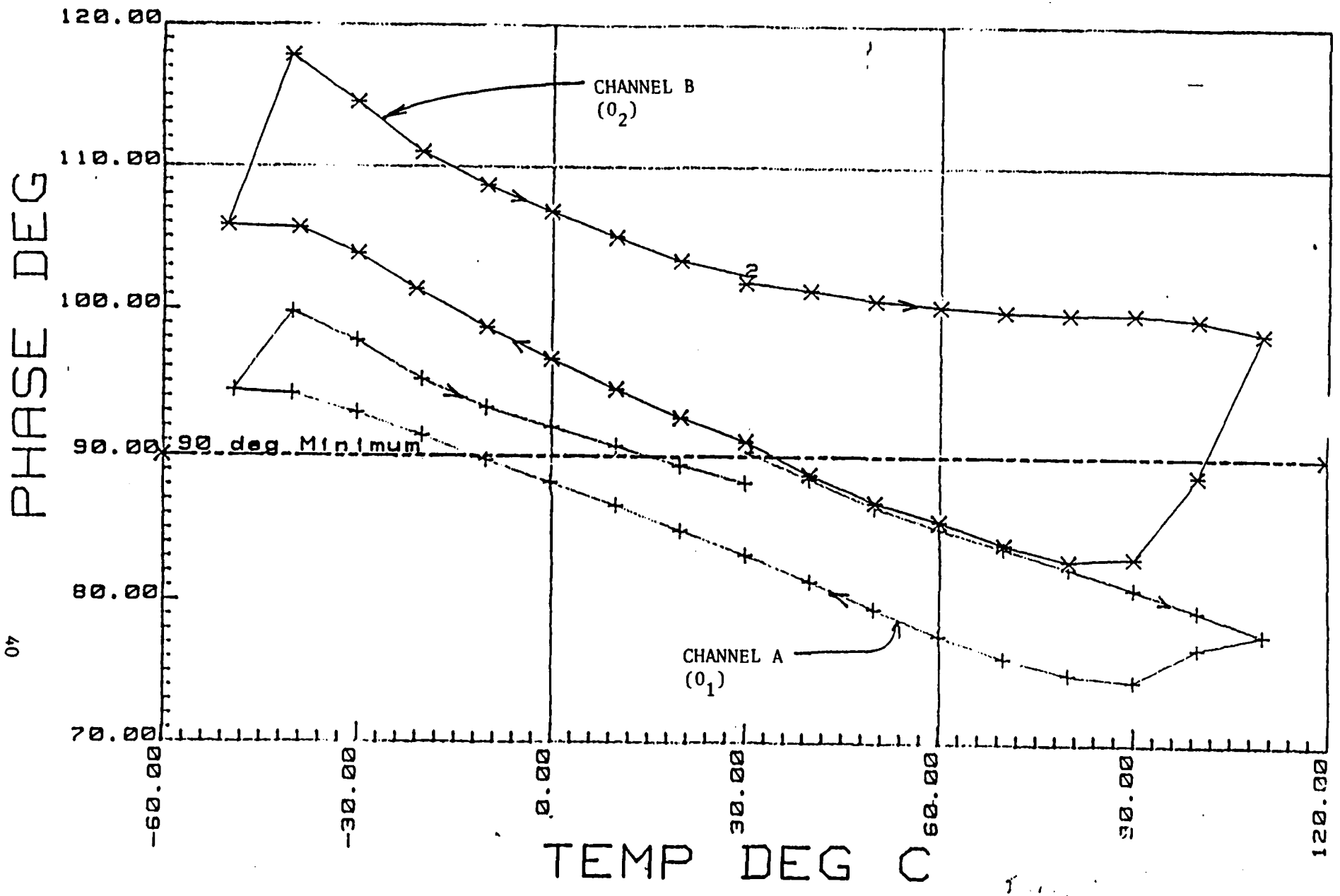

FIGURE 3-4

* Phase difference (90° desired) between short and long state each channel as a function of temperature.

POTENTIAL STRESSES

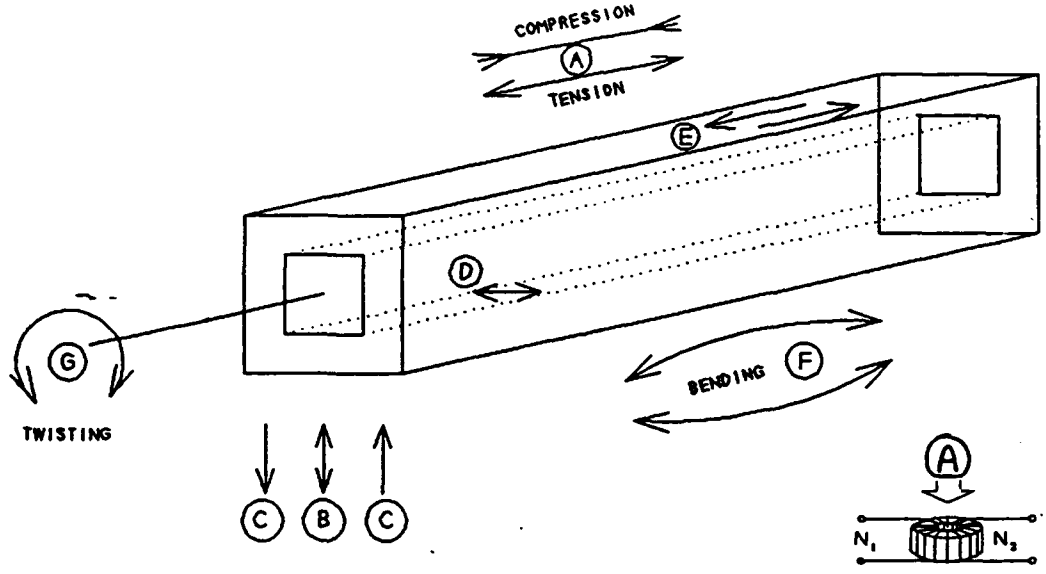

(A) Compression/Tension along the length occurs from differential expansin of the housing and ferrite material with temperature. Extremely Detrimental to phase shifters.

(B) Crush Compression and Relief: top to bottom of Phase Shifter: Necessary for good RF performance: can be very detrimental to phase shifter performance with temperature.

(BC) Differential Stress from soft top RF structures (more stress on outside leg than center leg in dual toroid structures.

(D) Side to side stress - not believed to be a major stress problem in phase shifters.

(E) Differential Expansion of ferrite material due to RF heating - (more in center leg than in outside leg): may be detrimental to performance at high RF power.

(F) Bending from tolerances in structure: Ferrite hysteresis properties very sensitive to this type of stress.

(G) Twisting - Structure related - not believed to be a major stress problem in phasers.

FIGURE 3-5

stresses are due to physical dimensions and associated tolerances; some result from structural/assembly requirements of the phaser and others result from environmental performance requirements (structural changes with temperature and RF power).

These potential stresses are listed and illustrated in Figure 3-5.

3.3 STATIC STRESS TEST FIXTURES

The program plans include both static and RF tests with stress. Comparative evaluation of these data hopefully would allow in the future for full evaluation with accurate stress sensitivity assessment from only static tests of materials.

A standard test fixture in the ferrite lab was available to stress donut shaped toroid samples (standard material test samples in the Ferrite Lab). Figure 3-5 (inset A) shows this configuration. It was desired to perform controlled static stress tests on the specific square toroids to be used in the dual toroid phaser structure. A special test fixture was designed and fabricated for this purpose. Schematics of this structure are shown in Figures 3-6 and 3-7. The S-shaped component in this fixture is a pressure (strain) gauge with a voltage output calibrated in pounds of pressure. With knowledge of the dimensions of the samples a pressure in pounds per square inch (PSI) could be computed.

Rather thin walled toroids were to be evaluated and it was observed in experimenting with this fixture that any distortion of the sample (bending, twisting, bulging out of the side walls) severely distorted the observed hysteresis loop. The desire was to provide a unidirectional stress (relative to M) without sample distortion. Sample flatness was very important. It was observed that the test fixture was best suited for longitudinal compressive stress on the phaser toroids. This stress direction is perpendicular to the average direction of the remanent magnetization in the toroid sample. The "crush" direction (top to bottom, partially parallel to M) was studied on many of the samples; however

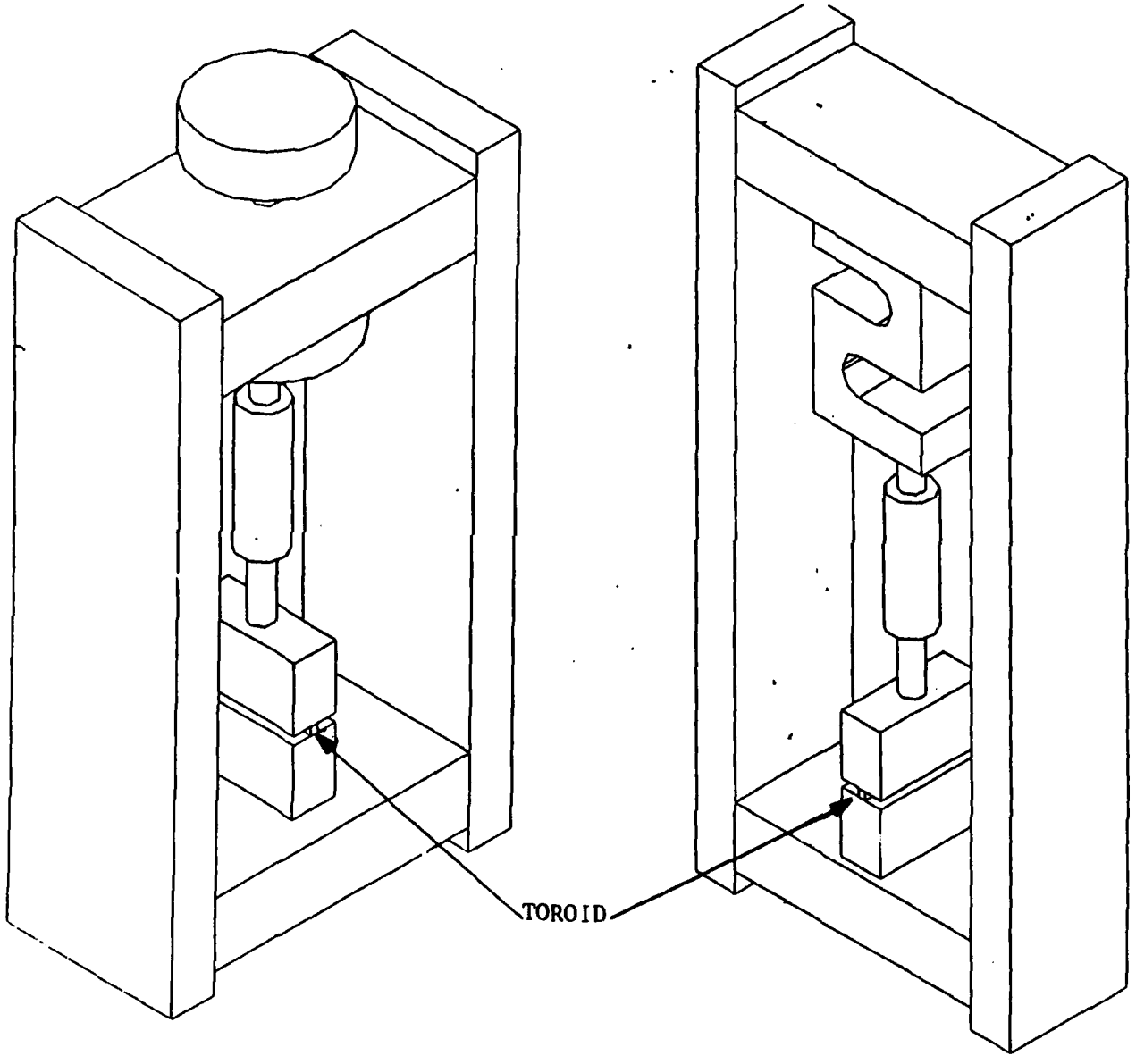

FIGURE 3-6

SCHEMATIC OF FIXTURE FOR STATIC STRESS TESTS
(Top to Bottom Stress on Toroid)

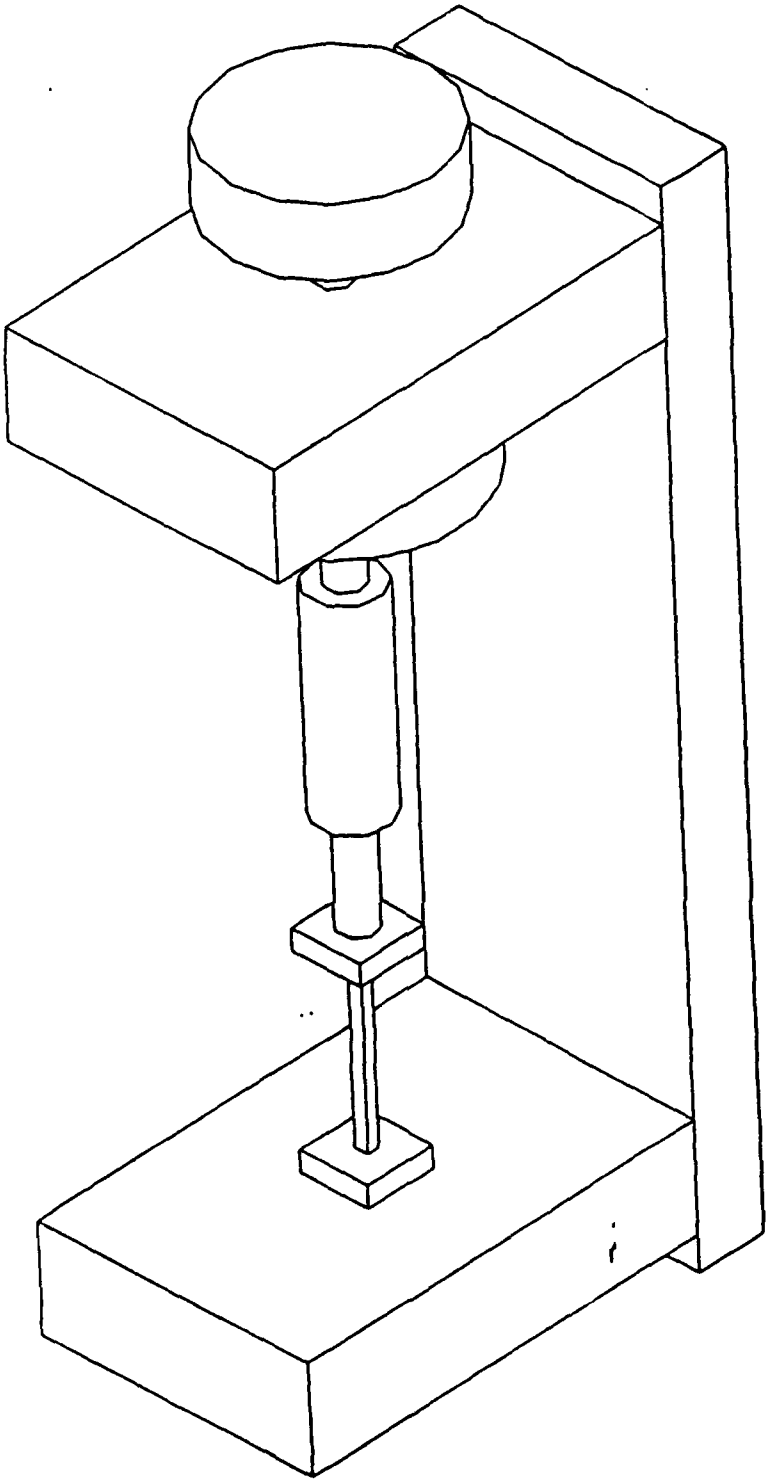

FIGURE 3-7

SCHEMATIC OF FIXTURE FOR STRESS TESTS
(Longitudinal Stress)

flatness and wall distortion of the toroids appeared to negate the intrinsic value of the measurement; thus longitudinal stress measurements were primarily conducted.

The level of stress in PSI experienced by the toroids in phase structures was unknown. Therefore, generally tests were conducted from 0 to 4000 PSI.

The test fixture was initially evaluated using the YIG-TbIG samples previously discussed in Section 2. Both thin walled square and round cylindrical toroids were available for evaluation. Figure 3-8 lists the anticipated magnetostrictive constants for the compounds available. These results are for solid solutions of YIG and TbIG using the single crystal λ_{100} and λ_{111} data reported by Iida (see Table 2-1). These test samples were polycrystalline and the expected changes in remanent magnetization with stress are noted in Figure 3-8. Figure 3-9 lists the observed changes in the hysteresis loops with stress. These observations are fully consistent with expected changes and the G-354 compound (16.7% TbIG) with a λ_{111} computed to be zero, exhibited no observable stress sensitivity to both top bottom and longitudinal compressive stress.

Photographs of the hysteresis characteristics with longitudinal compressive stress are presented in Figures 3-10, 3-11 and 3-12. Figure 3-10 is YIG which is very stress sensitive. Figure 3-11 is the 16.7% Tb substituted YIG. This compound exhibits no observable stress sensitivity. Figure 3-12 is a 35% Tb substituted YIG. In this compound λ_{111} has been molecularly changed to a positive value. Longitudinal compressive stress should support magnetocrystalline anisotropy in this case (tendency to increase Br and increase Hc).

These photos do not indicate any significant observed increase in Br but the loop does appear to be ballooned out, perhaps as a result from Hc increasing.

These data are significant in encouraging molecular engineering techniques to reduce stress sensitivity in garnets and the ability to observe improvements in static stress tests.

YIG - TbIG MATERIALS
At 25°C
(Thin Walled Square Toroid Samples)

Material		Magnetostrictive Constants	Expected Changes in Hysteresis Properties With Stress
G-352	YIG	$\lambda_{100} = -1.4 \times 10^{-6}$	Top to Bottom Br ↑
		$\lambda_{111} = -2.4 \times 10^{-6}$	End to End Br ↓
	TbIG	$\lambda_{100} = -3.3 \times 10^{-6}$	
		$\lambda 111 = +12 \times 10^{-6}$	
G-353	90% YIG · 10% TbIG	$\lambda_{100} = -1.6 \times 10^{-6}$	Top to Bottom Br ↑
		$\lambda_{111} = -0.96 \times 10^{-6}$	End to End Br ↓
G-354	83.3% YIG · 16.7% TbIG	$\lambda_{100} = -1.72 \times 10^{-6}$	
		$\lambda_{111} = 0$	0
G-355	75% YIG · 25% TbIG	$\lambda 100 = -1.88 \times 10^{-6}$	Top to Bottom Br ↓
		$\lambda 111 = +1.2 \times 10^{-6}$	End to End Br ↑
G-356	65% YIG · 35% TbIG	$\lambda_{100} = -2.07 \times 10^{-6}$	Top to Bottom Br ↓
		$\lambda_{111} = +2.64 \times 10^{-6}$	End to End Br ↑

FIGURE 3-8

FINGER APPLIED STRESS	G-352 YIG	G-353 90% YIG · 10% TbIG	G-354 83.3% YIG · 16.7% TbIG	G-355 75% YIG · 25% TbIG	G-356 65% YIG · 35% TbIG
	$\lambda_{100} = -1.4$ $\lambda_{111} = -2.4$	$\lambda_{100} = -1.6$ $\lambda_{111} = -0.96$	$\lambda_{100} = -1.75$ $\lambda_{111} = 0$	$\lambda_{100} = -1.88$ $\lambda_{111} = +1.2$	$\lambda_{100} = -2.07$ $\lambda_{111} = +2.64$
SQUARE TOROIDS Stress Top to Bottom Expected Change in Hysteresis loop	Br ↑	Br ↑	0	Br ↓	Br ↓
Observed	Br ↑; Hc ↑	Br ↑; Hc ↑	Br -; Hc -	Br ↓; Hc ↓	Br ↓; Hc -
SQUARE TOROIDS Stress End to End Expected	Br ↓	Br ↓	0	Br ↑	Br ↑
Observed	Br ↓; Hc ↓	Br ↓; Hc ↓	Br -; Hc -	Br ↑; Hc ↑	Br ↑; Hc ↑
ROUND TOROIDS Stress Top to Bottom Expected	?	?	?	?	?
Observed	Br ↓; Hc ↑	Br ↓; Hc ↑	Br -; Hc -	Br ↓; Hc -	Br ↓; Hc -
ROUND TOROIDS Stress End to End Expected	Br ↓	Br ↓	0	Br ↑	Br ↑
Observed	Br ↓; Hc ↓	Br ↓; Hc ↓	0	Br ↑; Hc ↑	Br ↑; Hc ↑

OBSERVED CHANGES IN HYSTERESIS LOOP WITH STRESS IN YIG-TbIG COMPOUNDS
(Square and Round Thin Walled Tubular Samples)
FIGURE 3-9

ILLUSTRATION OF HYSTERESIS CHARACTERISTIC OF YIG TOROID
UNDER LONGITUDINAL COMPRESSIVE STRESS

λ_{100} AND λ_{111} ARE BOTH NEGATIVE FOR YIG.

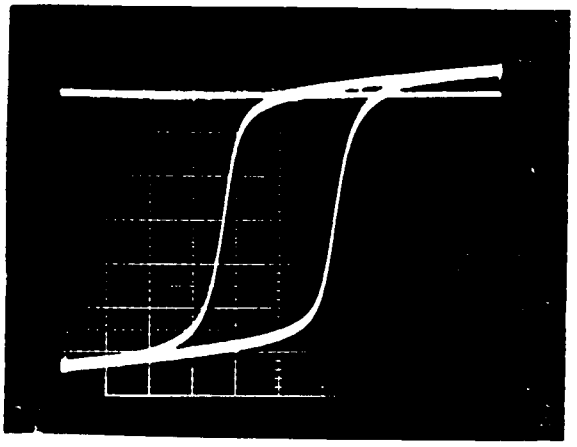

352 - YIG 0 PSI

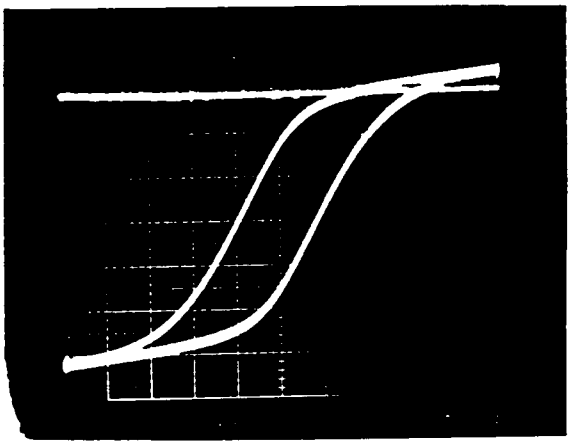

352 - YIG 1000 PSI

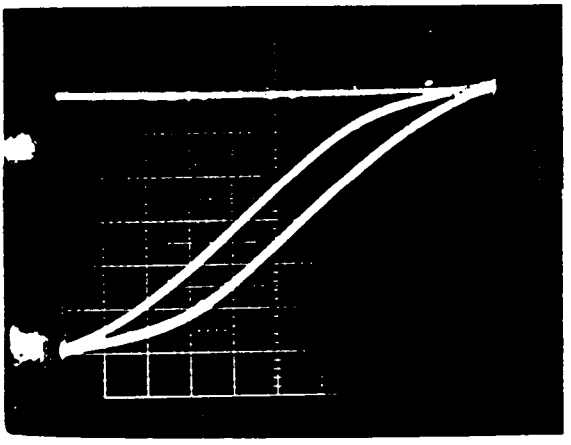

352 - YIG 2000 PSI

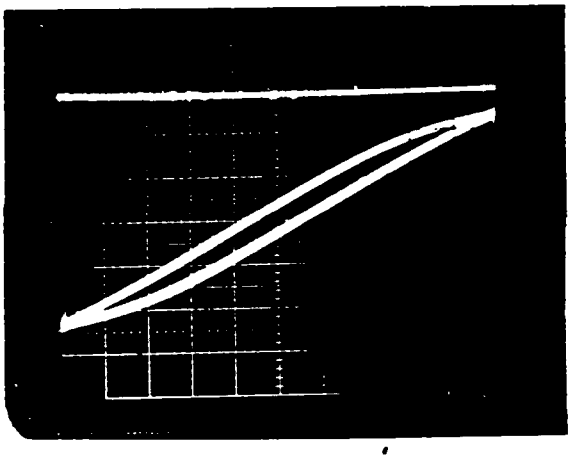

352 - YIG 3000 PSI

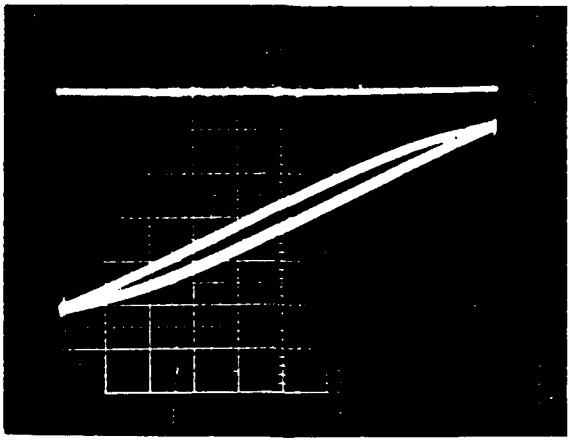

352 - YIG 4000 PSI

FIGURE 3-10

ILLUSTRATION OF HYSTERESIS CHARACTERISTIC OF (YIG . 16.7% TbIG) UNDER LONGITUDINAL COMPRESSIVE STRESS

λ_{100} IS NEGATIVE; $\lambda_{111} = 0$

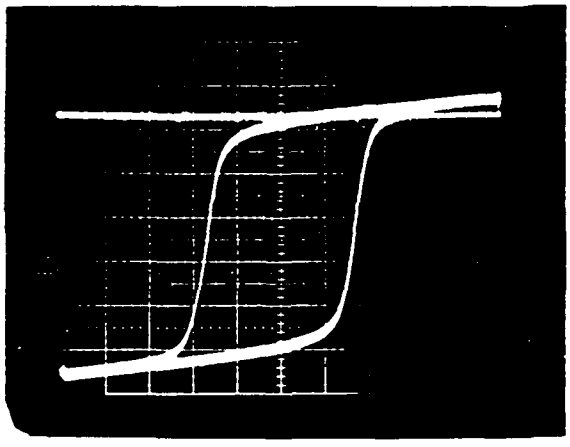

354 - YIG .167 Tb 0 PSI

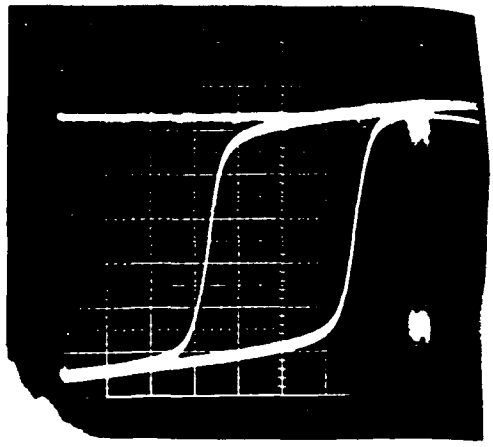

354 - YIG .167 Tb 1000 PSI

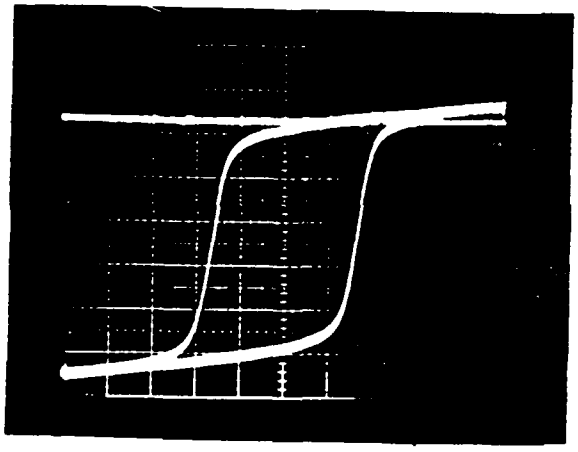

354 - YIG .167 Tb 2000 PSI

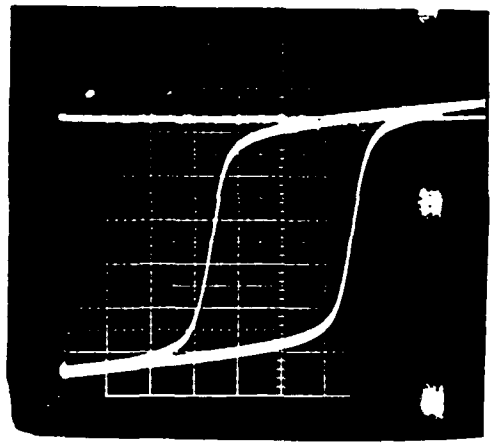

354 - YIG .167 Tb 3000 PSI

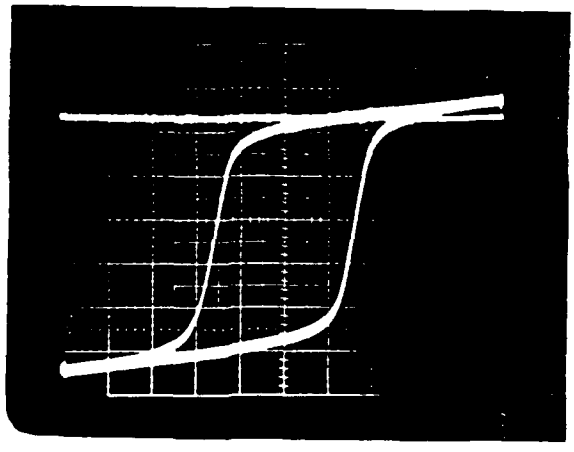

354 - YIG .167 Tb 4000 PSI

FIGURE 3-11

ILLUSTRATION OF HYSTERESIS CHARACTERISTIC OF (65% YIG . 35% TbIG) UNDER LONGITUDINAL COMPRESSIVE STRESS

λ_{100} IS NEGATIVE; λ_{111} IS POSITIVE

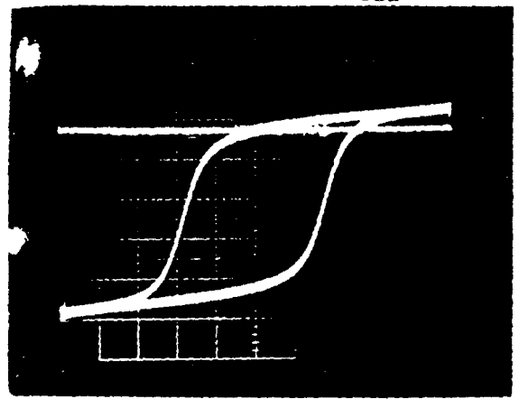

356 - YIG .35 Tb 0 PSI

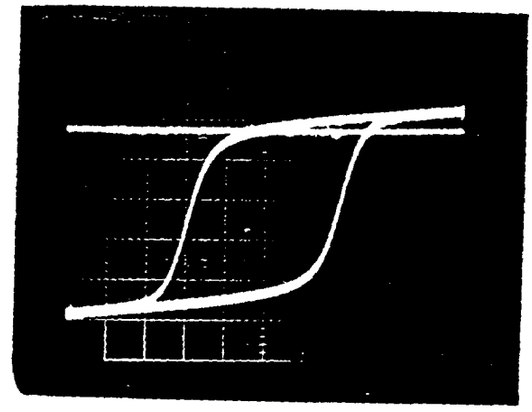

356 - YIG .35 Tb 1000 PSI

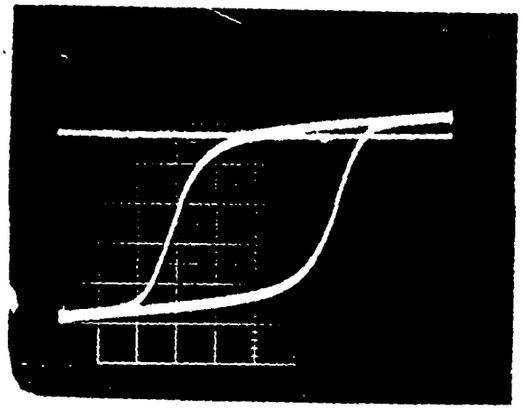

356 - YIG .35 Tb 2000 PSI

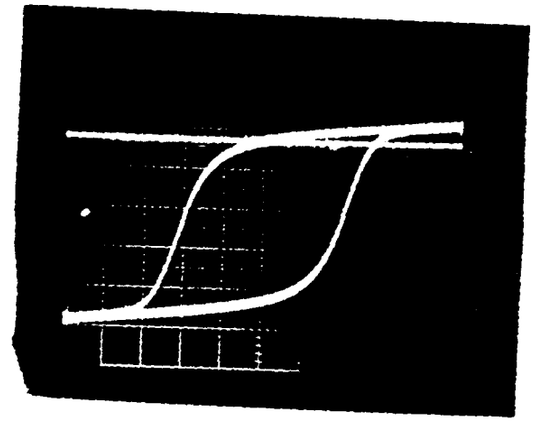

356 - YIG .35 Tb 3000 PSI

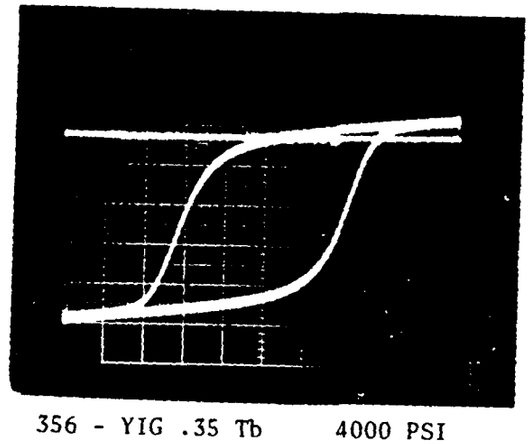

356 - YIG .35 Tb 4000 PSI

FIGURE 3-12

3.4 MANGANESE CHEMISTRY

As discussed in Section 2, Mn^{+3} substitution in garnets has been observed to reduce the stress sensitivity of these compounds. Mn^{+3} has been successfully substituted for Fe^{+3} in the structure in amounts up to 0.1 ions/formula unit without second phase detection. In amounts above this level, second phase formation is likely. The garnet structure readily accepts only +3 ions unless valance compensation is otherwise planned such as in the bismuth-calcium vanadium iron garnets.

Two areas of concern in planned studies regarding Mn^{+3} substitutions are the desire to prepare single phase compounds with Mn^{+3} substitutions up to 0.2 ions/formula unit and the assurance that Mn^{+3} is actually the ion entering the garnet structure.

Manganese can possess a valance from +2 to +7 as noted in Figure 3-13. Manganese in a +3 valance is not available in a stable oxide as a starting compound. Starting manganese compounds available are $MnCO_3$ (Mn^{+2}), MnO_2 (Mn^{+4}) and MnO (Mn^{+2}). Therefore to reach the Mn^{+3} ion desired in the structure, some solid state chemical reactions must take place to create this ionic state by forming $Mn_2^{+3}O_3$.

Some attention was given to this area in an effort to produce the Mn^{+3} substitution desired. Some of the characteristics of the various manganese compounds are listed in Figure 3-13. Figure 3-14 lists some of the possible solid state chemical reactions (under heat treatment) that may be encountered with starting compounds of $MnCO_3$, MnO_2 and MnO. Since the desired valance is +3, those reactions resulting in the possible formations of Mn_2O_3 are of prime interest for enhancement.

Manganese Carbonate ($MnCO_3$) is the compound containing manganese that is most commonly used for substitution into ferrites and garnets. MnO_2 is also available but is a less pure, more coarse compound and thus less desirable to formulate.

SOME CHARACTERISTICS OF MANGANESE COMPOUNDS

Valance	Compound	Mol. Wt	Comments
+2	$Mn^{+2}\ CO_3$	114.94	Density 3.125 gm/cm^3 Decomposes with heat Solubility in H_2O- .0065 gms/100 ml of Cold H_2O Color: Rose pink or Light brown Powder
+2	$Mn^{+2}O$	70.93	Density 5.45 gm/cm^3 Melting Point 1650°C Stable Color: Green
+2, +3	Mn_3O_4 $Mn^{+2}Mn_2^{+3}O_4$	228.79	Density 4-85.6 gm/cm^3 Melting Point 1705°C Color: Black
+3	$Mn_2^{+3}O_3$	157.86	Density 4.5 gm/cm^3 Decomposes with loss of O_2 at 1080°C $2Mn_2O_3$ -->1080°C $4MnO+O_2$? Color: Black
+4	$Mn^{+4}O_2$	86.93	Density 5.026 gm/cm^3 Decomposes with loss of oxygen at 535°C $2MnO_2$ -->535°C $1MnO+O_2$? Color: Brown/Black
+6	MnO_3		
+7	Mn_2O_7		

FIGURE 3-13

MANGANESE CHEMISTRY

Desire/Require Mn^{+3} in Garnet structure

Oxides/Carbonates Available

$Mn^{+2}CO_3$	Molecular Wt. 114.94
$Mn^{+4}O_2$	Molecular Wt. 86.93
$Mn_3^{+2,+3}O_4$	Molecular Wt. 157.86
$Mn^{+2}O$	Molecular Wt. 70.93

Possible Reactions:

1) $Mn^{+2}CO_3$ heat $Mn^{+2}O + CO_2$

2) $2\ Mn^{+2}CO_3$ heat $Mn^{2+3}O_3 + CO + CO_2$

600°C

-----> $2Mn^{+2}O + 2CO + O_2$

-----> $2Mn^{+2}O + 2CO_2$

3) $4Mn^{+2}O + O_2$ -----> $2Mn_2^{+3}O_3$

4) $2Mn^{+4}O2 + O_2$ -----> $Mn_2^{+3}O_3$

5) $2Mn^{+4}O_2$ -----> $2Mn^{+2}O + O_2$

6) $4\ Mn\ O+O_2$ -----> $2Mn_2^{+3}O_3$

7) $4MnO_2$ -----> $2Mn_2O_3 + O_2$

Molecular WT Mn_2O_3 - 157.86

FIGURE 3-14

EXPERIMENTAL STUDY

DECOMPOSITION OF MANGANGESE CARBONATE ($MnCO_3$)

Determine the decomposition products of $MnCO_3$ by observing weight loss and color changes in powder heat treated under various conditions.

1) Heat treat a sample of MnCO3 at 600°C for 4 hours in air. Observe the weight loss and color change of the powder.

2) Repeat the first experiment using a flowing oxygen atmosphere. Observe the weight loss and color change for this powder.

3) Using the material from experiment #2 continue heat treatment cycles at 800°C and 1200°C for 4 hours in an air atmosphere. Determine the weight loss for each of these heat treatments.

RESULTS:

Heat Treatment Cycle	Measured Weight Loss	Color
#1 600°C/4 hrs AIR	32.5 %	Black Powder
#2 600°C/4 hrs OXYGEN	32.5 %	Black Powder
#3 800°C/4 hrs AIR	1.2 %	Black Powder
1200°C/4 hrs AIR	10.1 %	Brown/Black

Possible Decomposition Reaction for $MnCO_3$:

	Calculated Weight Loss
$2\ MnCO_3 \xrightarrow{600°C} Mn_2O_3 + CO + CO_2$	31.3 %
$Mn_2O_3 \xrightarrow{800°C} Mn_2O_3$ (No decomposition)	0.0 %
$2\ Mn_2O_3 \xrightarrow{1200°C} 4\ MnO + O_2$	10.1 %

FIGURE 3-15

Some heat treatment studies were conducted on $MnCO_3$ as outlined in Figure 3-15. $MnCO_3$ is a light brown powder. As noted in Figure 3-15, after a heat treatment to 600°C this powder turned black with a weight loss of 32.5%. This suggests the formation of Mn_2O_3. Additional heat treatment at 800°C did not significantly change the result and powder. Further heat treatment at 1200°C resulted in a brown/black powder and a weight loss of 10.1%. This suggests the decomposing of Mn_2O_3 to MnO and a Mn valence of +2.

This observation is of some concern since the garnet compounds are sintered at temperature above 1400°C. However, presintering of the mixed oxides is conducted near 1200°C and, at this point in the present study, it is assumed that the desired Mn^{+3} ion is locked into the garnet compound and thus not free to be reduced to Mn^{+2}. This possibility may also suggest that sintering should be conducted in an oxygen environment to enhance the possibility of maintaining the manganese in a +3 valance state.

Further analytical studies on the sintered garnet compounds are planned to verify single phase microstructures.

3.5 MANGANESE SUBSTITUTION IN HYBRID YIG-GdIG COMPOUND

A mixed yttrium - gadolinium ion garnet (YIG-GdIG) compound ($4\pi M_s$ near 1000 gauss) was selected for the investigation of Mn^{+3} substitution to achieve an improved stress insensitive material for X-band phaser applications.

The compound selected was a 56 2/3% YIG/43 1/3% GdIG compound. Assuming a solid solution of these two garnets substituted with Mn^{+3}, the magnetostrictive characteristics presented in Figure 3-16 would be expected. These data are computed using weighted percentages and Dionne's magnetostrictive constants presented in Section 2.

With no Cobalt (Co) in the structure (Y=0), λ_{111} would reach 0 near a Mn^{+3} substitution of 0.2. At this substitution, λ_{100} would be a fairly large positive value of near +16.

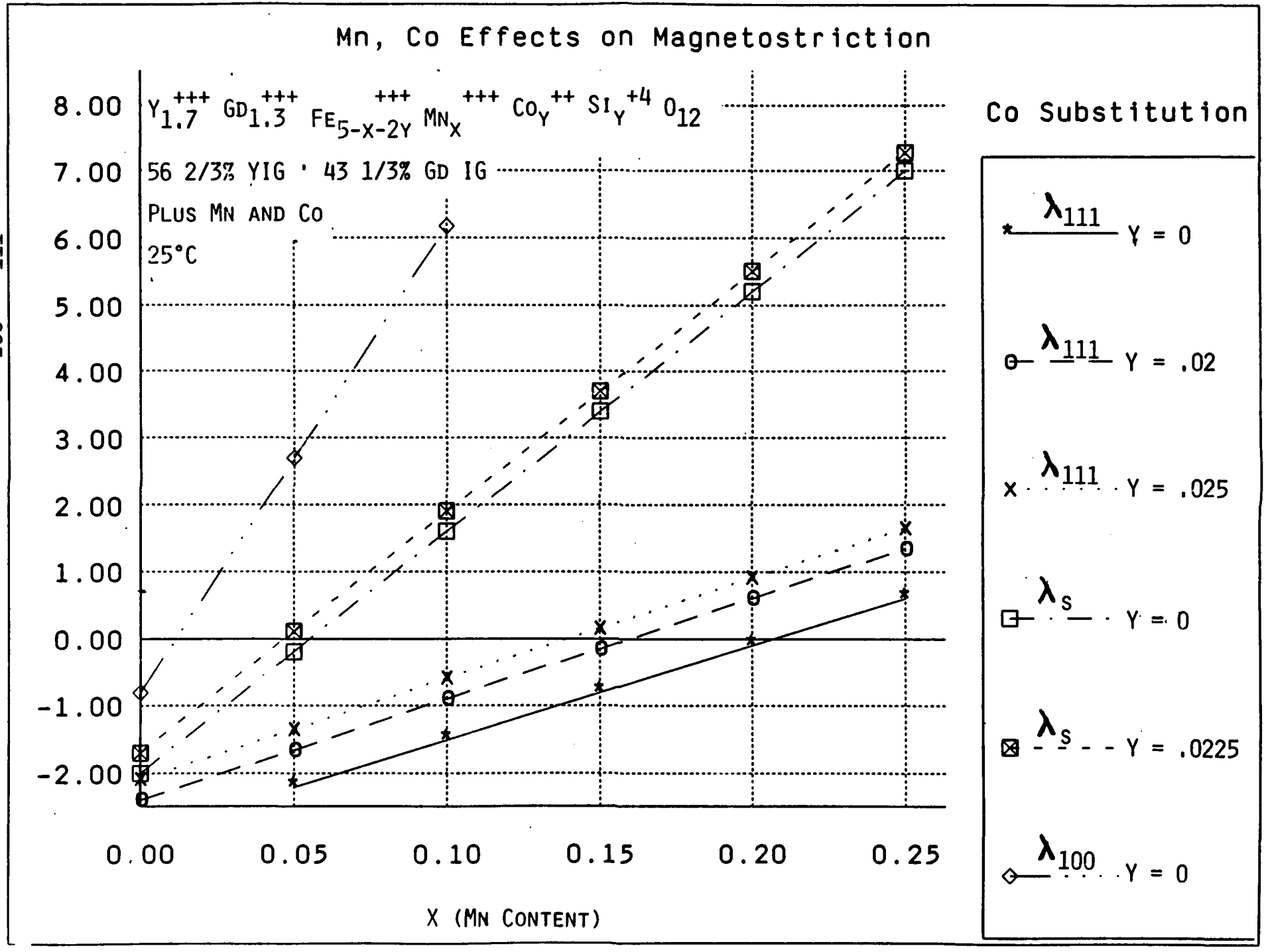
Mn, Co Effects on Magnetostriction
$Y_{1.7}^{+++}\ GD_{1.3}^{+++}\ Fe_{5-x-2Y}^{+++}\ Mn_X^{+++}\ Co_Y^{++}\ Si_Y^{+4}\ O_{12}$
56 2/3% YIG · 43 1/3% GD IG
PLUS MN AND CO
25°C
MAGNETOSTRICTIVE CONSTANTS λ_{100}, λ_{111} x 10^6
8.00
7.00
6.00
5.00
4.00
3.00
2.00
1.00
0.00
-1.00
-2.00
0.00
0.05
0.10
0.15
0.20
0.25
X (MN CONTENT)
Co Substitution
λ_{111} Y = 0
λ_{111} Y = .02
λ_{111} Y = .025
λ_S Y = 0
λ_S Y = .0225
λ_{100} Y = 0

FIGURE 3-16

To achieve the characteristics of $K_1>0$ and $\lambda_{111}=0$, as discussed in Section 2 as a stress insensitive condition, Co^{+2}/Si^{+4} can be substituted into this compound for Fe^{+3}. As indicated in Figure 3-16 and 3-17, a Co^{+2}/Si^{+4} amount of 0.0225 would appear sufficient to increase K_1 to a slightly positive value with a Mn^{+3} content for $\lambda_{111}=0$ of near 0.15.

This analysis formed the initial basis for formulating the Mn^{+3} substituted garnet compounds for preparation and evaluation.

STRESS INSENSITIVE GARNET COMPOUND

CONDITIONS: $K_1 > 0$

$\lambda_{111} = 0$

$$Y_{1.7}^{+++}\ Gd_{1.3}^{+++}\ Fe_{4.8}^{+++}\ Mn_{0.155}^{+++}\ Co_{0.0225}^{++}\ Si_{0.0225}^{+4}\ O_{12}$$

$\lambda_{111} = 0$; $\lambda_{100} = +10.1$

$K_1 = +1 \times 10^3$ ergs/cm^3

$K_2 = -3.2 \times 10^3$ ergs/cm^3

FIGURE 3-17

4.0 MATERIALS FORMULATED

A series of manganese substituted yttrium-gadolinium ion garnets were studied on this program with compositions given by:

$$Y^{+3}_{1.7}\ Gd^{+3}_{1.3}\ Fe^{+3}_{5-X}\ Mn^{+3}_{X}\ O_{12}$$

Consistent with the discussion of Section 3.5, manganese substitution levels from X=0.09 to X=0.21 were investigated. These compositions are solid solutions of 56 2/3 YIG and 43 1/2% GdIG with Mn^{+3} substituted for Fe^{+3}. They are similar to the Trans Tech commercial product TT G-1002+09Mn; which served as a baseline material.

4.1 MATERIAL PREPARATION

EMS and other ferrite manufacturers have had some difficulty in preparing high quality garnets with relatively high Mn contents. Some previous experience has indicated problems in achieving good hysteresis properties together with low dielectric and magnetic loss. In the early stages of this project the standard preparation processes were varied slightly to establish procedures that would facilitate the substitution of up to 0.21 Mn ions per formula unit.

In the normal ceramic processes of milling and mixing iron is always picked up, and adjustments of starting iron stoichiometry are made to compensate, so as to yield a final end product that is on stoichiometry. This is particularly important in the case of garnets, where single phase materials are produced for only a very narrow compositional field. An initial study was done on the 0.15 Mn substituted material to determine the range of acceptable starting iron deficiencies. Table 4-1 below shows results obtained.

Table 4-1 Study of Effect of Iron Stoichiometry on Material Properties

Iron Deficiency	Density (gms/cc)	Magnetic Loss Tangent	Relative Permittivity Er	Dielectric Loss Tangent	4πMs gauss	Br gauss	Hc oersteds
1%	5.59	.00429	15.0	.00019	1058	654	1.61
2%	5.57	.00087	14.7	.00012	1015	654	1.58
2.5%	5.69	.00087	15.4	.00012	1068	717	1.29
3%	5.67	.00092	15.3	.00009	1045	774	1.3
3.6%	5.72	.00051	15.0	.00029	1010	457	2.15

At small iron deficiency the iron picked up in processing produces an iron rich end product that apparently has a second magnetic phase (magnetite?) which increases the magnetic loss.

Too large an iron deficiency yields an yttrium rich end product with a second phase that is probably the orthoferrite. This low magnetization phase serves as a non-magnetic inclusion and results in a low value of remanent magnetization.

The 2.5 and 3 percent starting iron deficiencies produce good hysteresis properties and low loss. All materials later tested on this program were prepared in this range.

It was found that the decrease in remanent magnetization often observed at large Mn substitution levels could be mitigated by sintering at somewhat lower temperatures. Table 4-2 contains a summary of results of this study. Also shown there are the results obtained when the sintering atmosphere was changed from air to oxygen.

Negligible differences were found in properties as the firing temperature was changed from 1425 to 1450 degrees, until relatively high Mn contents were reached. Negligible differences in material properties were also seen when oxygen was substituted for air in the firing cycle until the higher temperature and manganese contents were reached. Then the oxygen fired samples showed a greater tolerance for high firing temperatures. Remanent magnetization was found to be the most sensitive parameter.

Some relevant Br data are shown in the table below.

Table 4-2 Effect of Firing Temperature and Atmosphere on Material Properties For Firings Done in Air/Oxygen

Mn Content	Br (gauss)		Hc (Oe)	
	@1425°C	@1450°C	@1425°C	@1450°C
.09	728/710	743/767	1.53/1.58	1.10/1.1
.15	774/754	697/751	1.25/1.3	1.2 /1.1
.17	689/	491/	1.39/	1.55/
.21	602/645	381/433	1.58/1.4	2.0 /1.7

In an attempt to study the effects of processing parameters on oxidation state of the Mn ions, some batches of materials were prepared using an oxygen atmosphere in the calcine stage. These results, shown in Table 4-3, are compared to those obtained when calcining in air. The oxygen calcine ("OxCalc" under "Comments") produced results that do not differ in any property (outside of experimental error) from those of material prepared by the standard ("STD") process.

As a part of the study of manganese chemistry described in Section 3.4, some batches of the 0.15 Mn compositions were prepared with preoxidized Mn added before ("Mnprecalc") the calcine step, rather than as a carbonate (Mn^{+2}) in the initial mix. In other batches the preoxidized Mn^{+3} was added after the calcine step ("Mnpostcalc") rather than as the carbonate (Mn^{+2}) in the initial mixing. Both of these approaches as seen in Table 4-4 led to somewhat lower densities and markedly lower values of remanent magnetization than obtained in the standard ("STD") process. This result is probably a reflection of less thorough mixing and a less uniform end product, rather than any effect from altering the valence of the Mn ions.

The evidence obtained, however, indicates that the divalent manganese ions initially mixed as a carbonate do convert to a trivalent state as required by the garnet chemical balance.

sample#	density	Ms	Tandm	tande	ke	Br	Bd	Hc	Dbr	DH	DHk	Comments
G265-39A	5.68	999	0.00093	0.0001	15.3	751	826	1.1	0.9	112	9.8	STD(1100-1450@1/min/O2
G265-39B	5.58	964	0.00107	0.00015	15.2	697	794	1.2	0.88	121	9.3	STD(1100-1450@1/min/air
G265-39C	5.66	1061	0.00085	0.00009	15.2	754	858	1.3	0.96	101	10.3	STD(1075-1425@1/min/O2
G265-39D	5.67	1047	0.00092	0.00009	15.3	774	867	1.25	0.95	114	9.99	STD(1075-1425@1/min/air
G265-40A	5.68	1028	0.00086	0.0001	15.1	724	816	1.1	0.92	121	9.9	OxCalc/Std/1100-1450@1/minO2
G265-40B	5.59	1038	0.00114	0.0001	15.2	651	776	1.3	0.85	144	10	OxCalc/Std/1100-1450@1/minair
G265-40C		1044	0.00092	0.00009	15.3	753	836	1.24	0.93	109	9.76	OxCalc/Std/1075-1425@1/minO2
G265-40D		973				730	825	1.3	0.95	113	9.43	OxCalc/Std/1075-1425@1/minair

Table 4-3 Results of Study of Effect of Oxygen Calcine Treatment Conducted on a .15 Mn Composition.

NRL Materials Property Tabulation

Results of Pre-treatment of Mn addition to G-265 for a .15 Mn content and 3% Fe starting deficiency

sample#	density	Ms	Tandm	tande	Er	Br	Bd	Hc	Dbr	DH	DHk	Comments
G265-39A	5.68	999	0.00093	0.0001	15.3	751	826	1.1	0.9	112	9.8	STD(1100-1450@1/min/O2
G265-39B	5.58	964	0.00107	0.00015	15.2	697	794	1.2	0.88	121	9.3	STD(1100-1450@1/min/air
G265-39C	5.66	1061	0.00085	0.00009	15.2	754	858	1.3	0.96	101	10.3	STD(1075-1425@1/min/O2
G265-39D	5.67	1047	0.00092	0.00009	15.3	774	867	1.25	0.95	114	9.99	STD(1075-1425@1/min/air
G265-44A	5.69	1072	0.00085	0.00018	14.9	608	737	1.46	0.99	144	10.65	Mnpostcalc/1075-1425/AIR
G265-44B	5.62	1004	0.00078	0.00016	13.8	623	756	1.59	0.93	138		Mnpostcalc/1075-1425/O2
G265-44C	5.64	1031	0.00086	0.00018	14.7	603	759	1.42	0.89	125	9.89	Mnpostcalc/1100-1450/O2
G265-45A	5.65	1013	0.00078	0.00018	15.4	563	714	1.77	0.955	132	10.65	Mnprecalc/1075-1425/O2
G265-45B	5.65	1018	0.00085	0.00018	15.7	561	709	1.59	0.945	145	9.86	Mnprecalc/1100-1450/O2

Table 4-4 Results of Pre-treatment of Mn in a 0.15 Mn substituted G-265

Table 4-5 shows the six levels of Mn addition prepared and studied on this program. In addition, the baseline Trans Tech G-1002 + .09 Mn is included. The material properties listed were all measured in the EMS materials laboratory by standard measurement procedures (see Table 4-6). The properties are abbreviated as follows.

Ms	Saturation magnetization (in gauss)
Tandm	Magnetic loss tangent
tande	Dielectric loss tangent
ke	Relative permittivity
Br	Remanent magnetic flux (in gauss)
Bd	Drive flux level, when hysteresis is measured (in gauss)
Hc	Coercive field (in oersteds)
Dbr	Remanent flux at 3000 PSI axial stress/Remanent flux at no stress
DH	Resonance linewidth (in oersteds)
DHk	Spinwave linewidth (in oersteds)

...Mn..	sample#	density	..Ms..	Tandm	tande	...ke	....Br	....Bd	..Hc..	..Dbr.....	DH....	DHk
0.09	TransT1002		1099	0.00068	0.0009	15.7	669	818	1.08	0.72	114	10.3
0.09	G265-35	5.64	1097		0.00006	15.4	723	816	1.35	0.772	137	12.2
0.11	G265-36	5.65	1049		0.00006	15.4	758	849	1.25	0.789	170	12.1
0.13	G265-37	5.63	1071	0.00085	0.00006	15.3	722	828	1.25	0.858	145	11.8
0.15	G265-33	5.62	1038	0.00092	0.00009	15.3	721	818	1.29	0.958	128	12.2
0.17	G265-42	5.64	1106	0.00085	0.00025	15	601	730	1.5	0.935	141	
0.21	G265-41	5.66	1013	0.00099	0.00024	15.3	645	763	1.4	1	119	9.63

Table 4-5 NRL Materials Property Tabulation

TABLE 4-6

MATERIAL PROPERTY MEASUREMENTS

PROPERTY	MEASUREMENT TECHNIQUE	ACCURACY
Density	Water immersion	± 0.02 gm/cc
Magnetization, $4\pi Ms$ (Gauss)	Magnetometer	± 3 to 5 %
Remanent Magnetization, Br (Gauss)	Square Loop Tester	± 5 %
Coercive Field, Hc (Oe.)	Square Loop Tester	± 0.2 Oe.
Resonant Linewidth ΔH (3dB) (Oe.)	X-Band Transmission Cavity	± 3 %
Spinwave Linewidth ΔHk (Oe.)	X-Band Transmission Cavity	± 10 %
Dielectric Loss Tangent $\tan\delta\varepsilon'$	X-Band Transmission Cavity ASTM C525-63T	± 0.0002 (<0.001)
Dielectric Constant ε'	X-Band Transmission Cavity ASTM C525-63T	± 0.3
Magnetic Loss Tangent $\tan\delta m$	X-Band Transmission Cavity	± 0.0002 (<0.001)
Stress Sensitivity ΔBr	Square Loop Tester	

Stress is applied to the toroid by placing the toroid in fixture and applying a controlled torque to a screw. Axial stress applied in the direction as shown is perpendicular to the direction of magnetization. The amount of torque applied resulted in a compressive force of 2600 psi on the toroid.

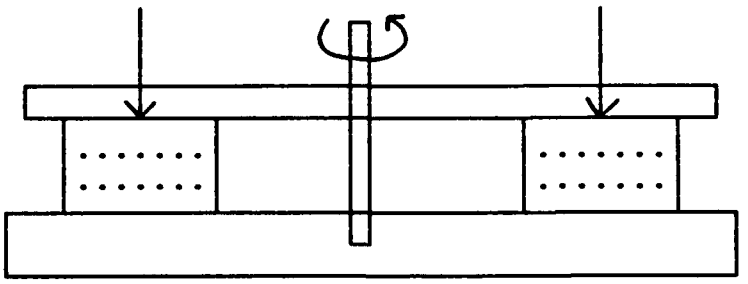

The measured remanent magnetization of round toroids is shown in Figure 4-1 as a function of axially applied stress. Manganese content is the parameter. The decreasing stress sensitivity with increasing Mn content is apparent.

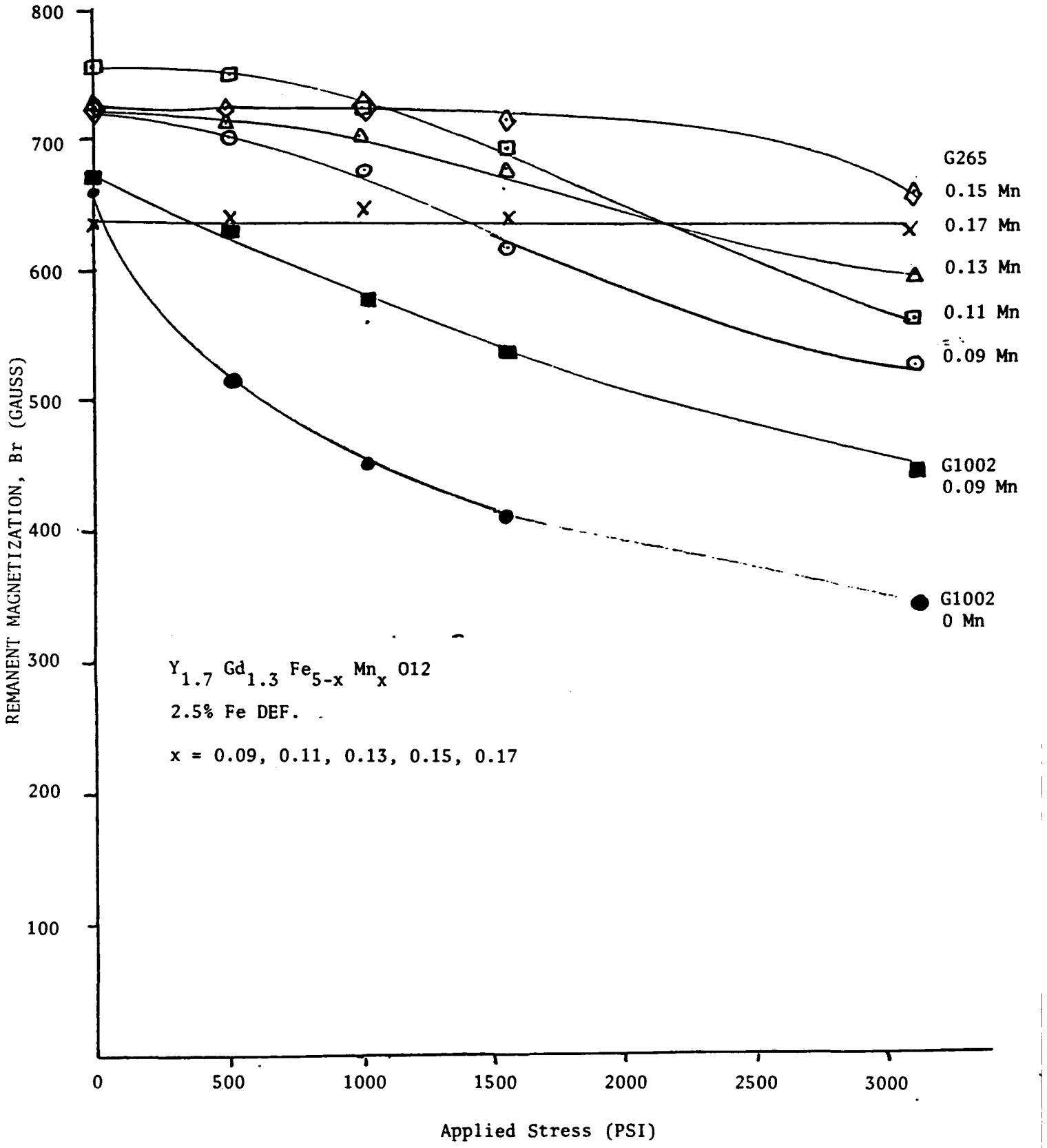

Figure 4-1 Remanent Magnetization Vs. Applied Stress in Y-Gd Garnet With Dependence on Mn Content.

Figure 4-2 Shows remanent magnetization measured on standard round test toroids as a function of temperature. All compositions have similar slopes of B_r versus temperature. The room temperature values of B_r are within $\pm$10% of 700 gauss.

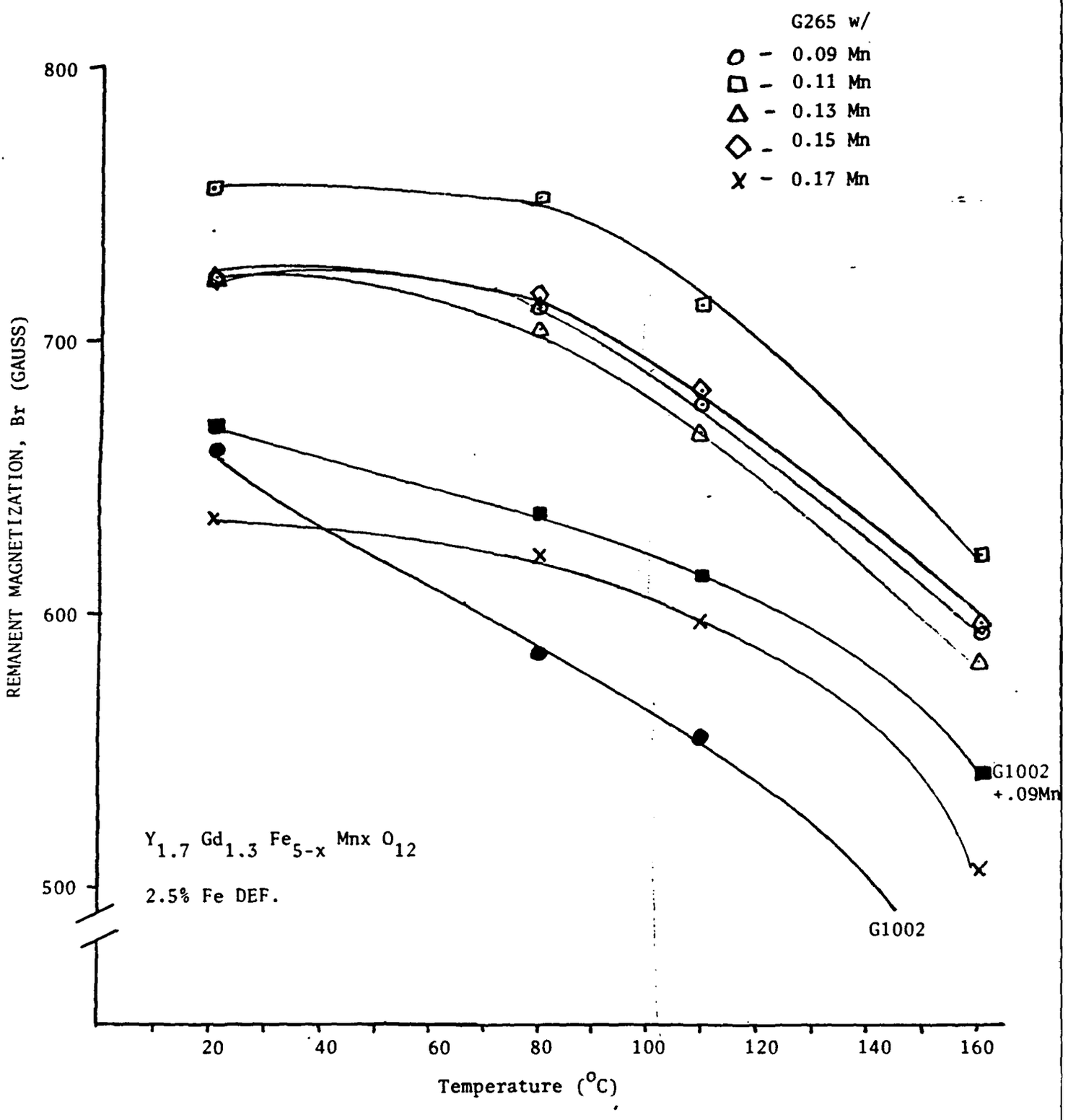

Figure 4-2 Remanent Magnetization Vs. Temperature in Y-Gd Garnet With Dependence on Mn Content.

5.0 STATIC STRESS DATA

5.1 INITIAL TESTS

The test fixture discussed in Section 3.3 and illustrated in Figures 3-6 and 3-7 was used to measure changes in the hysteresis characteristics of the materials as a function of applied stress. The fixture was most useful for studying longitudinal stress perpendicular to the average direction of the remanent magnetization.

The YIG-TbIG compound discussed in Section 3.3 were evaluated in this fixture. Figure 5-1 presents the changes observed in YIG (No TbIG), YIG (0.167TBIG) and YIG(0.35TbIG) for various stress conditions. Photographs of the hysteresis curves were presented in Section 3.3. As noted in Figure 5-1, the change in remanence ratio of the YIG (0.167TbIG) compound was very small up to 4000 PSI for both longitudinal and vertical compressive stress.

Figure 5-2 presents similar data for TTG-1002 (0.09 Mn). The test sample was a toroid prepared for phaser evaluation. It is observed that the material exhibits considerable change in the remanence ratio with stress in all directions; however the material is considerably more sensitive to longitudinal stress.

4.2 STATIC STRESS TESTS ON MANGANESE SUBSTITUTED G-265

The manganese substituted compounds prepared for study were discussed in Section 4.0 The EMS formulated YIG-GdIG compound is designated as G-265 with the following manganese substitution (0.09 Mn, 0.11 Mn, 0.13 Mn, 0.15 Mn, 0.17 Mn, and 0.21 Mn).

Toroids were prepared of each substitution and dimensional sized for phase shifter evaluation. These same toroids were used in the static stress tests.

Figures 5-3 through 5-7 present photographs of the hysteresis curves of these materials for longitudinal stress up to 4000 PSI. All of the

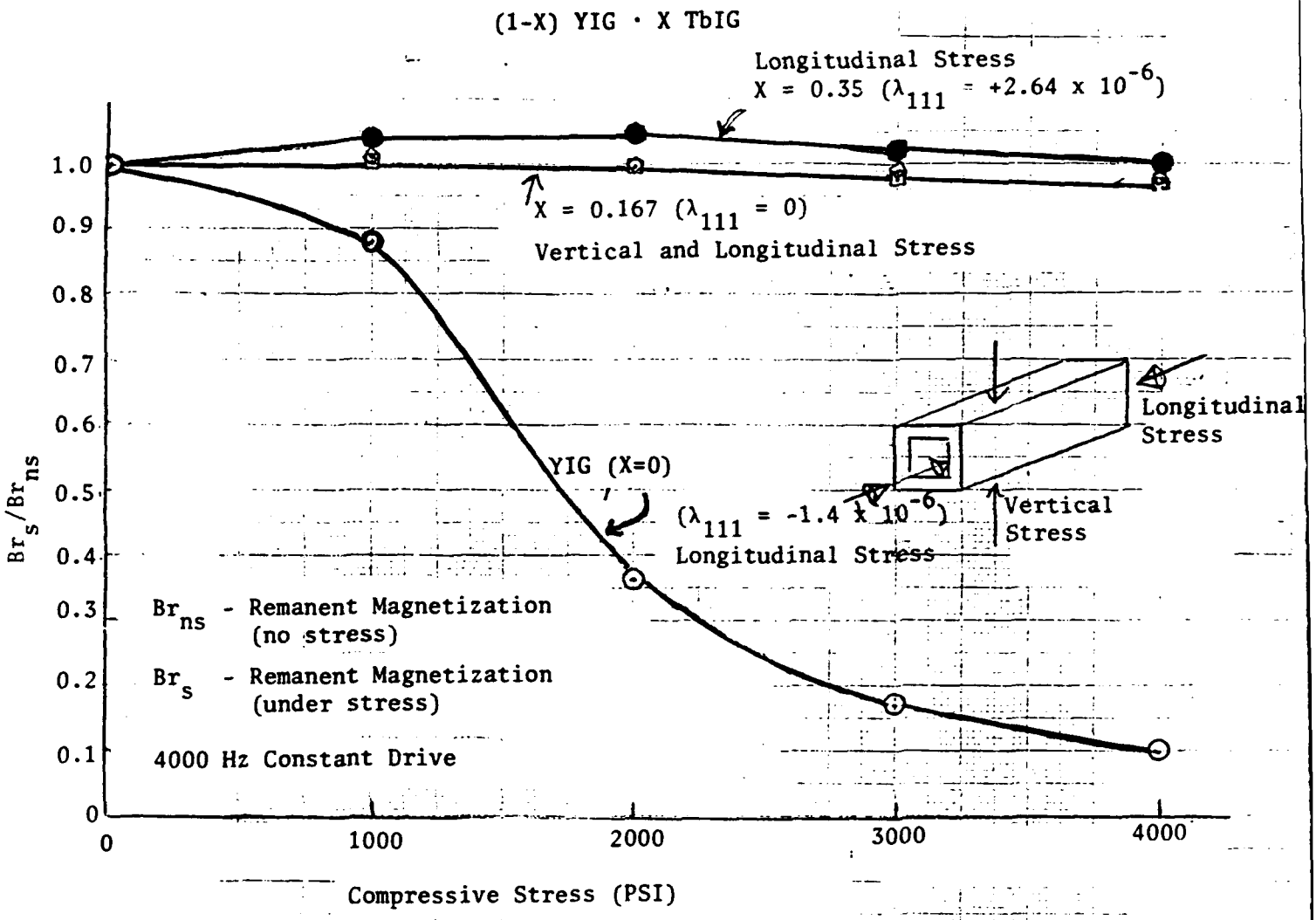

CHANGE IN REMANENCE RATIO WITH STRESS

(YIG - TbIG COMPOUND)

FIGURE 5-1

TTG-1002 (0:09 Mn)

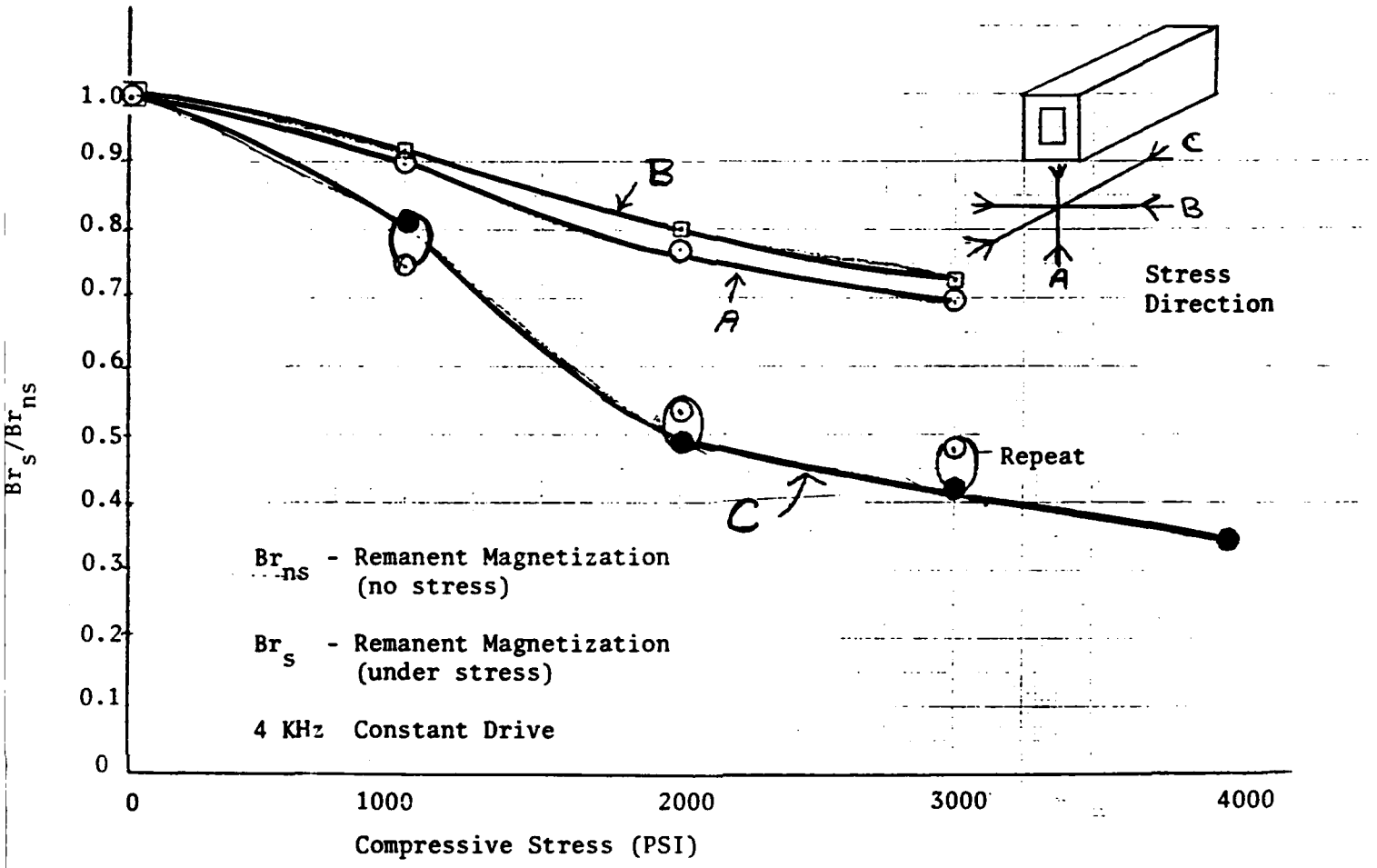

CHANGE IN REMANENCE RATIO WITH STRESS

FOR TTG1002 (0.09 Mn)

FIGURE 5-2

G-265 (0.09 Mn) ILLUSTRATION OF HYSTERESIS CHARACTERISTIC UNDER LONGITUDINAL COMPRESSIVE STRESS

λ_{100} IS POSITIVE
λ_{111} IS NEGATIVE

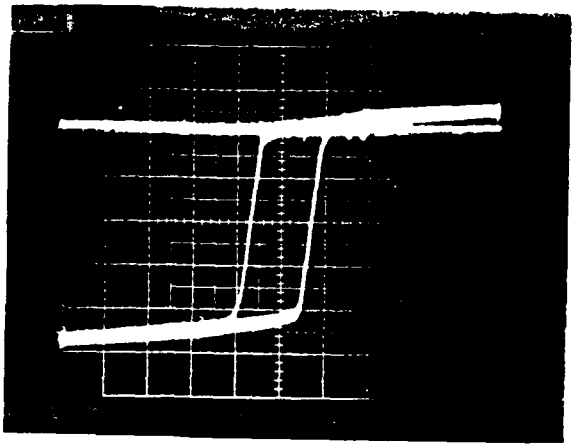

.09 Mn NRL 165 0 PSI Axial

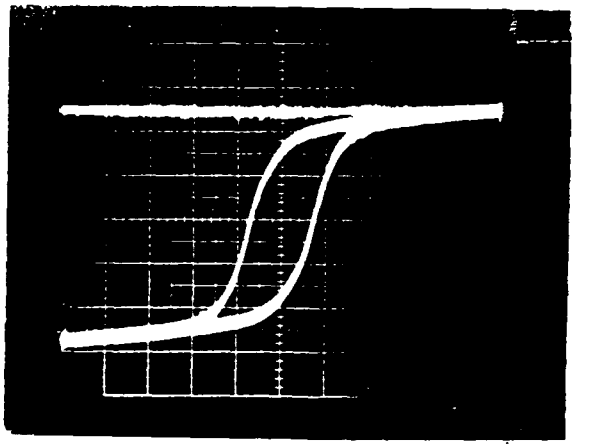

.09 Mn NRL 265 1000 PSI Axial

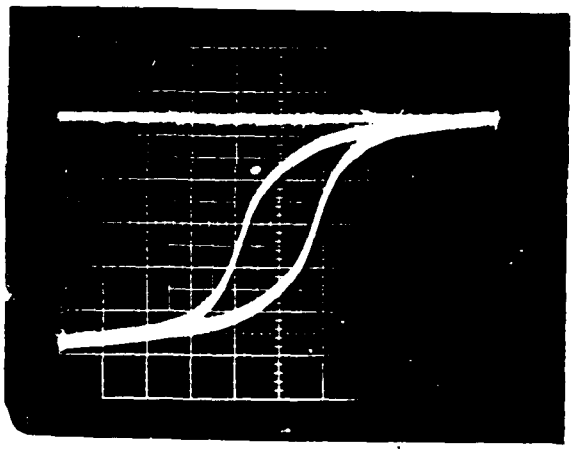

.09 Mn NRL 265 2000 PSI Axial

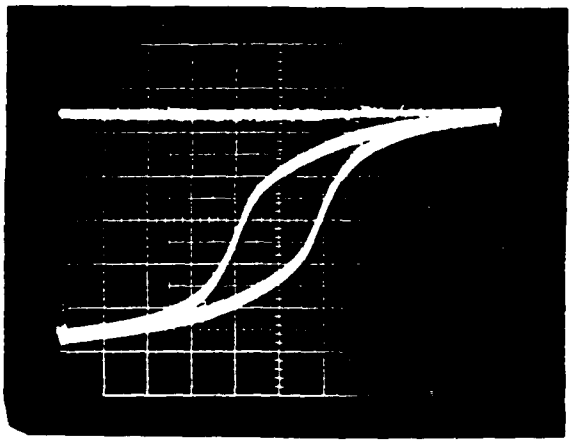

.09 Mn NRL 265 3000 PSI Axial

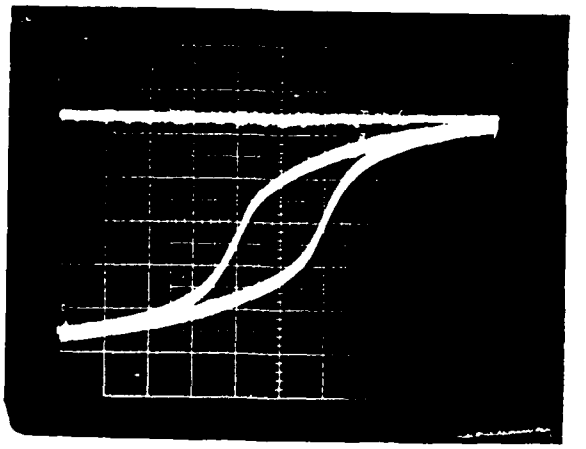

.09 Mn NRL 265 4000 PSI Axial

FIGURE 5-3

G-265 (0.11 Mn) ILLUSTRATION OF HYSTERESIS CHARACTERISTIC UNDER LONGITUDINAL COMPRESSIVE STRESS

λ_{100} IS POSITIVE
λ_{111} IS NEGATIVE

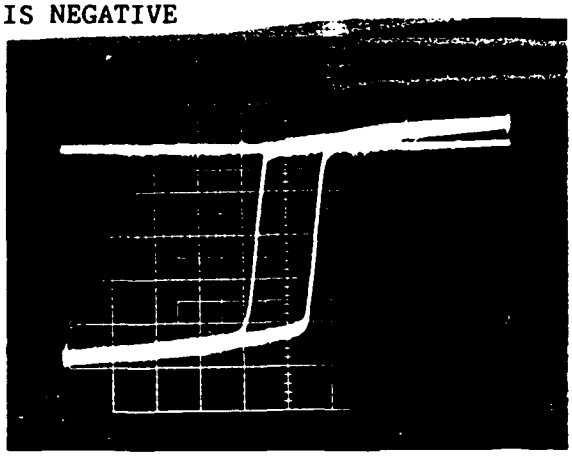

.11 Mn NRL 265 0 PSI Axial

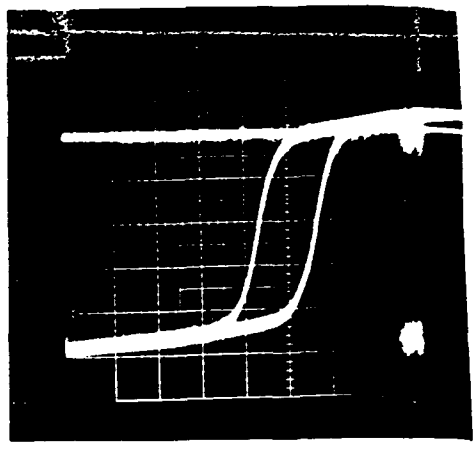

.11 Mn NRL 265 1000 PSI Axial

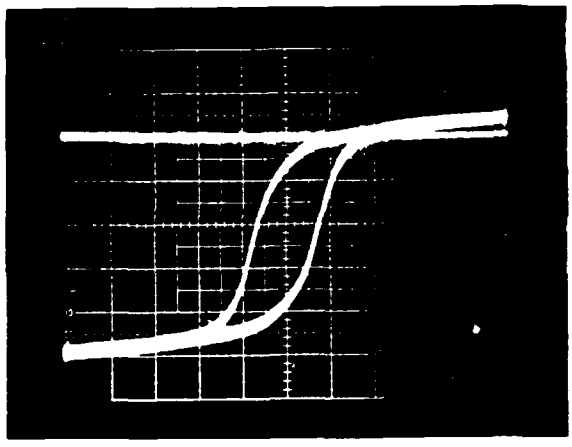

.11 Mn NRL 265 2000 PSI Axial

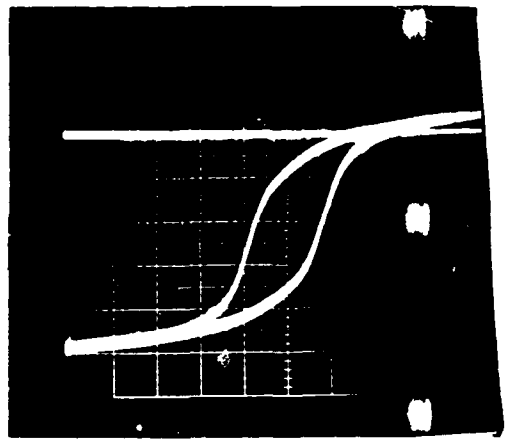

.11 Mn NRL 265 3000 PSI Axial

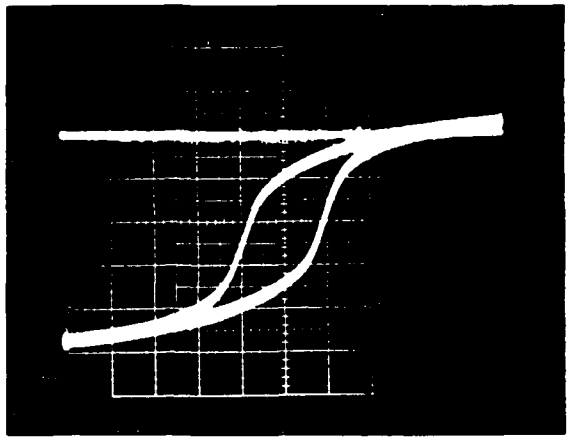

.11 Mn NRL 265 4000 PSI Axial

FIGURE 5-4

G-265 (0.13 Mn) ILLUSTRATION OF HYSTERESIS CHARACTERISTIC UNDER LONGITUDINAL COMPRESSIVE STRESS

λ_{100} IS POSITIVE
λ_{111} IS NEGATIVE

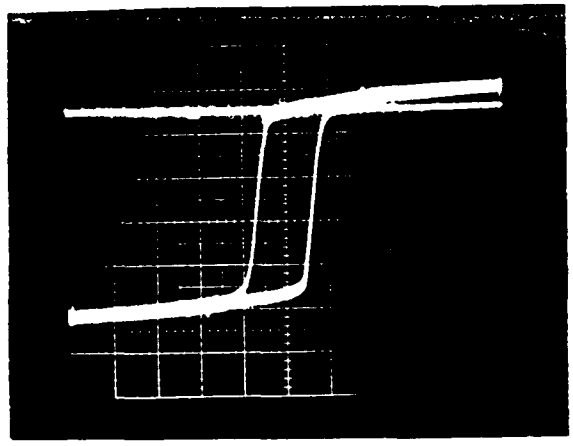

.13 Mn NRL 265 0 PSI Axial

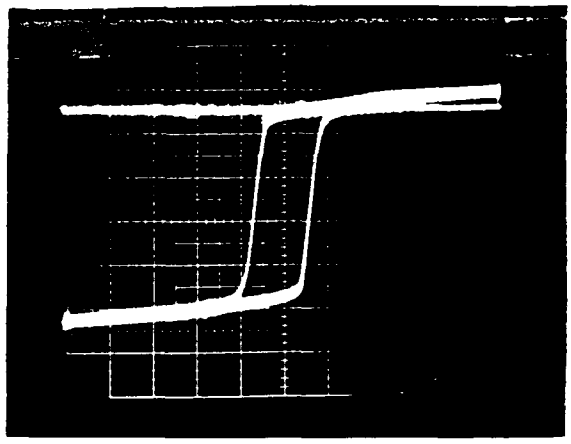

.13 Mn NRL 265 1000 PSI Axial

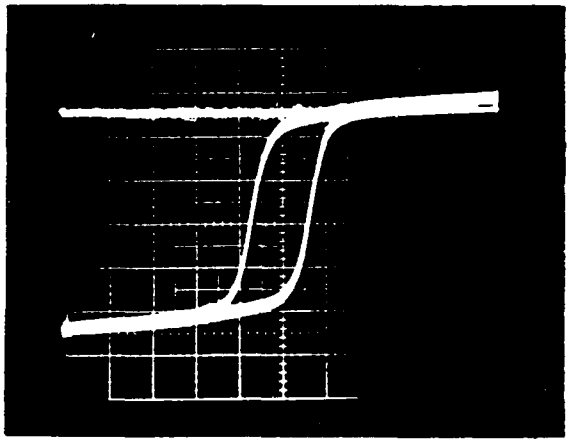

.13 Mn NRL 265 2000 PSI Axial

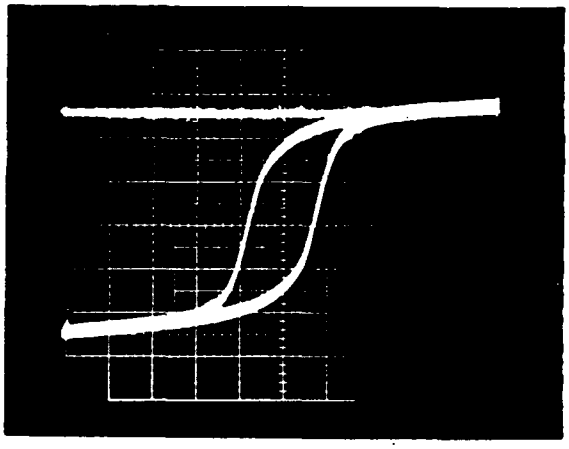

.13 Mn NRL 265 3000 PSI Axial

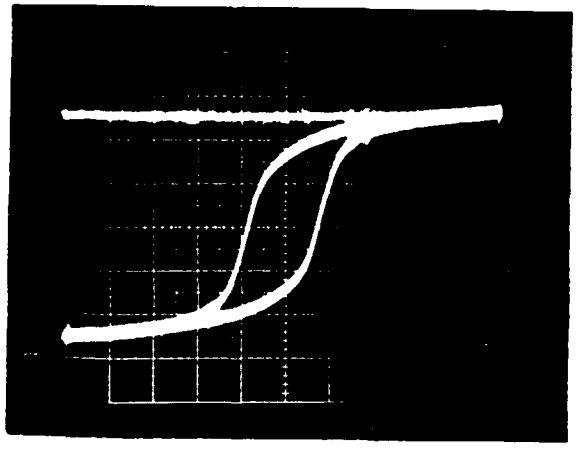

.13 Mn NRL 265 4000 PSI Axial

FIGURE 5-5

G-265 (0.15 Mn) ILLUSTRATION OF HYSTERESIS CHARACTERISTIC UNDER LONGITUDINAL COMPRESSIVE STRESS

λ_{100} IS POSITIVE
$\lambda_{111} \sim 0$

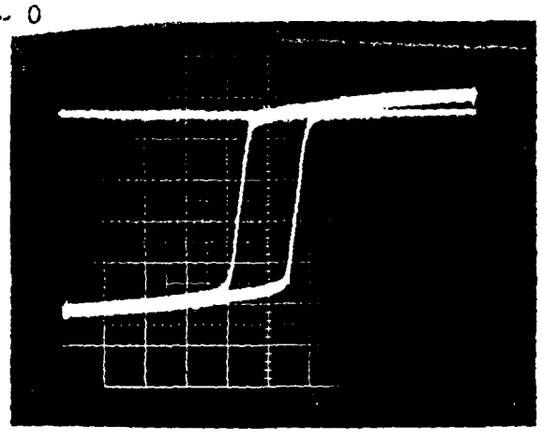

.15 Mn NRL 265 0 PSI Axial

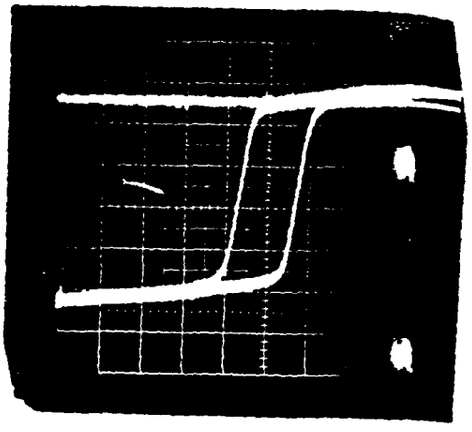

.15 Mn NRL 265 1000 PSI Axial

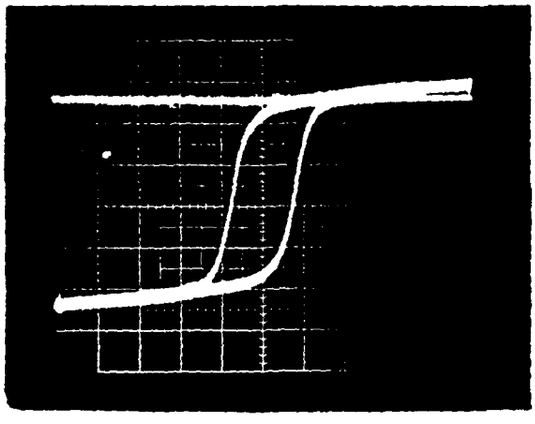

.15 Mn NRL 265 2000 PSI Axial

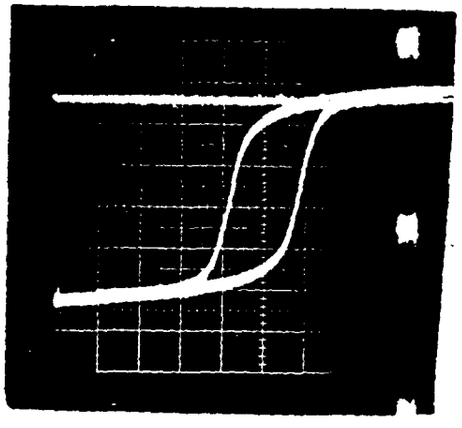

.15 Mn NRL 265 3000 PSI Axial

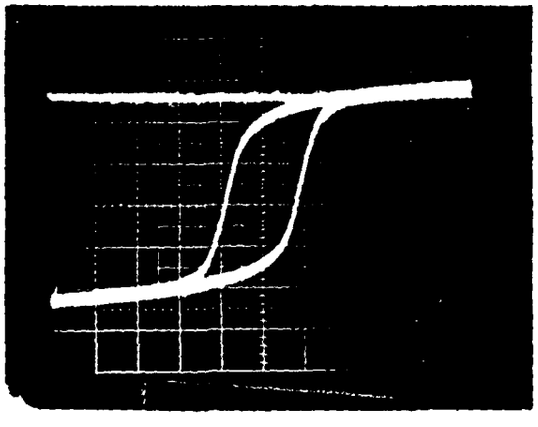

.15 Mn NRL 265 4000 PSI Axial

FIGURE 5-6

G-265 (0.17 Mn) ILLUSTRATION OF HYSTERESIS CHARACTERISTIC UNDER LONGITUDINAL COMPRESSIVE STRESS

λ_{100} IS POSITIVE
$\lambda_{111} \sim 0+$

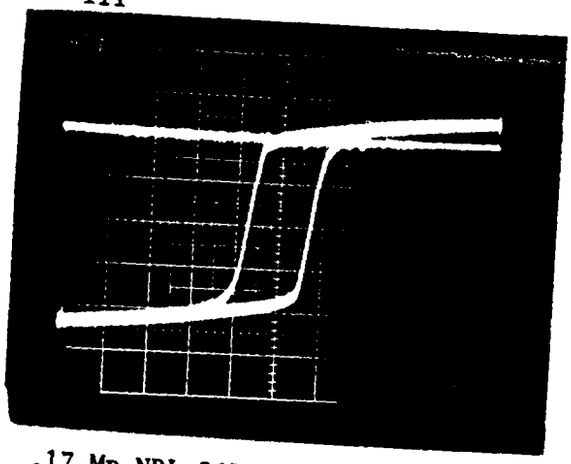

.17 Mn NRL 265 0 PSI Axial

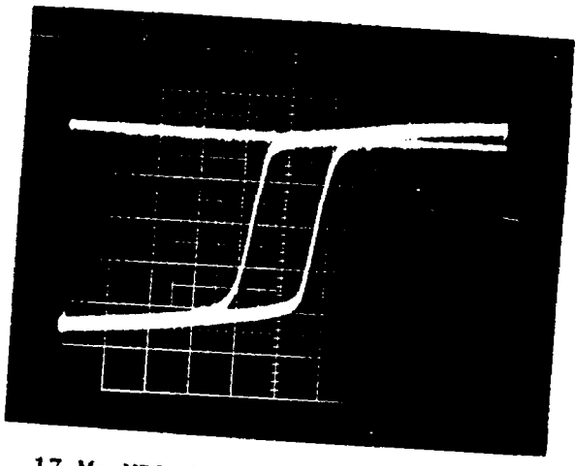

.17 Mn NRL 265 1000 PSI Axial

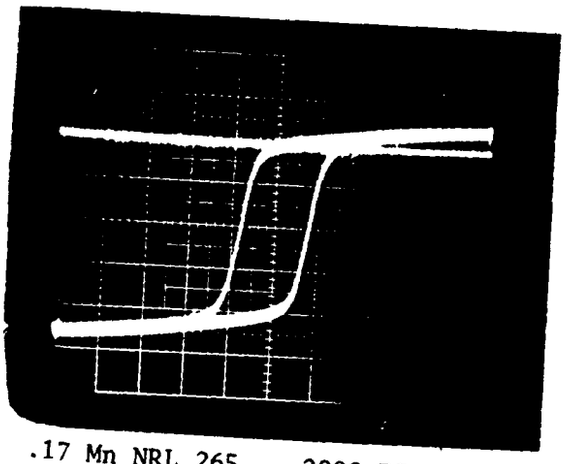

.17 Mn NRL 265 2000 PSI Axial

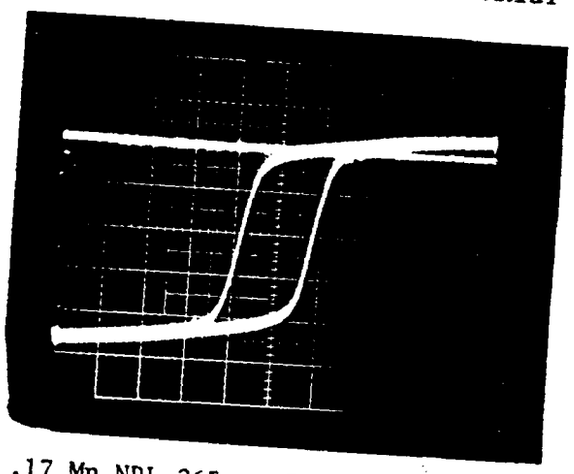

.17 Mn NRL 265 3000 PSI Axial

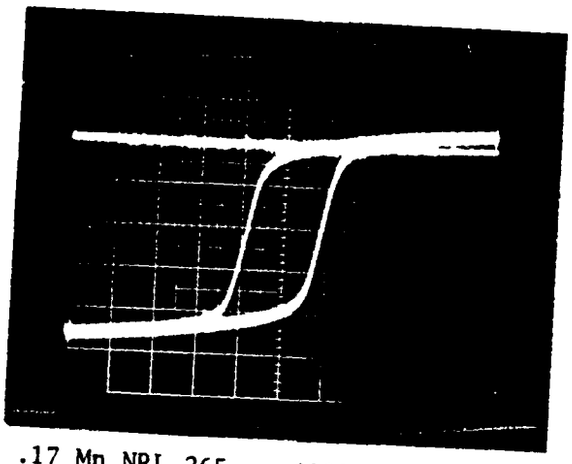

.17 Mn NRL 265 4000 PSI Axial

FIGURE 5-7

compounds exhibit some change in the hysteresis curve for stress above 2000 PSI. The observed change at the 0.17 Mn substitution (Figure 5-7) is very small with some beginning evidence of increasing coercive field with stress, indicating a positive λ_{111}.

These photographs suggest that above 1000 PSI of longitudinal stress, the toroids may be physically distorting (stress is not uni-directional) causing the observed changes in the hysteresis curves. Note that the 0.09 Mn and the 0.11 Mn compounds exhibit changes in the hysteresis curves between 0 and 1000 PSI and continue to change up to 4000 PSI. The 0.13 Mn, 0.15 Mn and 0.17 Mn compounds show almost no change in the hysteresis response up to 1000 PSI. Above this stress level some changes in the hysteresis curves are observed. This non-linear response suggests some minor distortion of the sample (such as bending) creating a stress on the sample that is not uni-directional.

The specific data collected on the change in Br (actually Br (stress)/Br (no stress)) with longitudinal compressive stress for all of the Mn substituted G-265 are presented in Figure 5-8. Note the data taken at 1000 PSI (some physical distortion may be present above this level as mentioned previously). At about 0.13 Mn there is no change in Br; below this level, Br decreases and above the 0.13 Mn substitution, the Br increases.

Figure 5-9 is the same data as Figure 5-8 but constant stress curves are plotted versus Mn content. The 0.13 Mn content appears to be the optimum Mn substituted compound for minimizing longitudinal stress sensitivity between 0 and 1000 PSI.

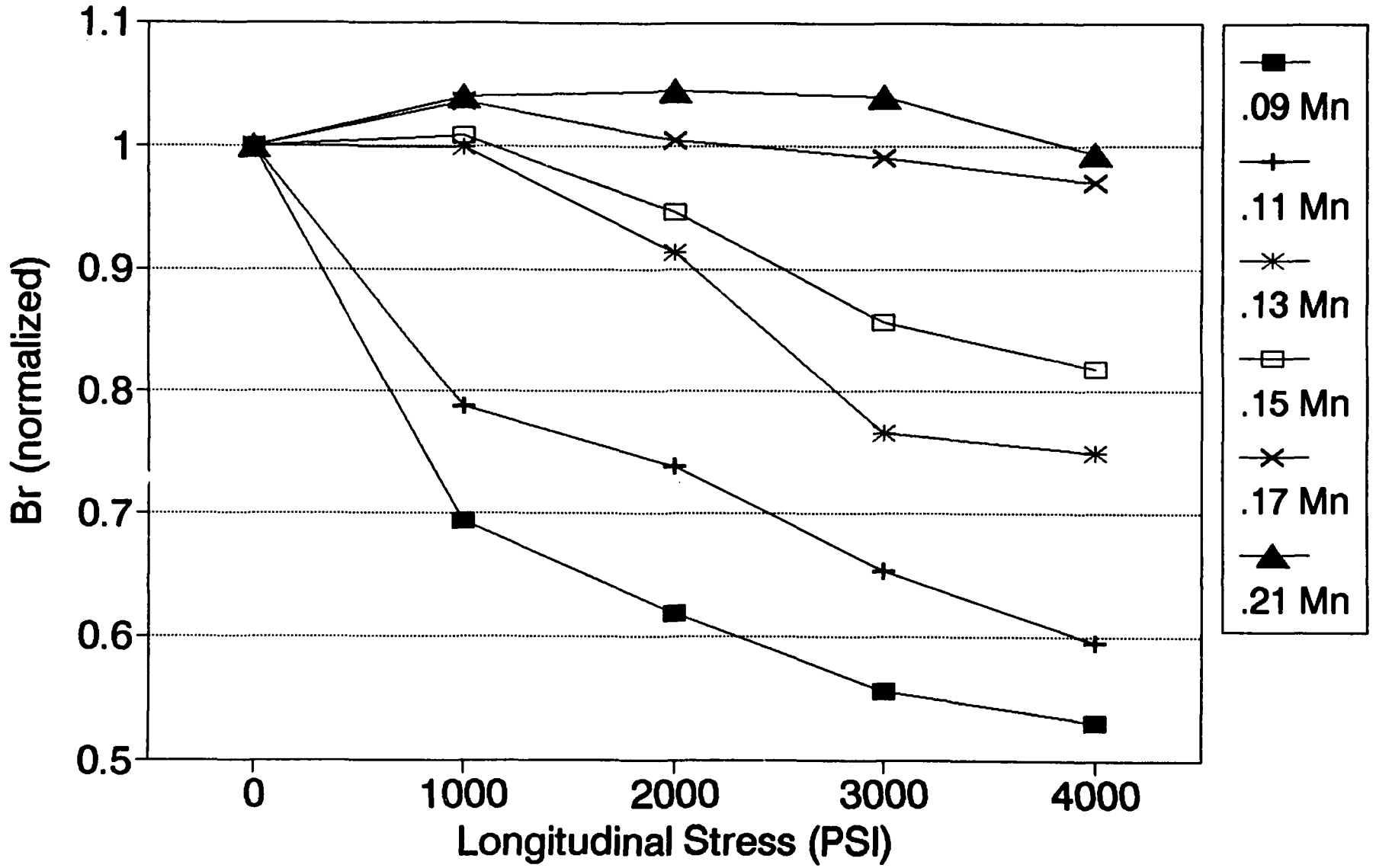
Br vs. Longitudinal Stress
EMS G265 / Various Mn Contents
Br (normalized)
1.1
1
0.9
0.8
0.7
0.6
0.5
0
1000
2000
3000
4000
Longitudinal Stress (PSI)
.09 Mn
.11 Mn
.13 Mn
.15 Mn
.17 Mn
.21 Mn

FIGURE 5-8

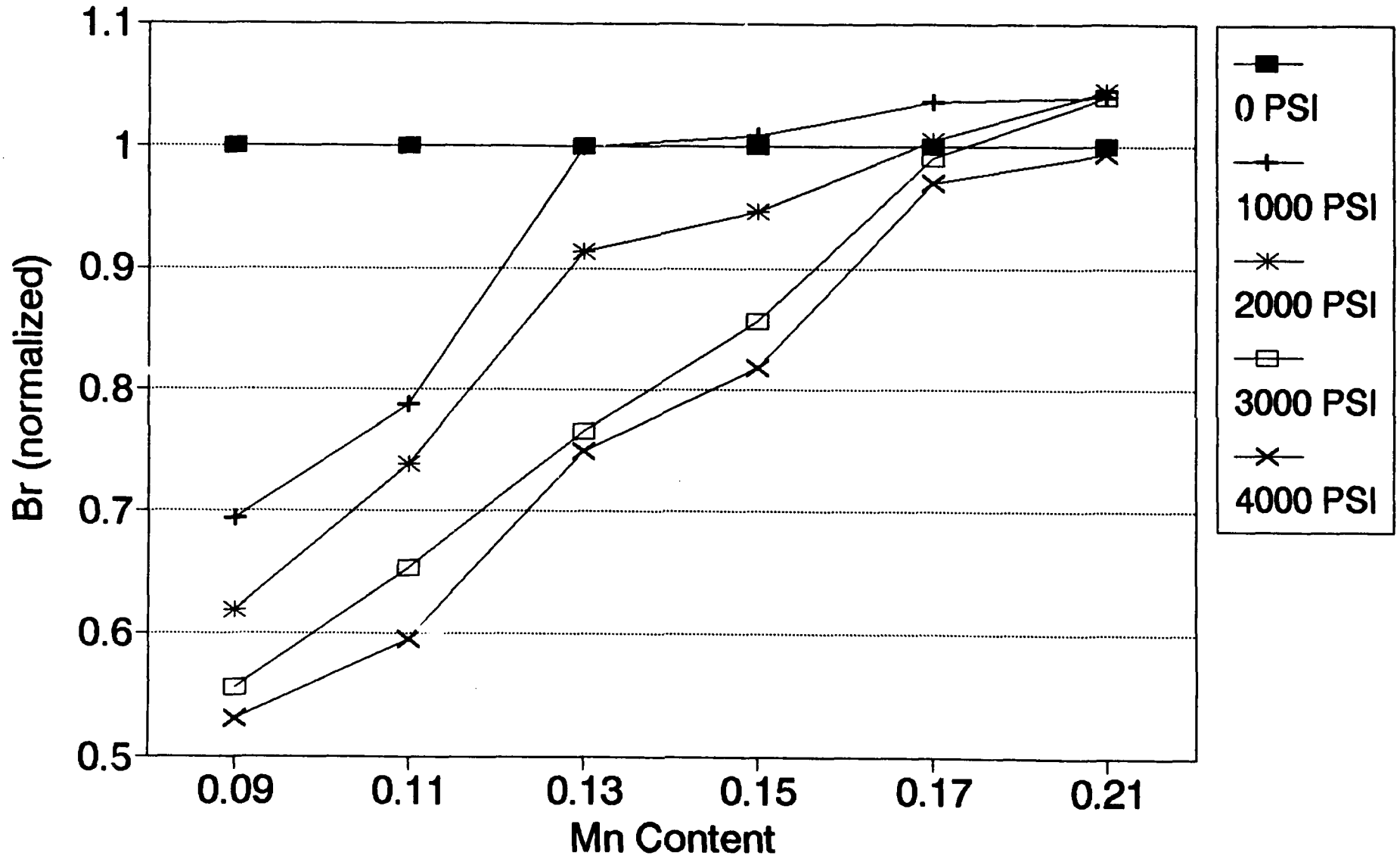
Br vs. Mn Content of EMS G265
Varying Longitudinal Stress
Br (normalized)
1.1
1
0.9
0.8
0.7
0.6
0.5
0.09
0.11
0.13
0.15
0.17
0.21
Mn Content
0 PSI
1000 PSI
2000 PSI
3000 PSI
4000 PSI

FIGURE 5-9

6.0 PHASER STRUCTURE TESTS

6.1 TEST PROGRAM

The program of measurements on the selected materials are described by the diagrams in Figure 6-1. Square phase shifter toroids were matched with a center dielectric slab to form a phaser unit. The schedule of measurements was designed to allow maximum correlation of hysteresis measurements with phase shift measurements. This is to our knowledge the first time that B-H loops have been obtained on actual phaser toroids in waveguide housings under high power conditions.

Hysteresis measurements were made of the B-H loop properties of phaser toroids (side 1 and side 2) loosely held in the housing as a function of temperature from room temperature (~25°C) to 100°C. The data (shown later) indicate no hysteresis with temperature, as one would expect.

Next these toroids were further assembled into the housing for low power RF tests as a function of temperature. The drum top (soft top) phase shifter housing was used to minimize non-repeatable changes resulting from top to bottom "crush" on the toroids. Hysteresis loops were again measured at each temperature and differential phase shift was also measured with the toroids driven by a latch box. These data show hysteresis with temperature in both remanent flux and differential phase shift.

Finally, the toroids (mounted in the housing) were tested at high RF average power with water cooling applied to the housing. Again the B-H loops were measured while the material was exposed to powers of up to 400 W average. The differential phase shift was also measured at each power level from 10 watts to 400 watts and for both increasing and decreasing powers. In these measurements the phaser is controlled by a flux driver, which does not produce as complete switching of the toroids as does the latch box. This high average RF power resulted in considerable heating of the ferrite and housing.

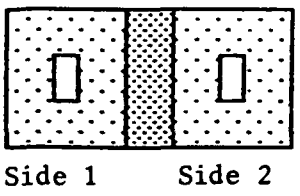

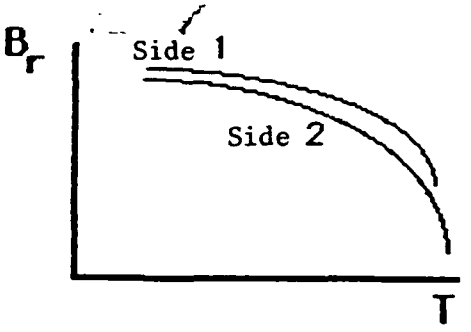

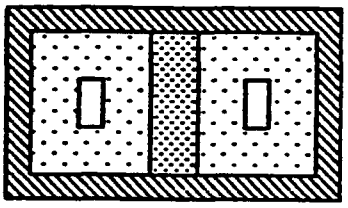

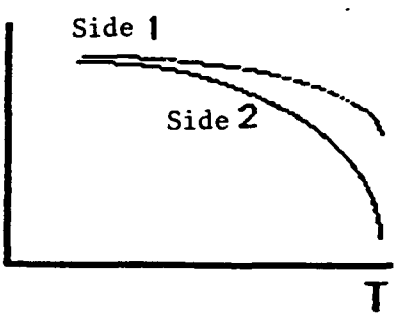

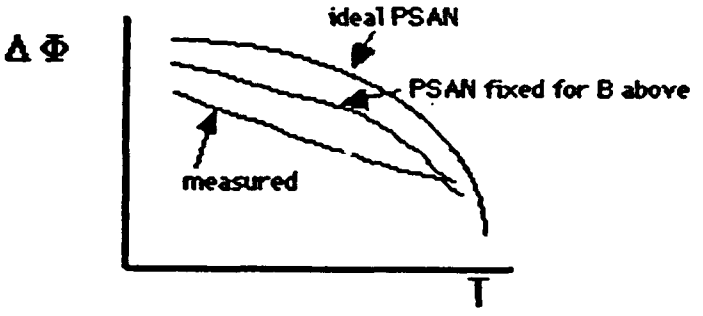

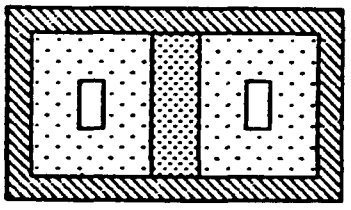

At high rf power

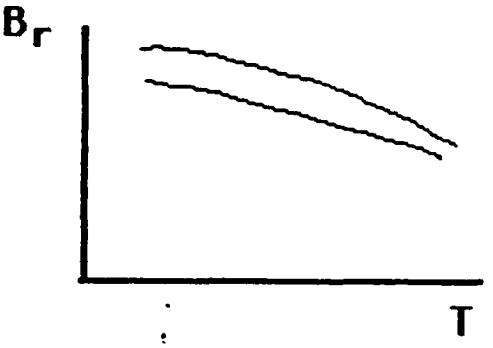

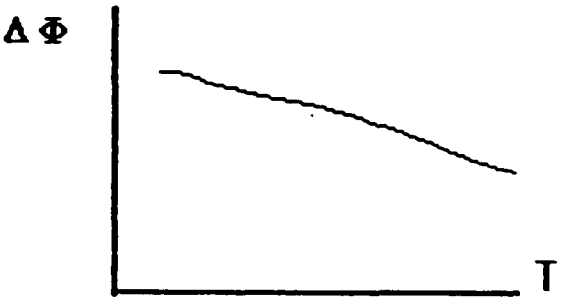

FIGURE 6-1

Theoretical comparisons of the effects of temperature and power are possible using the EMS generated computer analysis program called PSAN. By having measured values of Br available for each condition of operation we will be able to model these units more accurately.

6.2 TEMPERATURE DATA

Measurements of remnant magnetization (Br) and differential phase shift (Delta Phi) versus temperature are presented graphically in Figures 6-2 through 6-15. Seven (7) materials were tested, namely Trans-Tech's G-1002 (.09 Mn) and EMS G-265 (.09 Mn, .11 Mn, .13 Mn, .15 Mn, .17 Mn, and .21 Mn). For each material Br is plotted as a function of temperature both for toroids in a housing and for loose toroids. As expected the loose toroid data shows no hysteresis effects and is plotted for reference. The second plot for each material is a low power differential phase measurement with the Br measurement repeated to show how phase shift and remnant magnetization track one another. In each case the data is plotted on a normalized scale so that the materials may be compared easily. The differential phase shift for each material tested was near 115 degrees at 25°C. Note that the Trans-Tech G-1002 (.09 Mn) material is on a slightly different scale than the other materials due to its higher magnitude hysteresis. Additionally, arrows are included on each plot to indicate the sense of the hysteresis (clockwise or counterclockwise).

Figure 6-2 shows the clockwise sense hysteresis of Br for the Trans-Tech G-1002 (.09 Mn) material. Figure 6-3 shows differential phase hysteresis of the same sense and magnitude ($\approx$ 20%) as for Br of this material.

Figure 6-4 shows that EMS G-265 (.09 Mn) material has clockwise hysteresis just as the Trans-Tech material did, but with a much reduced magnitude (less than 1% relative to loose toroid data). Figure 6-5 shows that phase and Br measurements track closely.

Figures 6-6 and 6-7 show hysteresis results for the EMS G-265 (.11 Mn) material that has the same sense (clockwise) and nearly the same magnitude of hysteresis as that of the EMS G-265 (.09 Mn) material.

Figures 6-8 and 6-9 show results for the EMS G-265 (.13 Mn) material which indicate very little hysteresis of either Br or Delta Phi. The small amount of hysteresis (much less than 1%) that is displayed has a clockwise sense. This is significant because, as will be seen later, all materials measured with higher than .13 Mn content have counterclockwise hysteresis of phase and remnant magnetization. These results indicate a compensation point for a doping near .13 Mn.

Figures 6-10 and 6-11 show the counter clockwise hysteresis of Br and Delta Phi for the EMS G-265 (.15 Mn) material. The magnitude of the hysteresis is only slightly larger than that of the .11 Mn material (which is on the opposite side of the compensation point).

Figures 6-12 and 6-13 show the counterclockwise hysteresis of Br and Delta Phi for the EMS G-265 (.17 Mn) material. The magnitude of the hysteresis ($\simeq$ 4%) is much larger than that of materials with lower Mn dopings.

Figures 6-14 and 6-15 show the counterclockwise hysteresis of Br and Delta Phi for the EMS G-265 (.21 Mn) material with magnitude near 5%.

6.3 HIGH AVERAGE POWER DATA

Results of the high average power tests are presented in Figures 6-16 through 6-22. The seven materials tested are the same as those used in the temperature tests of section 6.2. CW power levels from 10 Watts to 400 Watts were used as indicated on each plot. Corresponding temperature due to RF heating is represented on the x-axis. The temperature was measured (and monitored) from a thermister mounted to the thin walled drum top part of the housing just above the ferrite section in the center of the waveguide. All plots are on a normalized scale with the scale for the Trans-Tech G-1002 (.09 Mn) material being slightly different due to its greater magnitude hysteresis. As before in the temperature data, arrows on the plots are used to indicate the sense of the hysteresis (clockwise or counterclockwise). For each material, both remanent magnetization (Br) and differential phase shift (Delta Phi) are plotted on the same graph.

Figure 6-16 shows that similar to the temperature testing, the Trans-Tech G-1002 (.09 Mn) material also exhibits considerable hysteresis with RF heating. The sense of the hysteresis is clockwise with a magnitude ≈ 6%.

Figure 6-17 shows that over the measured range of RF power, very little hysteresis is detectable for the EMS G-265 (.09 Mn) material. For comparison, it should be noted that the range of temperatures for the RF heating test (15°C to 30°C) is small compared to the range of temperatures used in the temperature tests (25°C to 100°C) of section 6.2. Therefore, in general much less hysteresis is seen in the RF heating data than in the temperature test data.

Similar to the .09 Mn material, Figures 6-18 and 6-19 show that very little hysteresis is associated with either the EMS G-265 (.11 Mn) or the EMS G-265 (.13 Mn) materials.

The data for the EMS G-265 (.13 Mn) material Figure 6-20 is significant because, as in the temperature data, all materials with higher than .13 Mn content have a counterclockwise sense of hysteresis. Again, it appears that a compensation point exists near the .13 Mn doping.

Figures 6-20 through 6-22 show the measured magnitude of the B_R and phase hysteresis to be increasing with the higher Mn content of the EMS G-265 (.15 Mn), EMS G-265 (.17 Mn), and EMS G-265 (.21 Mn) materials respectively. For the 0.21 Mn doping the hysteresis reaches a magnitude of about 4%. In each case the hysteresis is counterclockwise.

As noted in the figures, the temperature of the test phaser varied from near 15°C (temperature resulting from tap water flowing through mounting plate) to about 31°C (measured at the 400 watt in level with same cooling of mounting plate). Over this temperature and power range, the G-265 material with 0.09 Mn, 0.11 Mn, 0.13 Mn, and 0.15 Mn substitutions performed almost equally well. Large changes in ambient temperatures would effect data as noted in Figures 6-4 through 6-11. Figure 6-23 (a through i) present typical experimental data collected for the high power measurements.

As noted in these data, 128 phase states were measured at each power level. Thirty-two of these states were printed for each power level to investigate the stability of partially switched states. Figure 6-24 is a plot of change with power level for partial switched phase states. These results are typical of all the materials tested. The partially switched states show hysteresis responses that are appear to be percentage wise constant within experimental error.

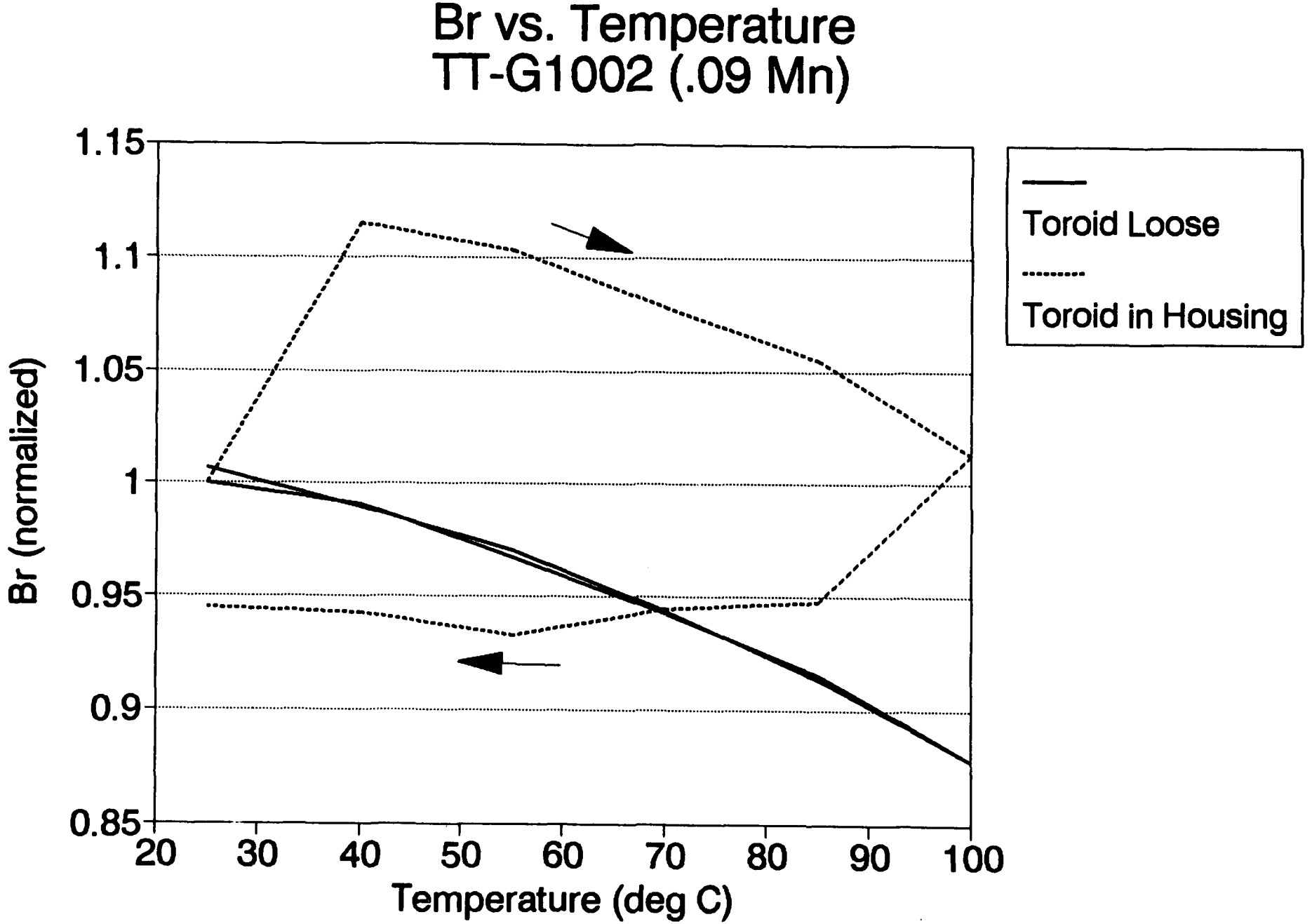
Br vs. Temperature
TT-G1002 (.09 Mn)
1.15
1.1
1.05
1
0.95
0.9
0.85
Br (normalized)
20
30
40
50
60
70
80
90
100
Temperature (deg C)
Toroid Loose
Toroid in Housing

FIGURE 6-2

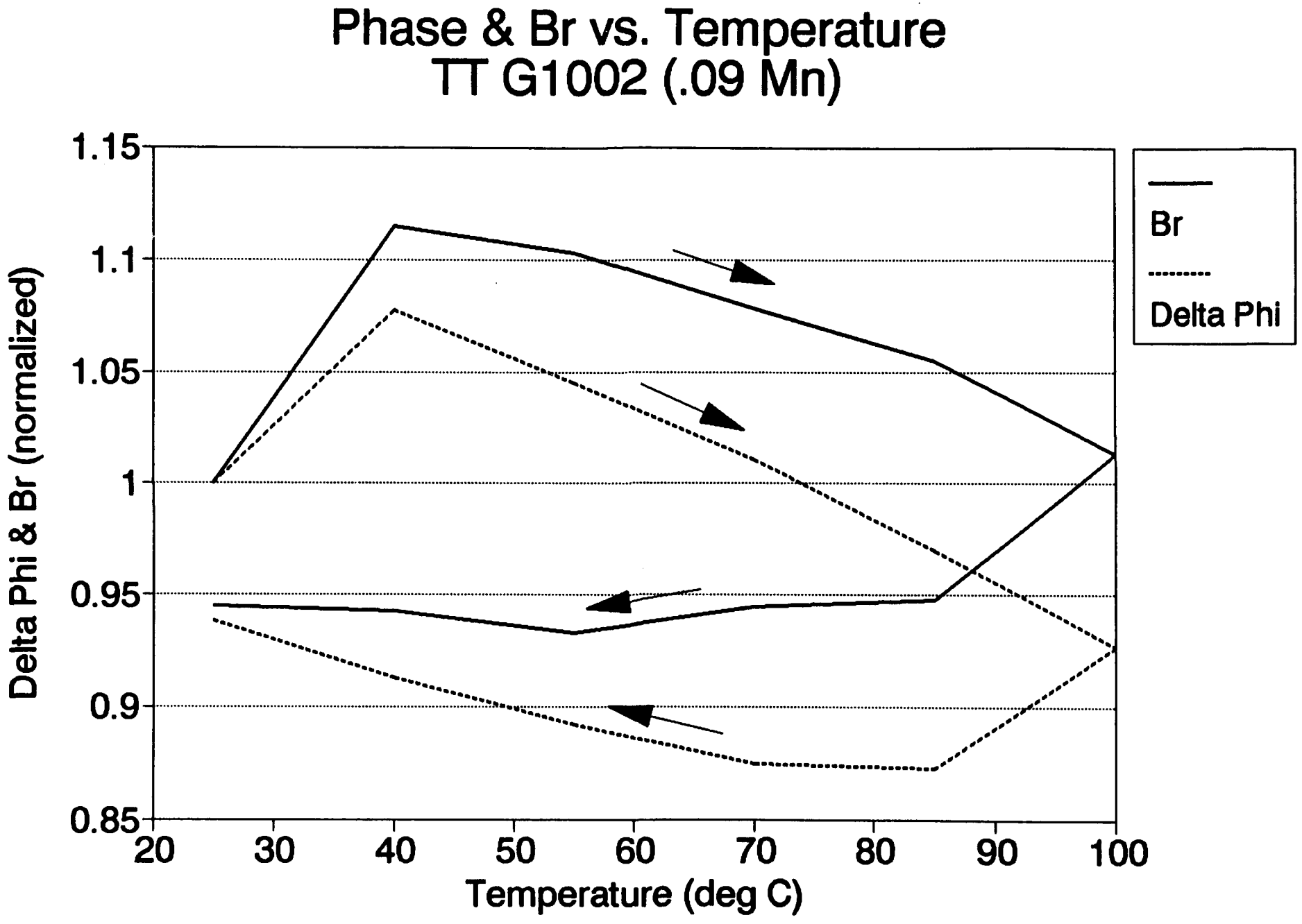
Phase & Br vs. Temperature
TT G1002 (.09 Mn)
Delta Phi & Br (normalized)
1.15
1.1
1.05
1
0.95
0.9
0.85
20
30
40
50
60
70
80
90
100
Temperature (deg C)
Br
Delta Phi

FIGURE 6-3

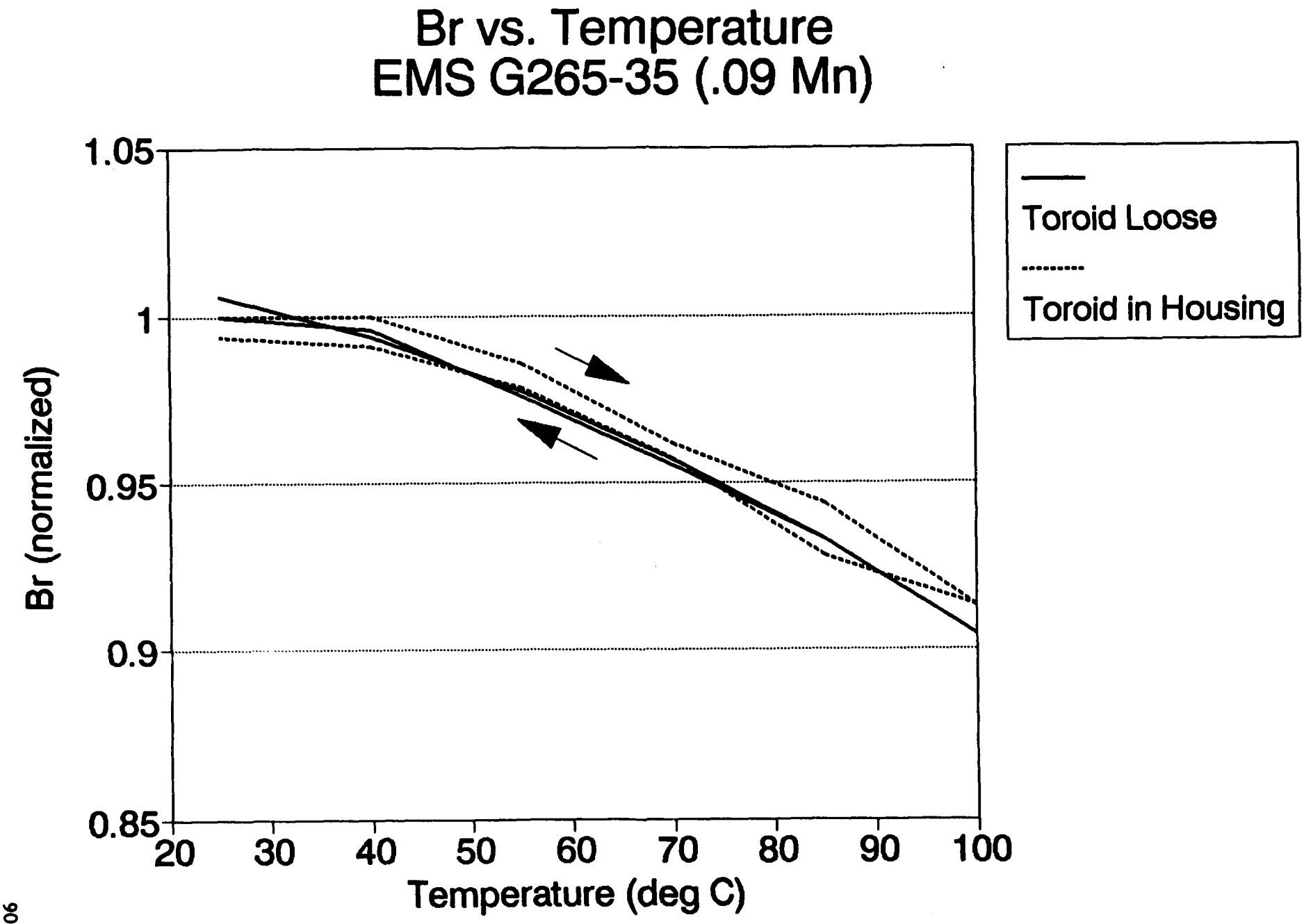
Br vs. Temperature
EMS G265-35 (.09 Mn)
1.05
1
0.95
0.9
0.85
Br (normalized)
20
30
40
50
60
70
80
90
100
Temperature (deg C)
Toroid Loose
Toroid in Housing

FIGURE 6-4

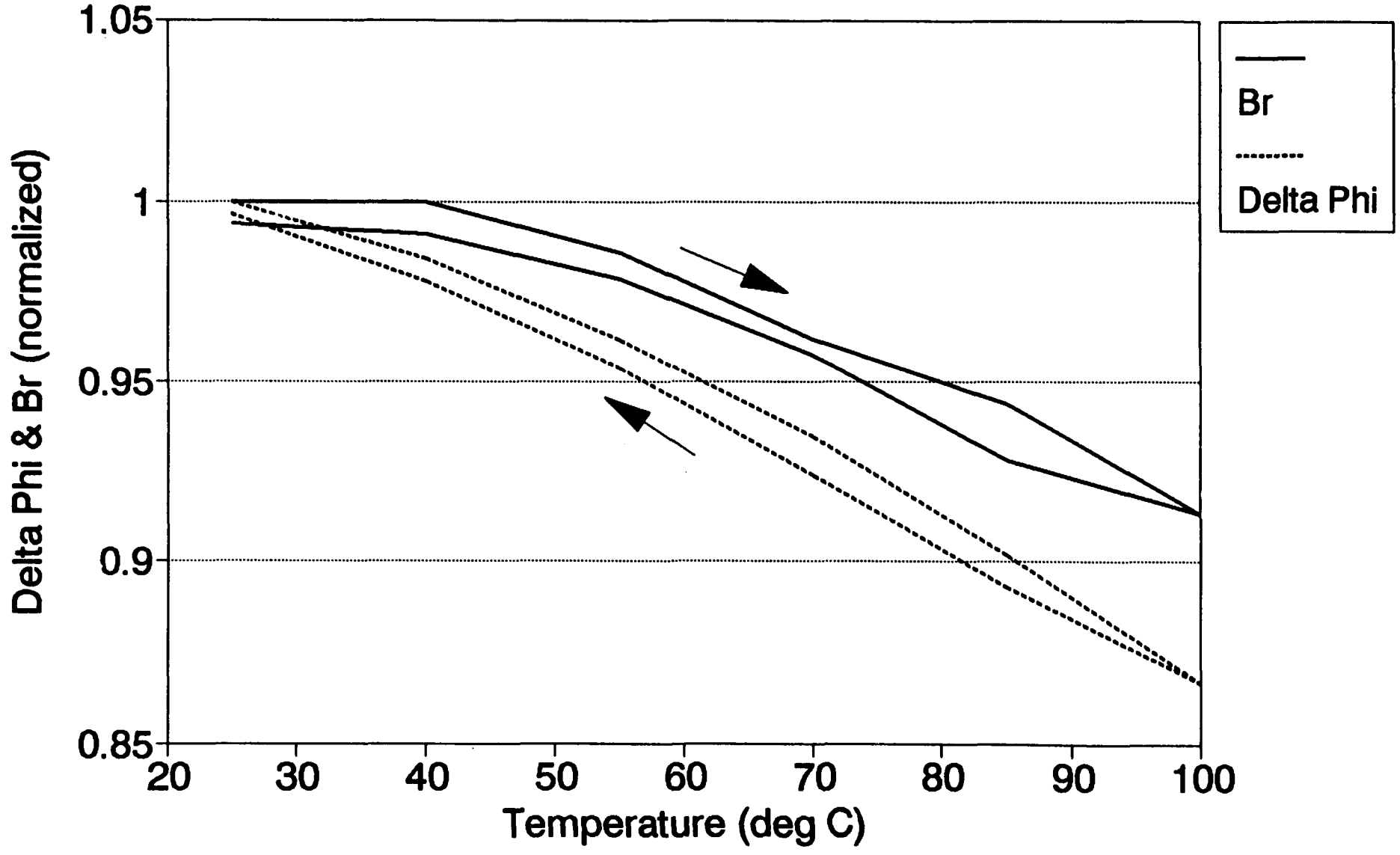
Phase & Br vs. Temperature
EMS G265-35 (.09 Mn)
Delta Phi & Br (normalized)
1.05
1
0.95
0.9
0.85
20
30
40
50
60
70
80
90
100
Temperature (deg C)
Br
Delta Phi

FIGURE 6-5

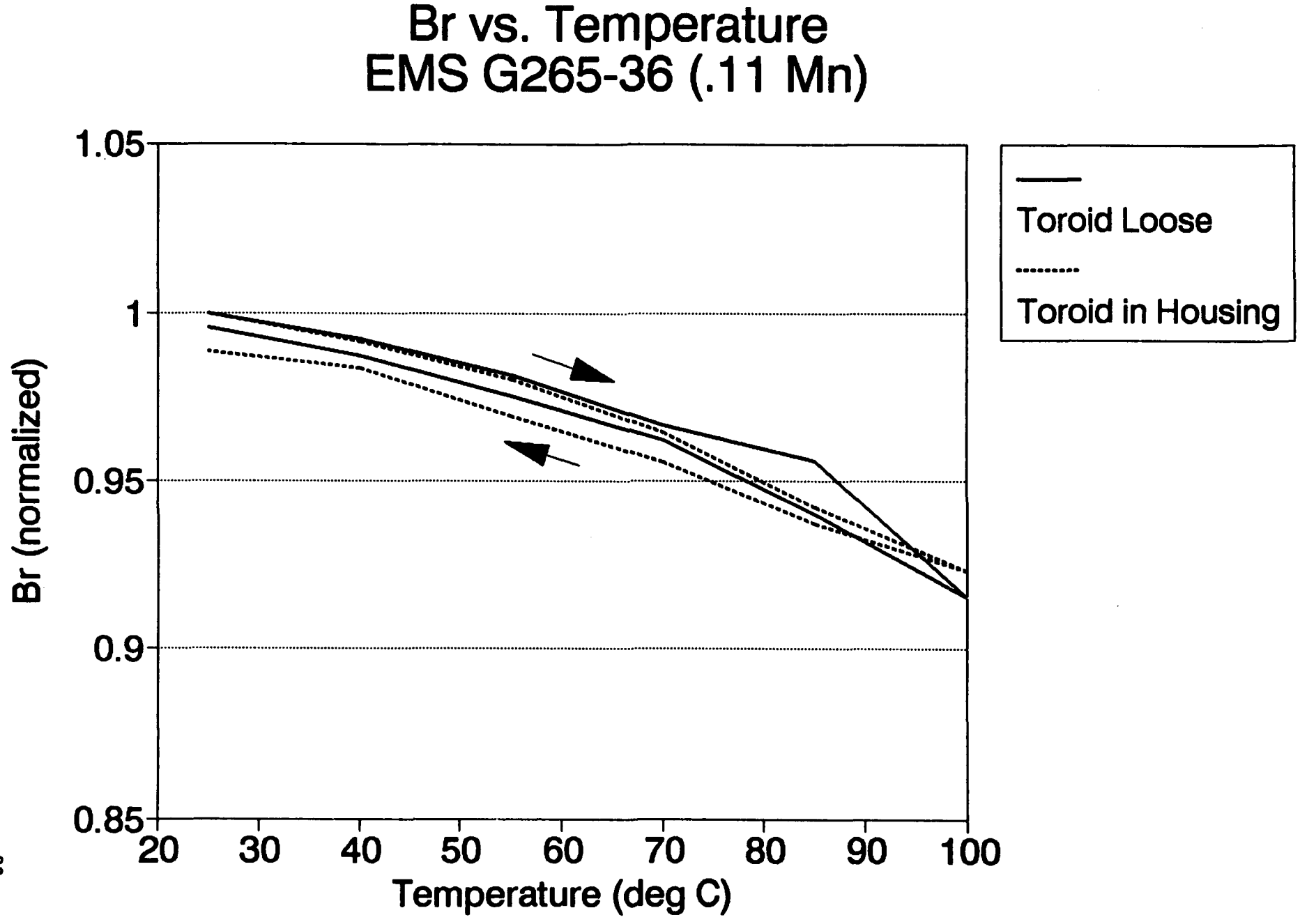
Br vs. Temperature
EMS G265-36 (.11 Mn)
1.05
1
0.95
0.9
0.85
Br (normalized)
20
30
40
50
60
70
80
90
100
Temperature (deg C)
Toroid Loose
Toroid in Housing

FIGURE 6-6

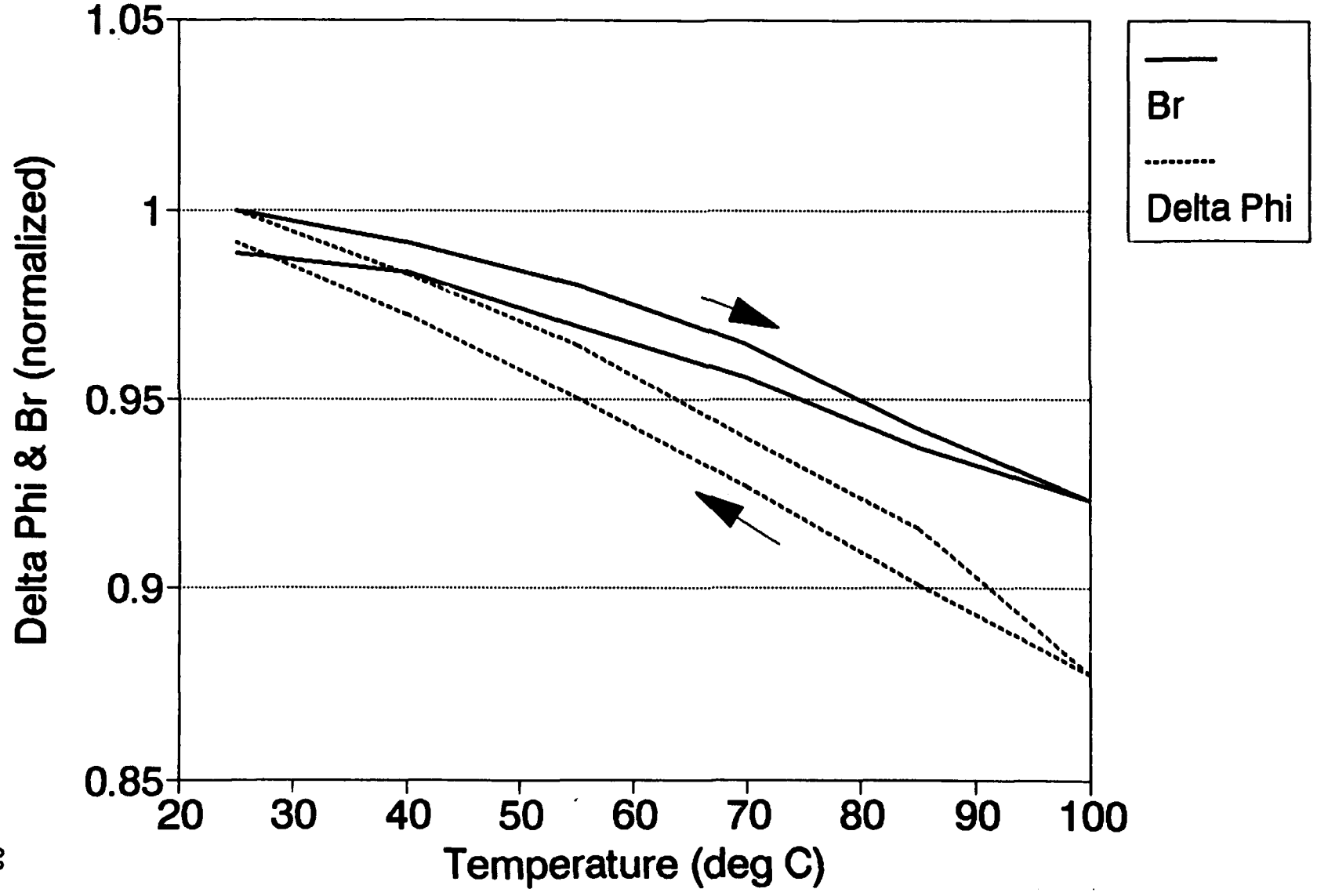
Phase & Br vs. Temperature
EMS G265-36 (.11 Mn)
Delta Phi & Br (normalized)
1.05
1
0.95
0.9
0.85
20
30
40
50
60
70
80
90
100
Temperature (deg C)
Br
Delta Phi

FIGURE 6-7

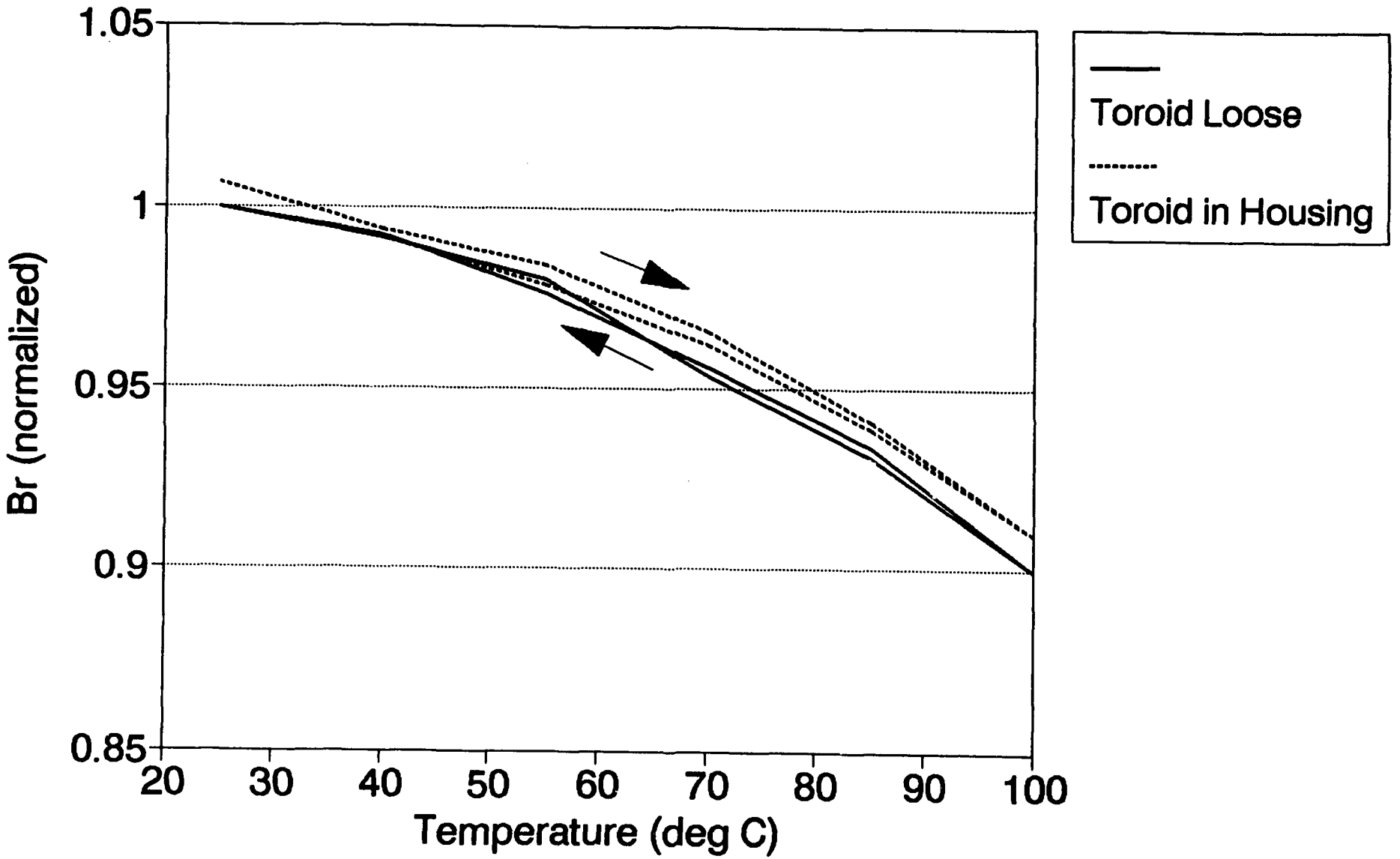
Br vs. Temperature
EMS G265-37 (.13 Mn)
1.05
1
0.95
0.9
0.85
Br (normalized)
20
30
40
50
60
70
80
90
100
Temperature (deg C)
Toroid Loose
Toroid in Housing

FIGURE 6-8

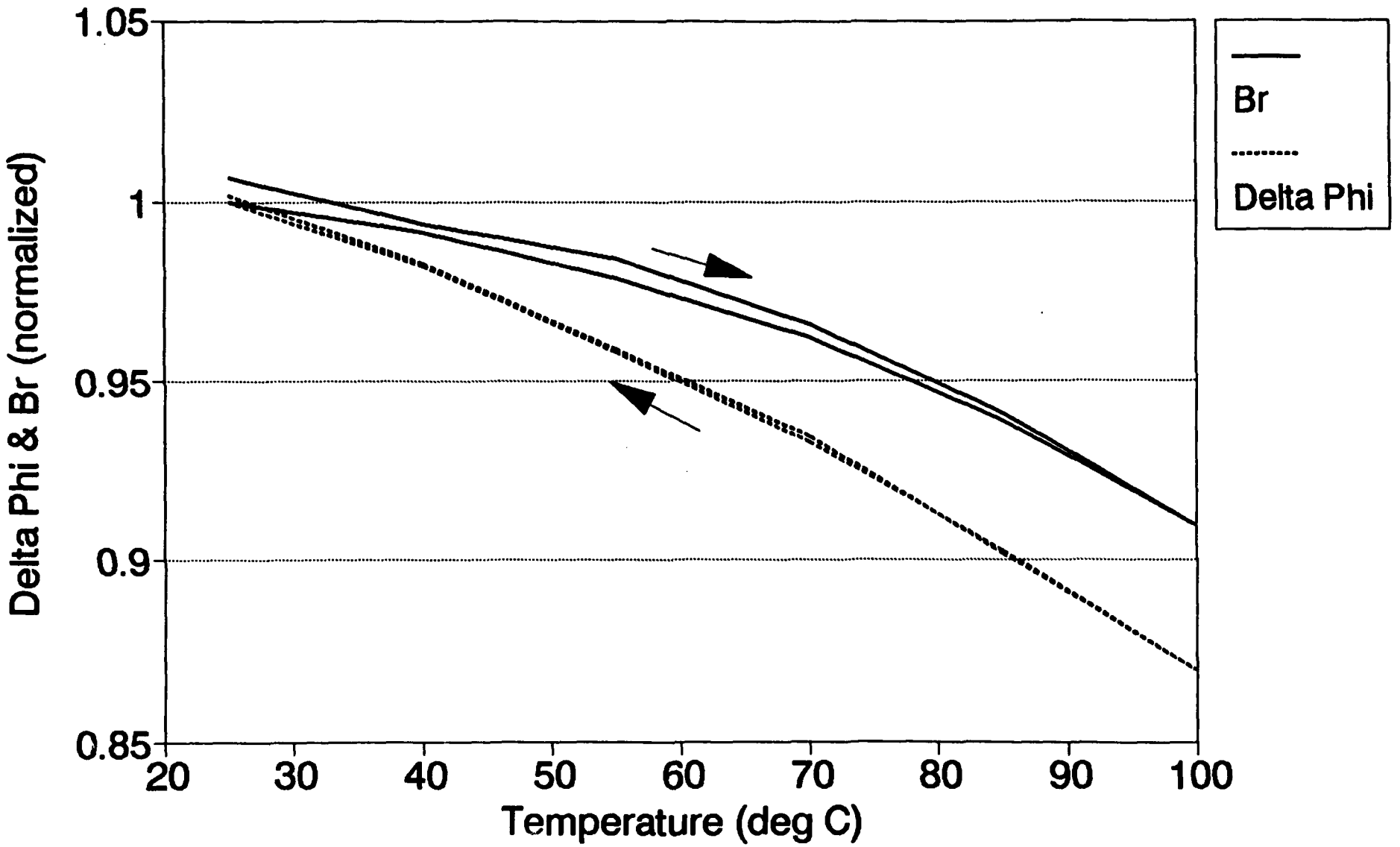
Phase & Br vs. Temperature
EMS G265-37 (.13 Mn)
Delta Phi & Br (normalized)
1.05
1
0.95
0.9
0.85
20
30
40
50
60
70
80
90
100
Temperature (deg C)
Br
Delta Phi

FIGURE 6-9

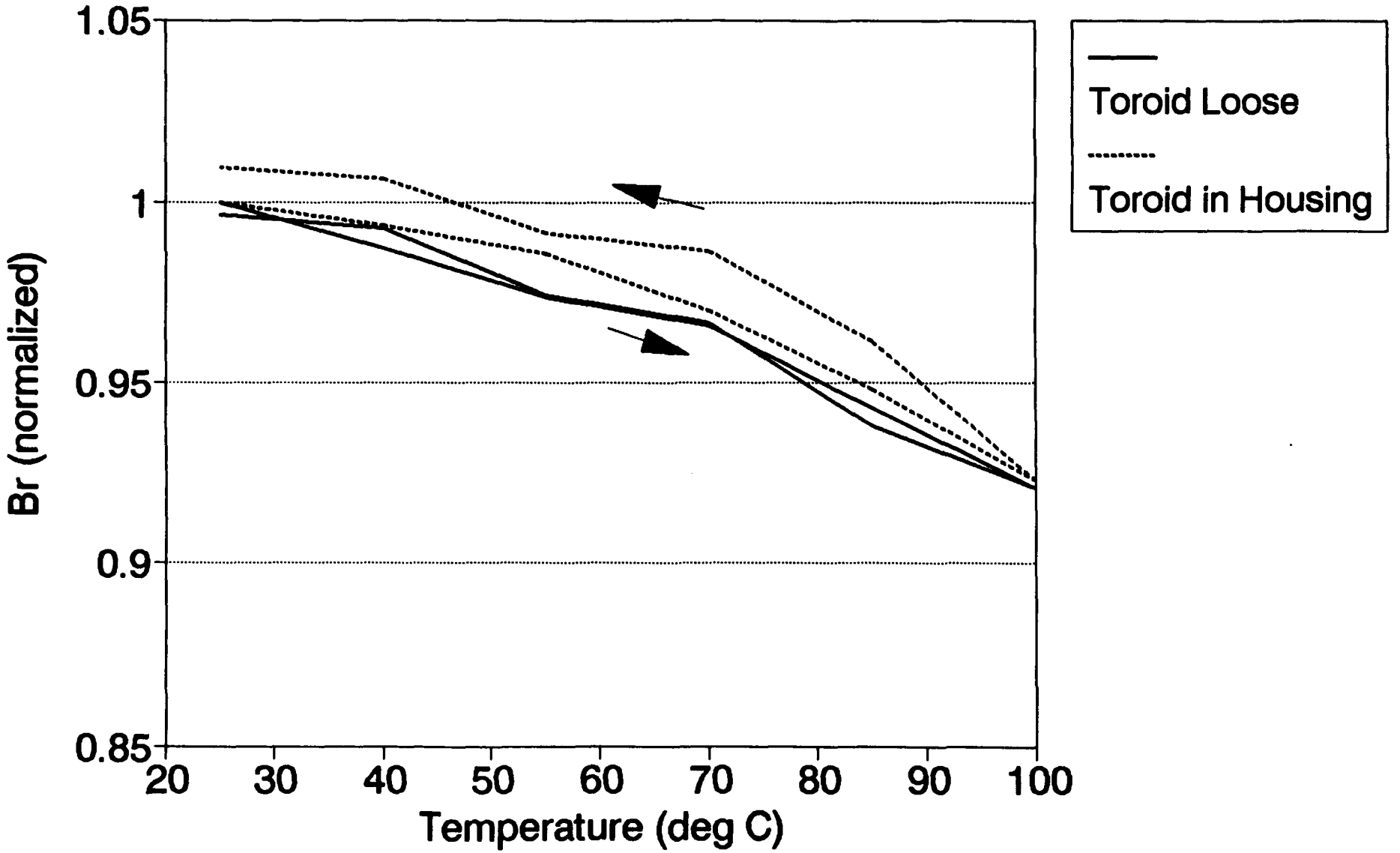
Br vs. Temperature
EMS G265-33 (.15 Mn)
1.05
1
0.95
0.9
0.85
Br (normalized)
20
30
40
50
60
70
80
90
100
Temperature (deg C)
Toroid Loose
Toroid in Housing

FIGURE 6-10

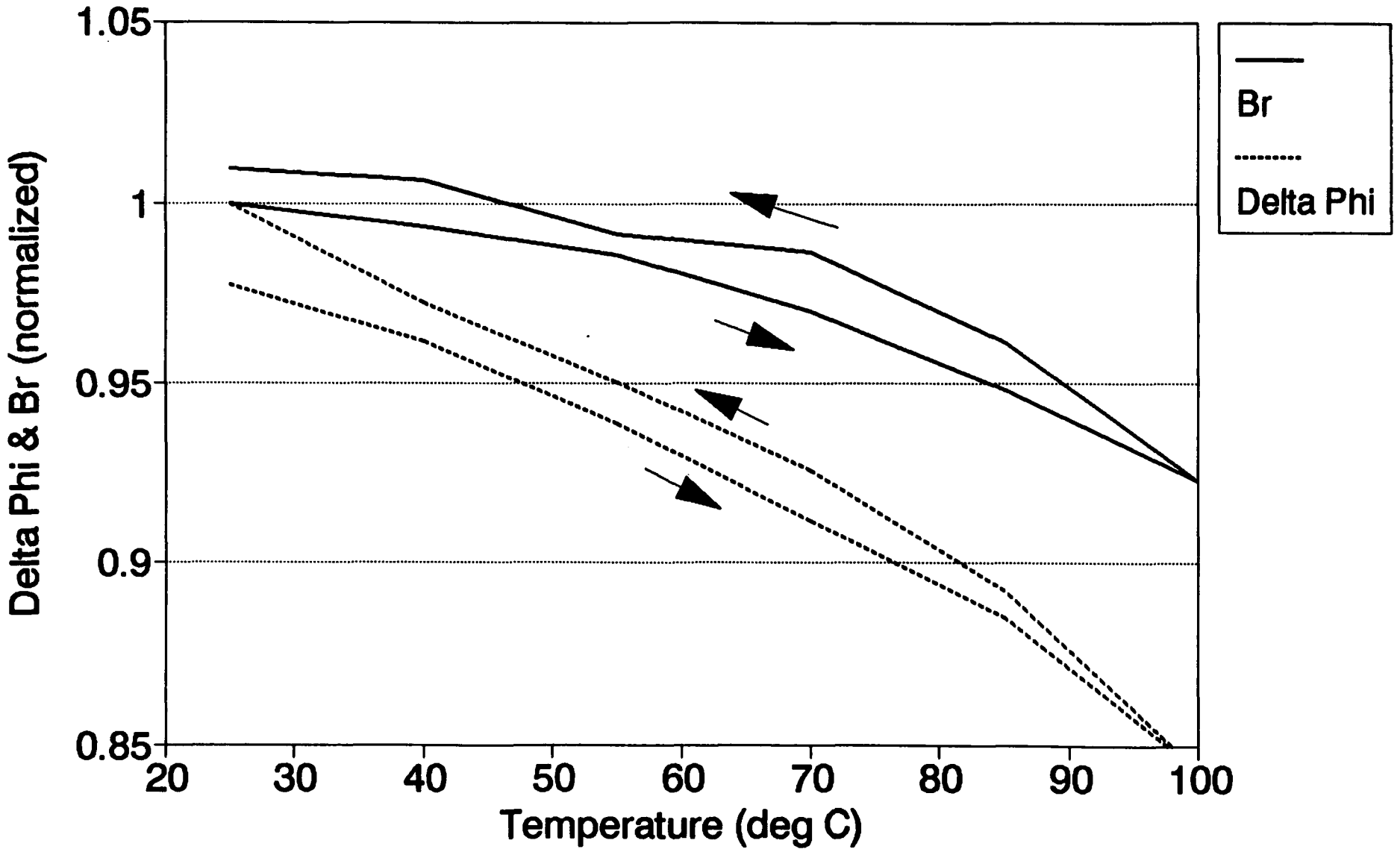
Phase & Br vs. Temperature
EMS G265-33 (.15 Mn)
Delta Phi & Br (normalized)
1.05
1
0.95
0.9
0.85
20
30
40
50
60
70
80
90
100
Temperature (deg C)
Br
Delta Phi

FIGURE 6-11

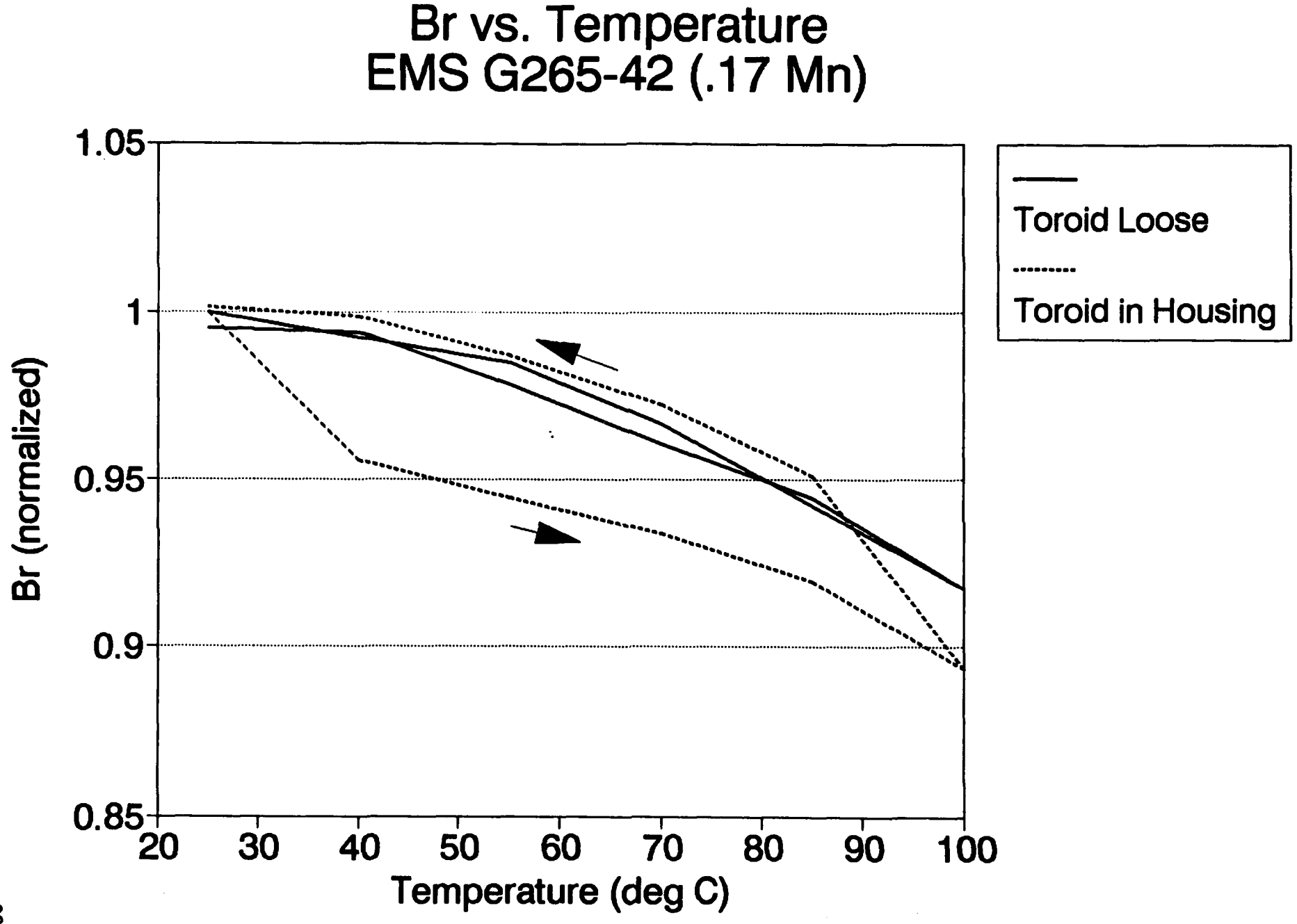
Br vs. Temperature
EMS G265-42 (.17 Mn)
1.05
1
0.95
0.9
0.85
Br (normalized)
20
30
40
50
60
70
80
90
100
Temperature (deg C)
Toroid Loose
Toroid in Housing

FIGURE 6-12

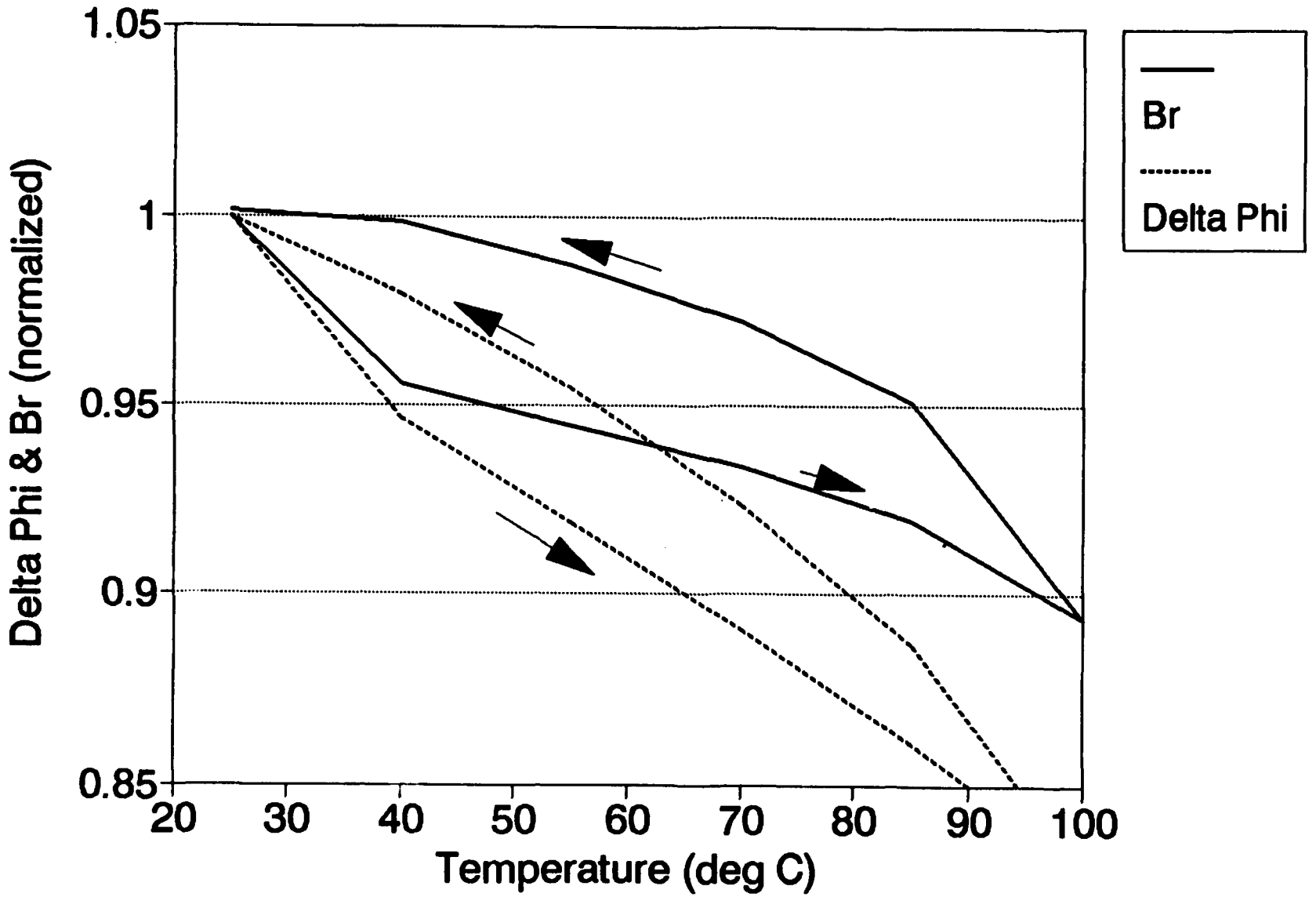
Phase & Br vs. Temperature
EMS G265-42 (.17 Mn)
Delta Phi & Br (normalized)
1.05
1
0.95
0.9
0.85
20
30
40
50
60
70
80
90
100
Temperature (deg C)
Br
Delta Phi

FIGURE 6-13

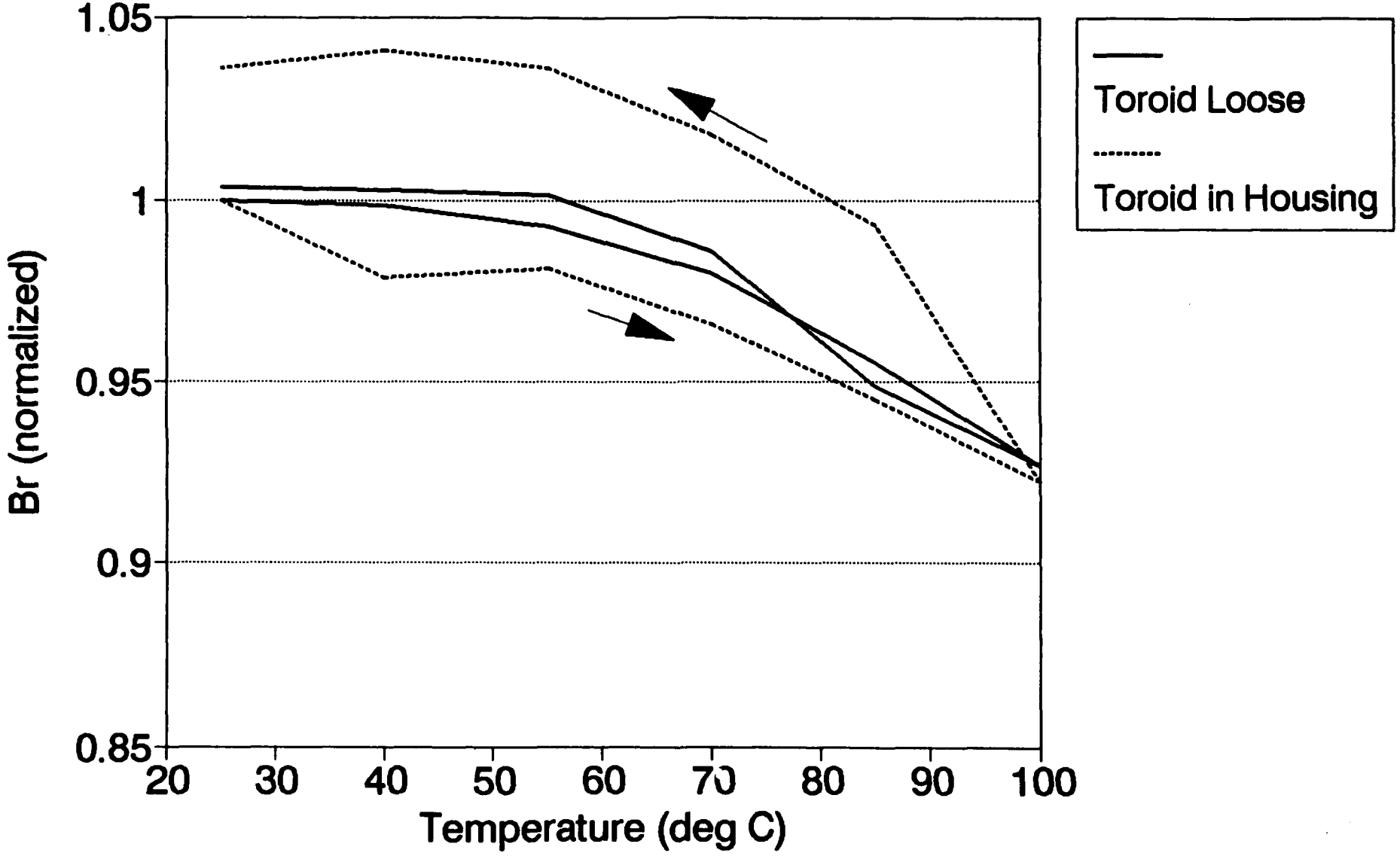
Br vs. Temperature
EMS G265-41 (.21 Mn)
1.05
1
0.95
0.9
0.85
Br (normalized)
20
30
40
50
60
70
80
90
100
Temperature (deg C)
Toroid Loose
Toroid in Housing

FIGURE 6-14

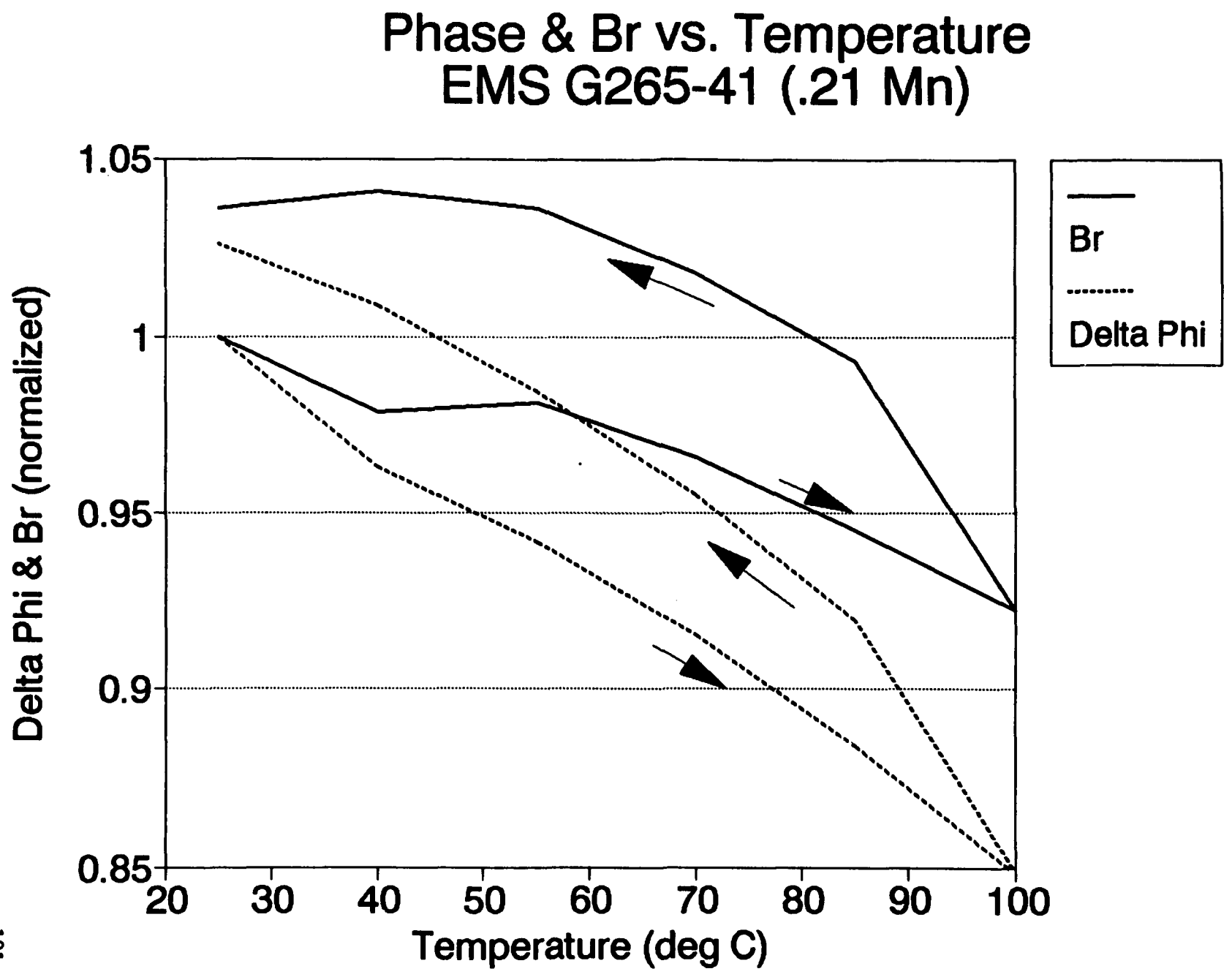
Phase & Br vs. Temperature
EMS G265-41 (.21 Mn)
Delta Phi & Br (normalized)
1.05
1
0.95
0.9
0.85
20
30
40
50
60
70
80
90
100
Temperature (deg C)
Br
Delta Phi

FIGURE 6-15

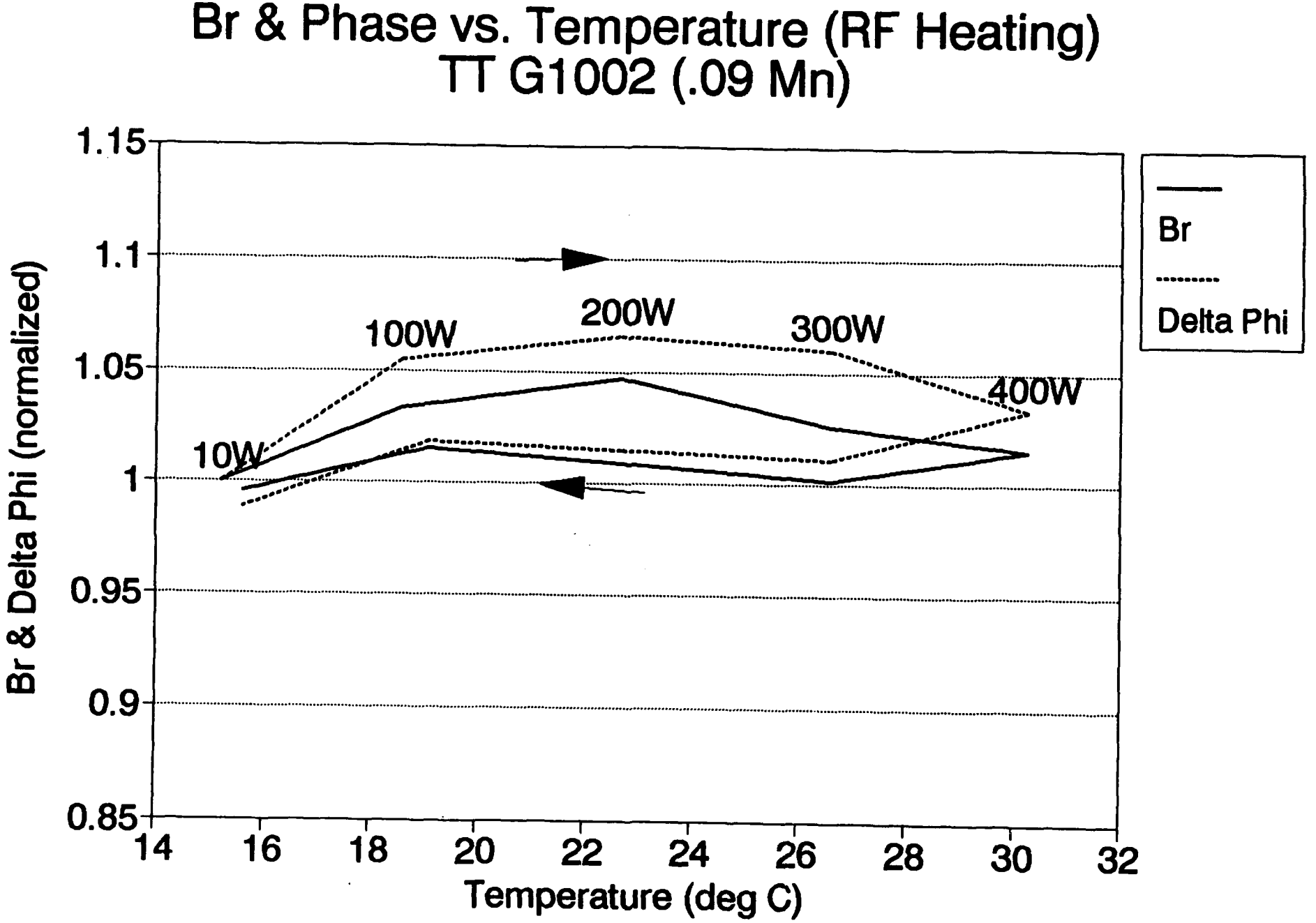
Br & Phase vs. Temperature (RF Heating)
TT G1002 (.09 Mn)
Br & Delta Phi (normalized)
1.15
1.1
1.05
1
0.95
0.9
0.85
14
16
18
20
22
24
26
28
30
32
Temperature (deg C)
Br
Delta Phi
10W
100W
200W
300W
400W

FIGURE 6-16

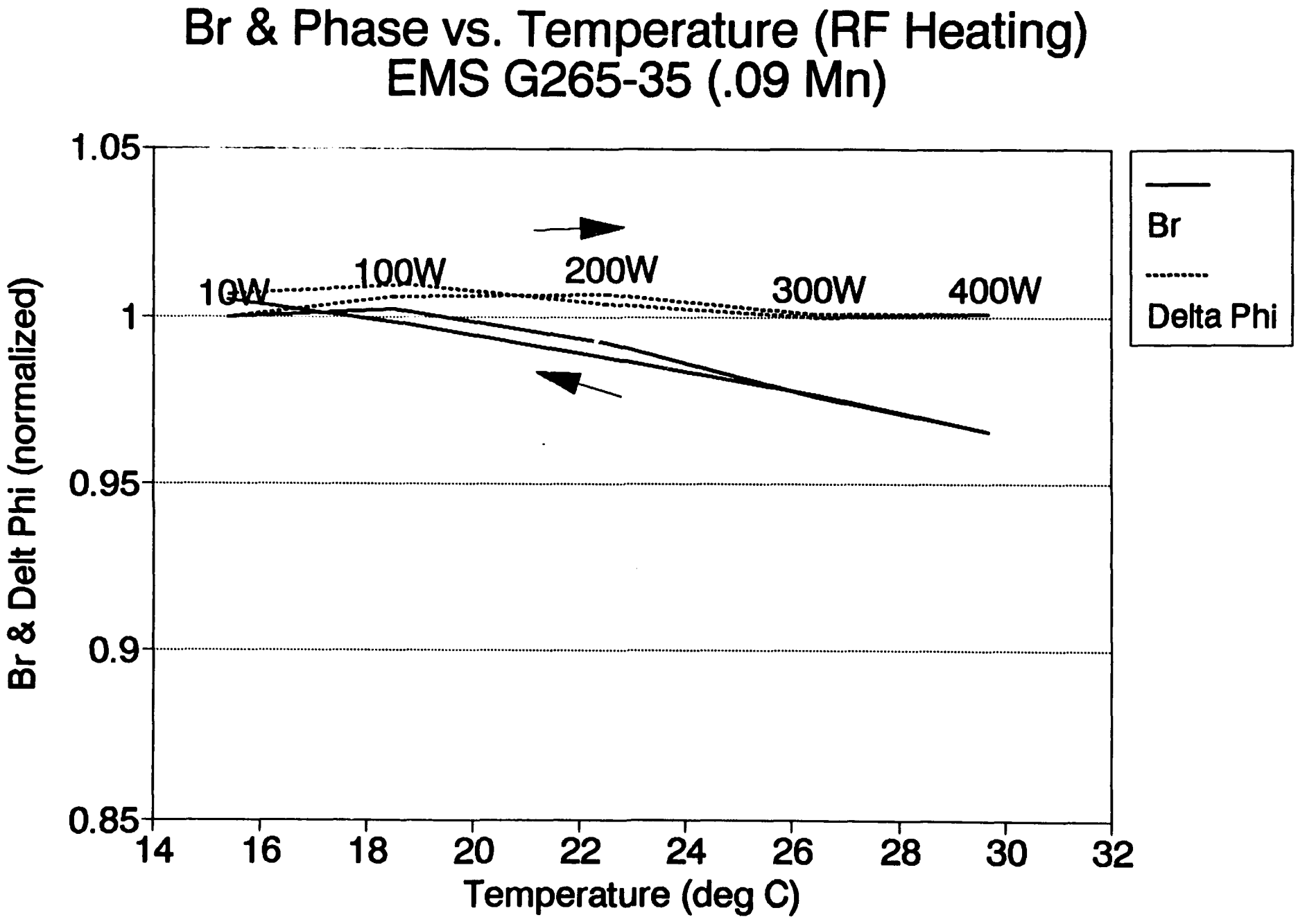
Br & Phase vs. Temperature (RF Heating)
EMS G265-35 (.09 Mn)
1.05
1
0.95
0.9
0.85
Br & Delt Phi (normalized)
10W
100W
200W
300W
400W
Br
Delta Phi
14
16
18
20
22
24
26
28
30
32
Temperature (deg C)

FIGURE 6-17

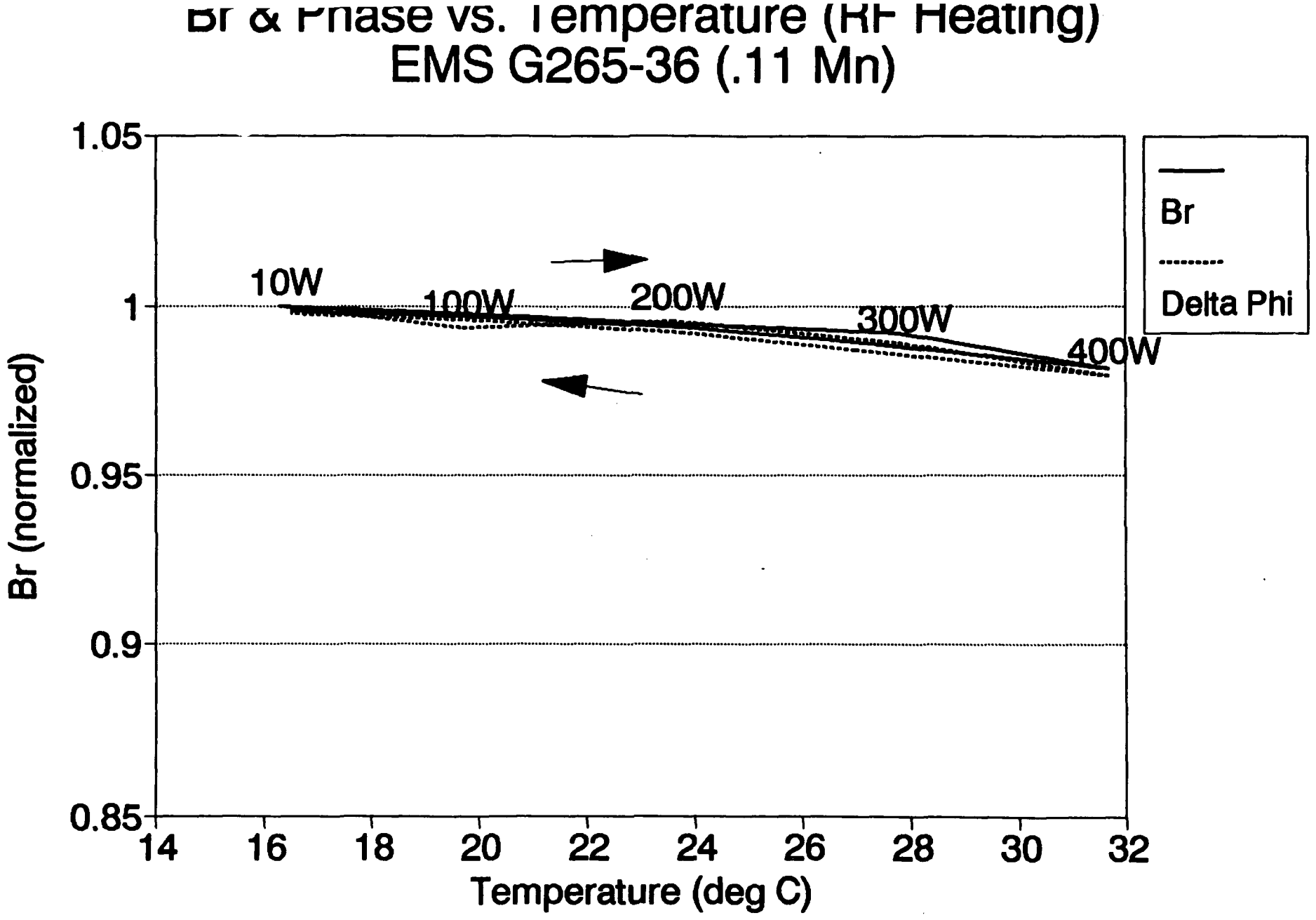
Br & Phase vs. Temperature (RF Heating)
EMS G265-36 (.11 Mn)
1.05
1
0.95
0.9
0.85
Br (normalized)
10W
100W
200W
300W
400W
Br
Delta Phi
14
16
18
20
22
24
26
28
30
32
Temperature (deg C)

FIGURE 6-18

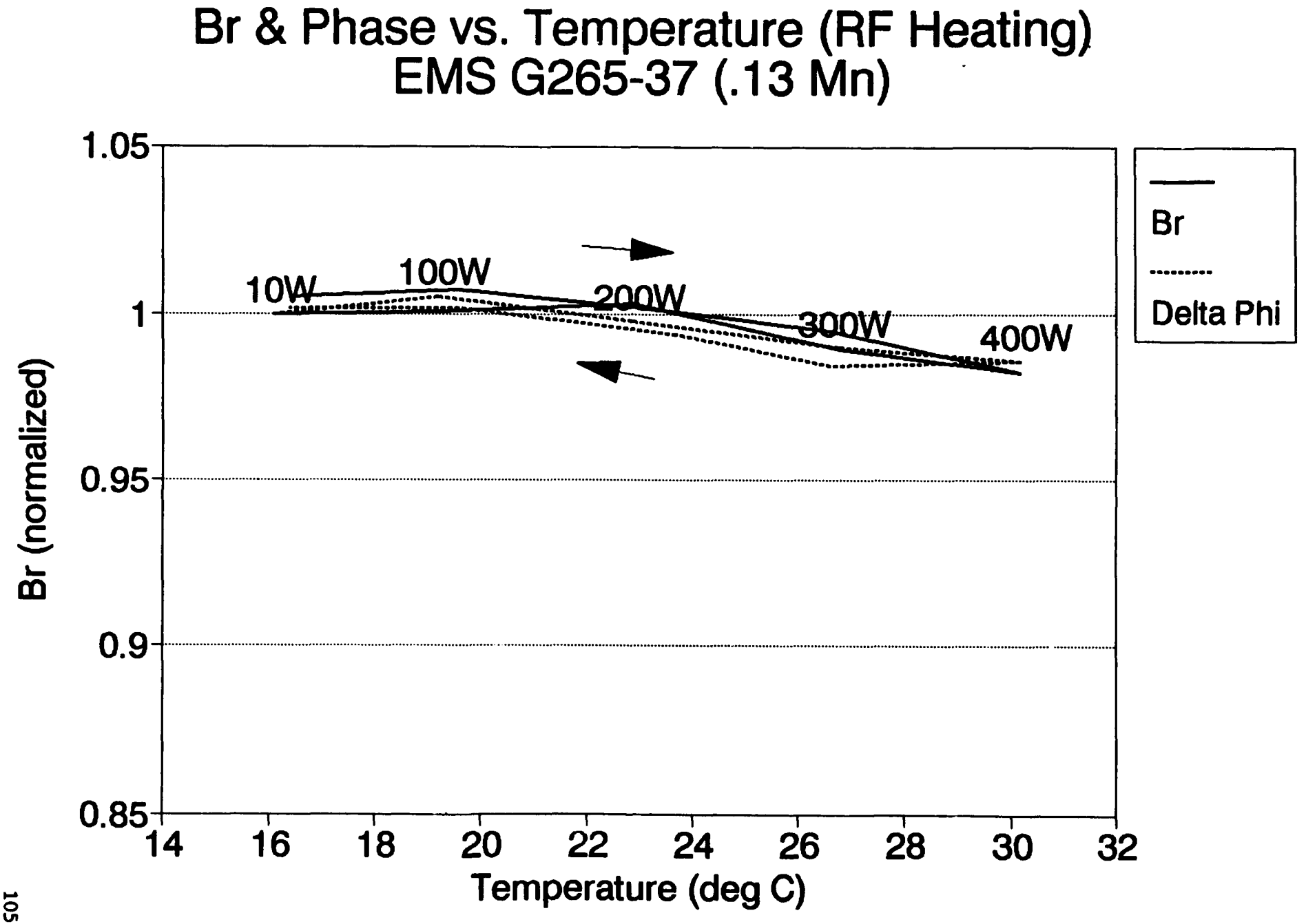
Br & Phase vs. Temperature (RF Heating)
EMS G265-37 (.13 Mn)
1.05
1
0.95
0.9
0.85
Br (normalized)
10W
100W
200W
300W
400W
Br
Delta Phi
14
16
18
20
22
24
26
28
30
32
Temperature (deg C)

FIGURE 6-19

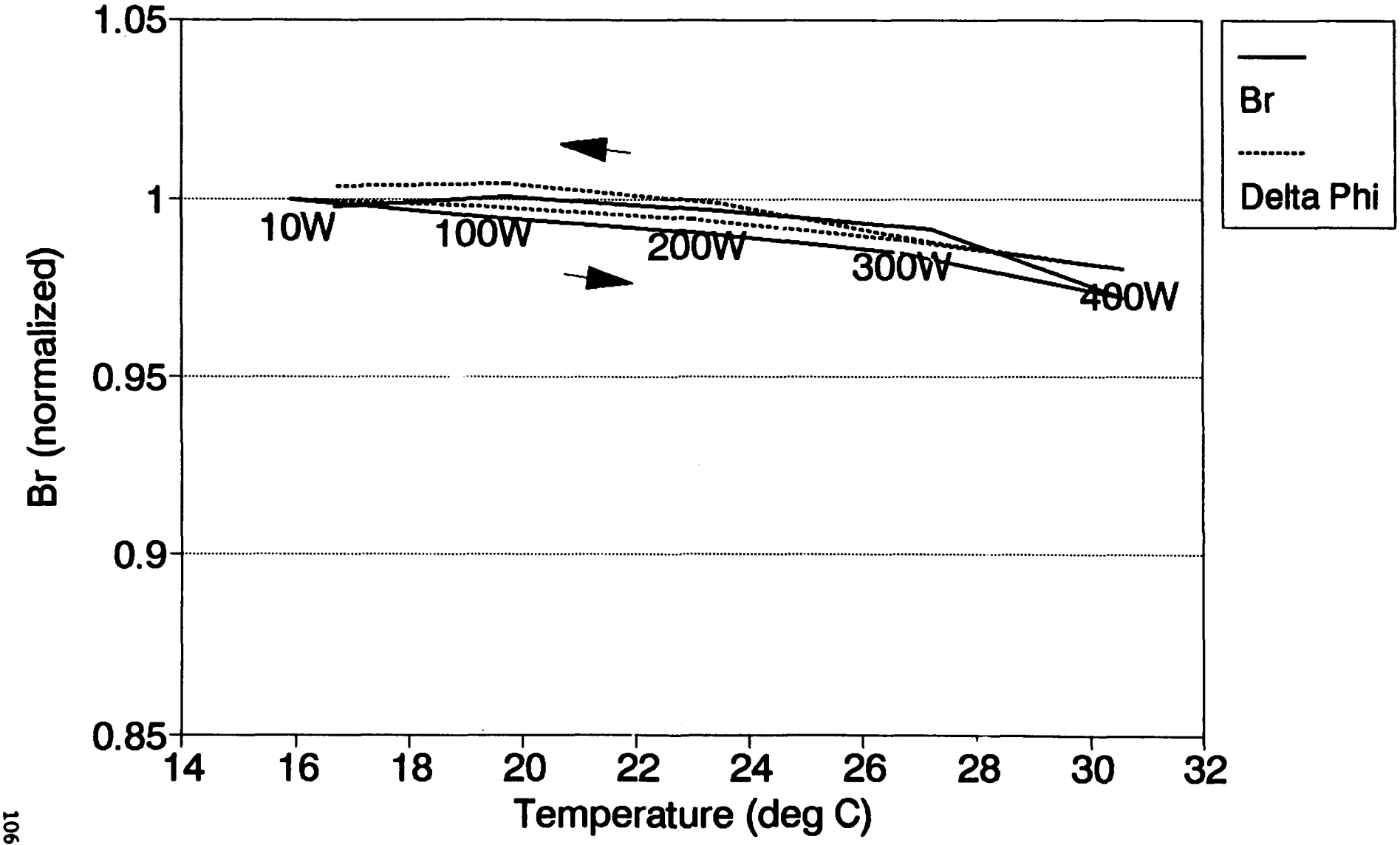
Br & Phase vs. Temperature (RF Heating)
EMS G265-33 (.15 Mn)
1.05
1
0.95
0.9
0.85
Br (normalized)
10W
100W
200W
300W
400W
Br
Delta Phi
14
16
18
20
22
24
26
28
30
32
Temperature (deg C)

FIGURE 6-20

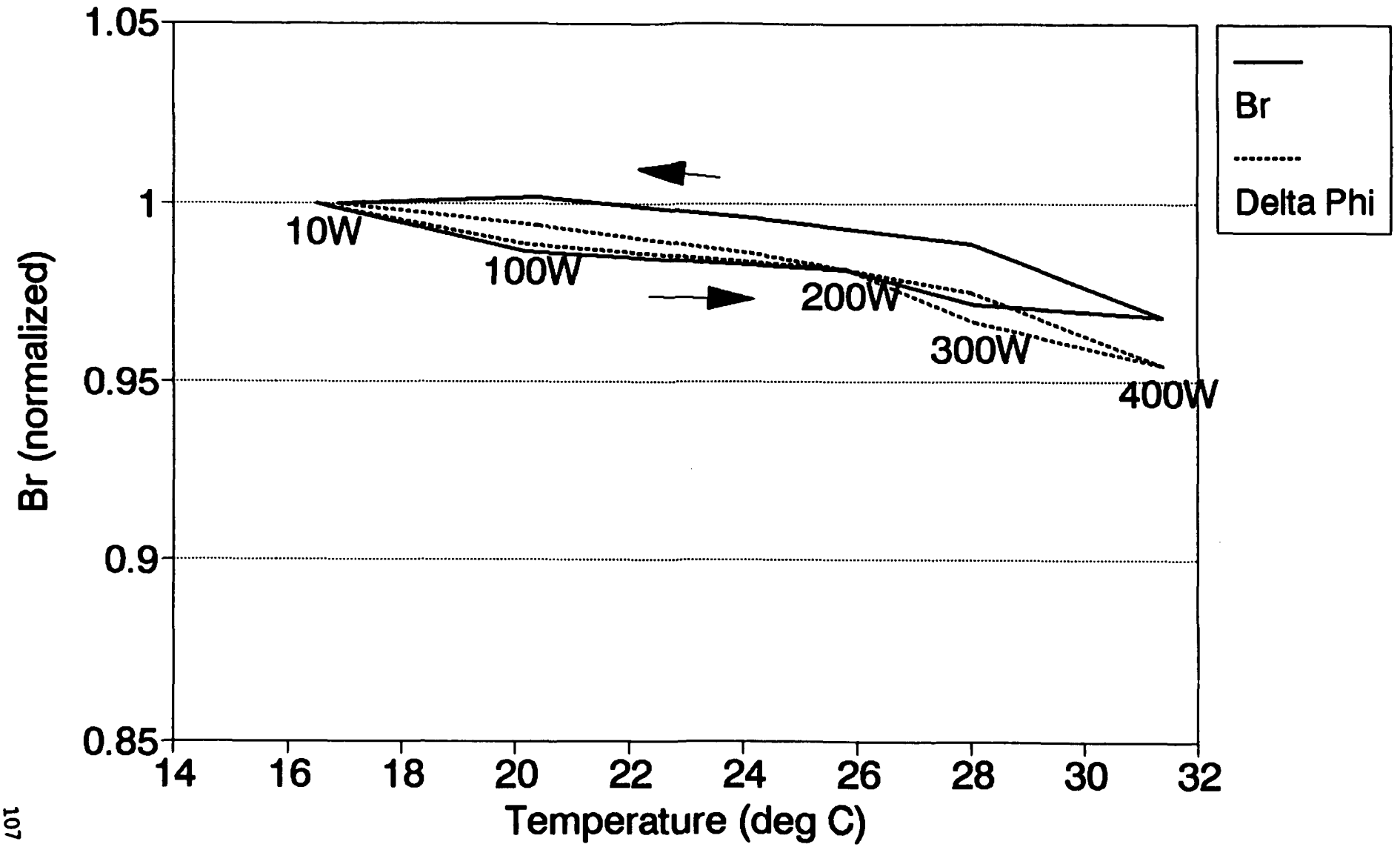
Br & Phase vs. Temperature (RF Heating)
EMS G265-42 (.17 Mn)
1.05
1
0.95
0.9
0.85
Br (normalized)
10W
100W
200W
300W
400W
Br
Delta Phi
14
16
18
20
22
24
26
28
30
32
Temperature (deg C)

FIGURE 6-21

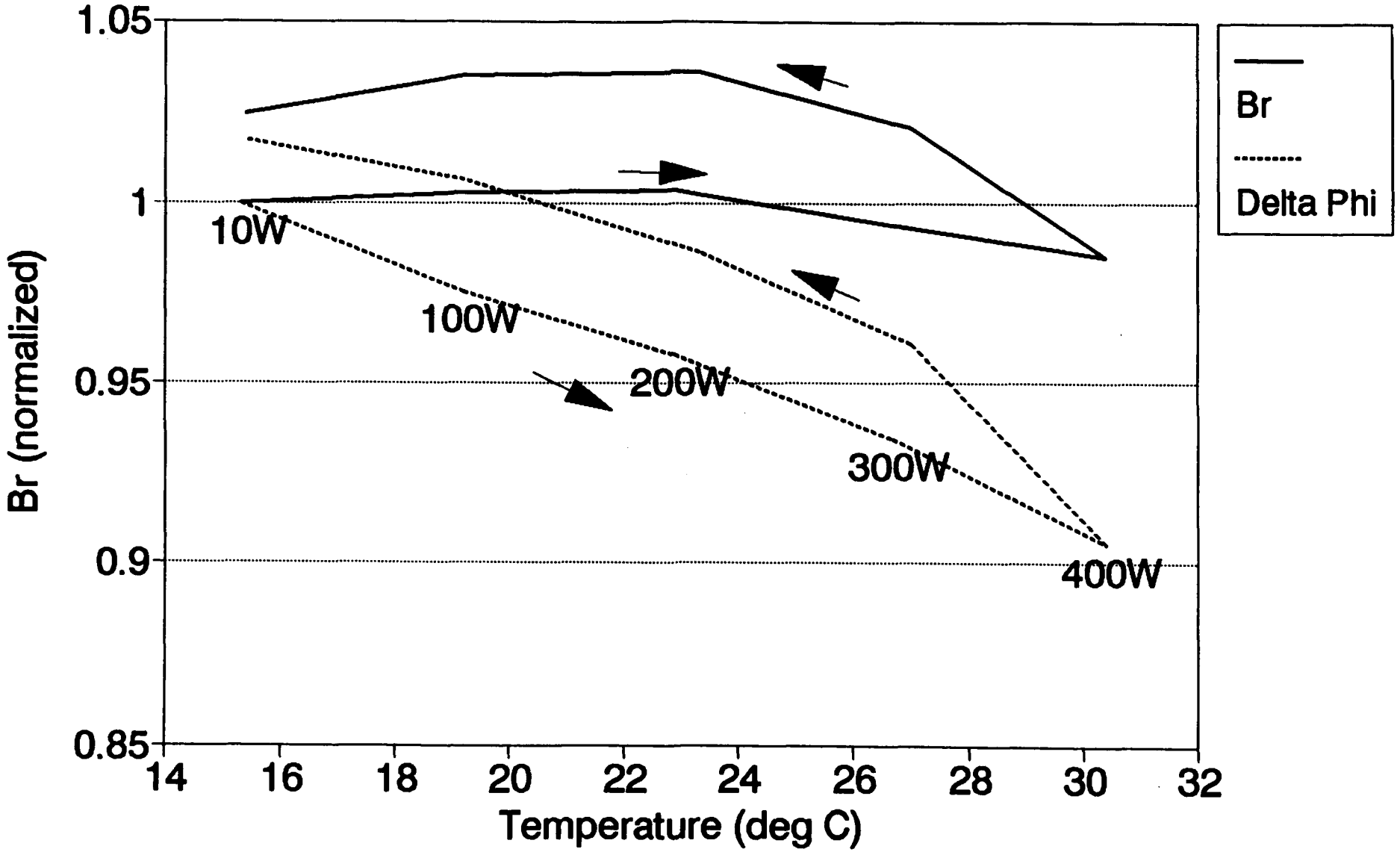
Br & Phase vs. Temperature (RF Heating)
EMS G265-41 (.21 Mn)
1.05
1
0.95
0.9
0.85
Br (normalized)
10W
100W
200W
300W
400W
Br
Delta Phi
14
16
18
20
22
24
26
28
30
32
Temperature (deg C)

FIGURE 6-22

NRL MATERIAL STUDY

HIPOWER TEST RESULTS

10 Apr 1992
11:06:10

37D/.13MN

TESTED AT 9.99 WATTS

MEASURED INSERTION LOSS= .55 dB
TEMP MEASURED ON DUT= 16.0789390692
TOTAL DELTA PHASE = 98.6952
128 STATES MEASURED

STATE	0	.0236	DEGREES
STATE	128	2.4353	DEGREES
STATE	256	5.8275	DEGREES
STATE	384	8.5032	DEGREES
STATE	512	9.86	DEGREES
STATE	640	13.3332	DEGREES
STATE	768	16.3039	DEGREES
STATE	896	20.848	DEGREES
STATE	1024	22.6985	DEGREES
STATE	1152	25.235	DEGREES
STATE	1280	27.1166	DEGREES
STATE	1408	29.3719	DEGREES
STATE	1536	31.7695	DEGREES
STATE	1664	32.272	DEGREES
STATE	1792	34.2508	DEGREES
STATE	1920	39.4567	DEGREES
STATE	2048	44.9412	DEGREES
STATE	2176	48.2636	DEGREES
STATE	2304	51.1002	DEGREES
STATE	2432	54.1755	DEGREES
STATE	2560	54.7646	DEGREES
STATE	2688	58.153	DEGREES
STATE	2816	62.1893	DEGREES
STATE	2944	66.1625	DEGREES
STATE	3072	69.327	DEGREES
STATE	3200	73.3723	DEGREES
STATE	3328	76.7207	DEGREES
STATE	3456	79.177	DEGREES
STATE	3584	85.7702	DEGREES
STATE	3712	90.2775	DEGREES
STATE	3840	93.3238	DEGREES
STATE	3968	99.1585	DEGREES

FIGURE 6-23 (a)

6265 37D/.13 Mn

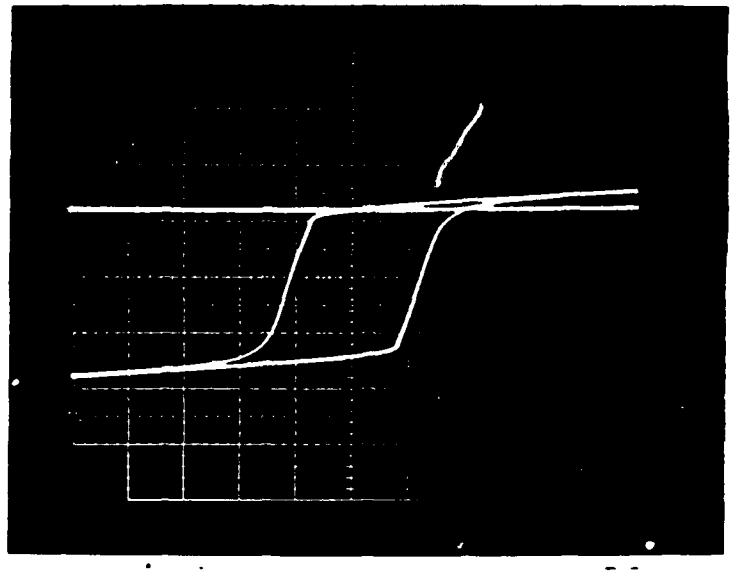

1110 10 APR 92 1332.67

BrAvg = 1332.67

NRL MATERIAL STUDY

HIPOWER TEST RESULTS

10 Apr 1992
11:27:05

37D/.13MN

TESTED AT 97.3 WATTS

MEASURED INSERTION LOSS= .53 dB
TEMP MEASURED ON OUT= 19.1539986035
TOTAL DELTA PHASE = 99.2122
128 STATES MEASURED

STATE	0	.1864	DEGREES
STATE	128	.2137	DEGREES
STATE	256	5.4131	DEGREES
STATE	384	8.4267	DEGREES
STATE	512	9.6348	DEGREES
STATE	640	12.9396	DEGREES
STATE	768	16.115	DEGREES
STATE	896	20.5391	DEGREES
STATE	1024	22.3576	DEGREES
STATE	1152	24.6363	DEGREES
STATE	1280	26.5158	DEGREES
STATE	1408	28.7138	DEGREES
STATE	1536	31.1541	DEGREES
STATE	1664	34.2209	DEGREES
STATE	1792	37.3569	DEGREES
STATE	1920	41.0827	DEGREES
STATE	2048	44.3229	DEGREES
STATE	2176	47.5889	DEGREES
STATE	2304	50.435	DEGREES
STATE	2432	53.6011	DEGREES
STATE	2560	54.2	DEGREES
STATE	2688	57.6614	DEGREES
STATE	2816	61.6592	DEGREES
STATE	2944	65.2377	DEGREES
STATE	3072	68.0237	DEGREES
STATE	3200	73.2216	DEGREES
STATE	3328	76.2593	DEGREES
STATE	3456	81.3484	DEGREES
STATE	3584	86.1661	DEGREES
STATE	3712	90.8777	DEGREES
STATE	3840	94.3796	DEGREES
STATE	3968	100.1216	DEGREES

FIGURE 6-23 (b)

6265 37D/.13-Mn 100W

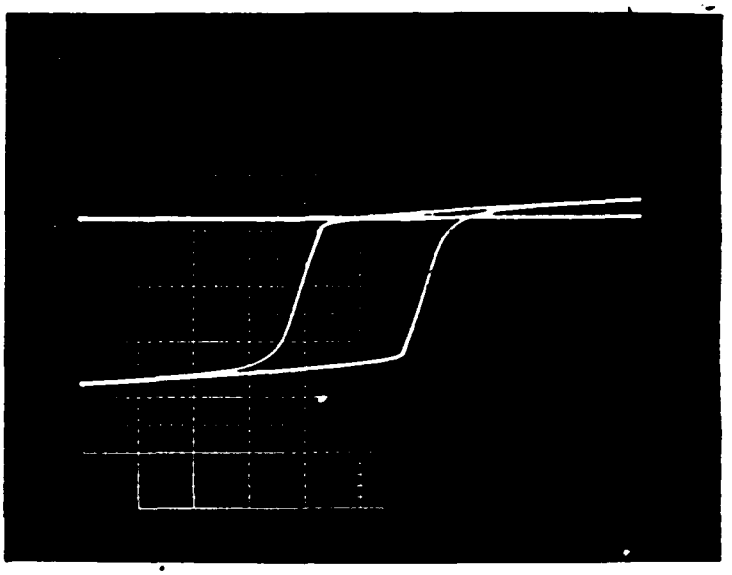

428 10 APR 92 1333.67

BrAvg = 1333.67

NRL MATERIAL STUDY

HIPOWER TEST RESULTS

10 Apr 1992
11:48:53

37D/.13MN

TESTED AT 199.4 WATTS

MEASURED INSERTION LOSS= .52 dB
TEMP MEASURED ON DUT= 22.8728227587
TOTAL DELTA PHASE = 98.5227
128 STATES MEASURED

STATE	0	.1932	DEGREES
STATE	128	.5547	DEGREES
STATE	256	5.4895	DEGREES
STATE	384	7.9082	DEGREES
STATE	512	9.0003	DEGREES
STATE	640	11.5098	DEGREES
STATE	768	14.7419	DEGREES
STATE	896	19.0392	DEGREES
STATE	1024	20.7443	DEGREES
STATE	1152	23.0107	DEGREES
STATE	1280	24.3223	DEGREES
STATE	1408	26.2757	DEGREES
STATE	1536	28.5746	DEGREES
STATE	1664	31.3581	DEGREES
STATE	1792	35.3842	DEGREES
STATE	1920	38.5961	DEGREES
STATE	2048	41.8918	DEGREES
STATE	2176	45.239	DEGREES
STATE	2304	48.1034	DEGREES
STATE	2432	51.2023	DEGREES
STATE	2560	51.7893	DEGREES
STATE	2688	55.3132	DEGREES
STATE	2816	59.3356	DEGREES
STATE	2944	63.5372	DEGREES
STATE	3072	67.4732	DEGREES
STATE	3200	71.161	DEGREES
STATE	3328	75.1647	DEGREES
STATE	3456	79.6644	DEGREES
STATE	3584	84.7049	DEGREES
STATE	3712	89.6172	DEGREES
STATE	3840	94.4	DEGREES
STATE	3968	97.8403	DEGREES

FIGURE 6-23 (c)

G265 37D/.13 Mn 200W

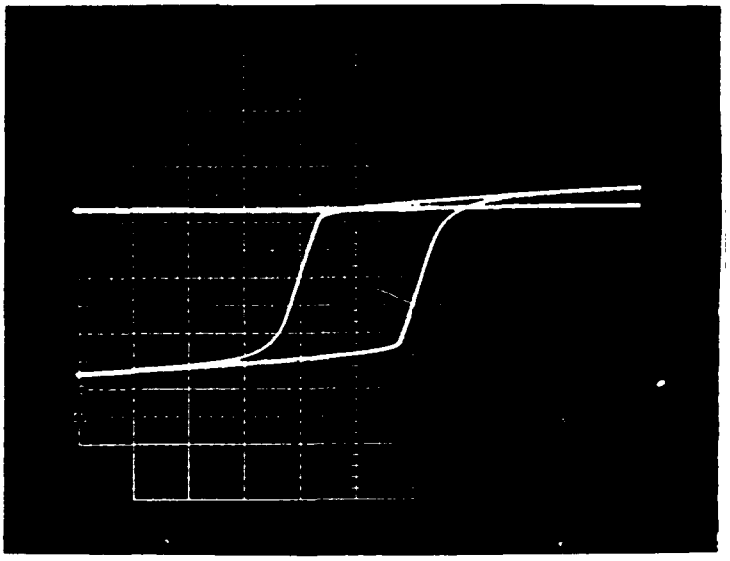

1151 10 APR 92 1337.33

Br Avg = 1337.33

NRL MATERIAL STUDY

HIPOWER TEST RESULTS

10 Apr 1992
12:05:32

37D/.13MN

TESTED AT 305.8 WATTS

MEASURED INSERTION LOSS= .52 dB
TEMP MEASURED ON DUT= 26.8241621678
TOTAL DELTA PHASE = 97.7171
128 STATES MEASURED

STATE	0	.3819	DEGREES
STATE	128	.9434	DEGREES
STATE	256	5.4841	DEGREES
STATE	384	7.5478	DEGREES
STATE	512	8.5721	DEGREES
STATE	640	10.3613	DEGREES
STATE	768	13.6365	DEGREES
STATE	896	17.7026	DEGREES
STATE	1024	19.2025	DEGREES
STATE	1152	21.2297	DEGREES
STATE	1280	22.9668	DEGREES
STATE	1408	24.9353	DEGREES
STATE	1536	27.2202	DEGREES
STATE	1664	30.1011	DEGREES
STATE	1792	33.1412	DEGREES
STATE	1920	36.3358	DEGREES
STATE	2048	39.8442	DEGREES
STATE	2176	42.7996	DEGREES
STATE	2304	45.7926	DEGREES
STATE	2432	48.9511	DEGREES
STATE	2560	49.5777	DEGREES
STATE	2688	53.1978	DEGREES
STATE	2816	57.2696	DEGREES
STATE	2944	61.5869	DEGREES
STATE	3072	65.7565	DEGREES
STATE	3200	69.8423	DEGREES
STATE	3328	73.8238	DEGREES
STATE	3456	78.1226	DEGREES
STATE	3584	81.272	DEGREES
STATE	3712	88.8982	DEGREES
STATE	3840	93.8076	DEGREES
STATE	3968	98.0067	DEGREES

FIGURE 6-23 (d)

6265 37D/.13 Mn 300W

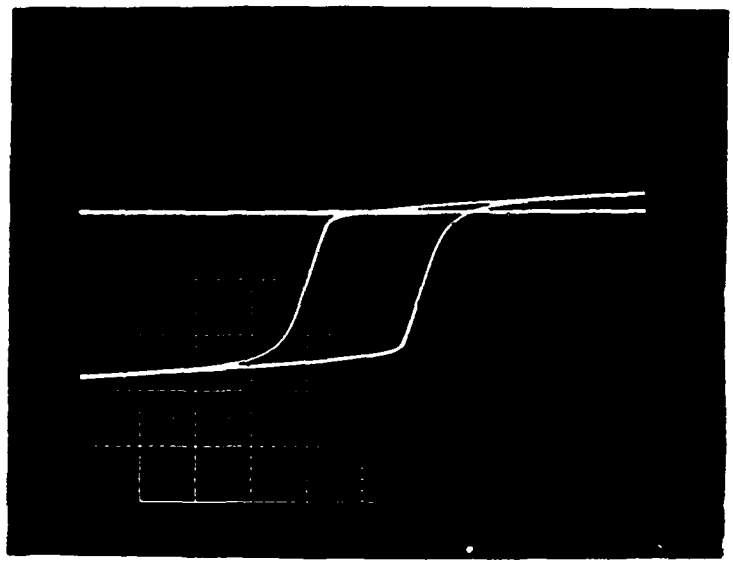

1207 10 APR 92 1319.0

Br Avg = 1319.0

NRL MATERIAL STUDY

HIPOWER TEST RESULTS

10 Apr 1992
12:24:12

37D/.13MN

TESTED AT 395.3 WATTS

MEASURED INSERTION LOSS= .51 dB
TEMP MEASURED ON DUT= 30.15762554
TOTAL DELTA PHASE = 97.2764
128 STATES MEASURED

STATE	0	.0622	DEGREES
STATE	128	3.5505	DEGREES
STATE	256	4.7353	DEGREES
STATE	384	6.6435	DEGREES
STATE	512	7.5482	DEGREES
STATE	640	9.081	DEGREES
STATE	768	12.2577	DEGREES
STATE	896	15.8431	DEGREES
STATE	1024	17.3742	DEGREES
STATE	1152	19.2932	DEGREES
STATE	1280	21.0341	DEGREES
STATE	1408	22.9259	DEGREES
STATE	1536	25.128	DEGREES
STATE	1664	27.945	DEGREES
STATE	1792	30.9498	DEGREES
STATE	1920	34.4058	DEGREES
STATE	2048	37.5667	DEGREES
STATE	2176	40.809	DEGREES
STATE	2304	43.5957	DEGREES
STATE	2432	46.5839	DEGREES
STATE	2560	50.4703	DEGREES
STATE	2688	54.6296	DEGREES
STATE	2816	58.8495	DEGREES
STATE	2944	63.0027	DEGREES
STATE	3072	66.9984	DEGREES
STATE	3200	68.0615	DEGREES
STATE	3328	72.3803	DEGREES
STATE	3456	77.2612	DEGREES
STATE	3584	82.6892	DEGREES
STATE	3712	87.882	DEGREES
STATE	3840	91.6164	DEGREES
STATE	3968	97.9365	DEGREES

FIGURE 6-23 (e)

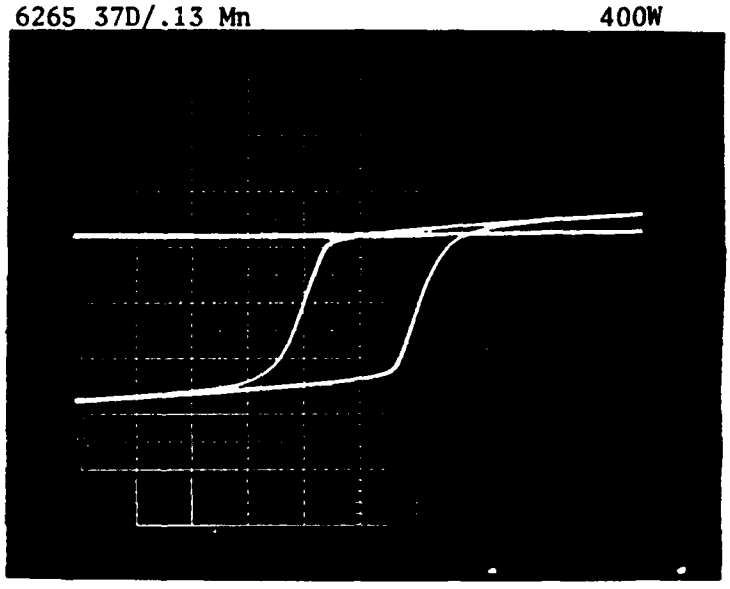

Br Avg = 1309.67

NRL MATERIAL STUDY

HIPOWER TEST RESULTS

10 Apr 1992
12:44:25

37D/.13MN

TESTED AT 293.5 WATTS

MEASURED INSERTION LOSS= .52 dB
TEMP MEASURED ON DUT= 26.6072032902
TOTAL DELTA PHASE = 97.2372
128 STATES MEASURED

STATE	0	.0176	DEGREES
STATE	128	.1766	DEGREES
STATE	256	4.9514	DEGREES
STATE	384	7.1226	DEGREES
STATE	512	8.1732	DEGREES
STATE	640	9.8289	DEGREES
STATE	768	13.1085	DEGREES
STATE	896	16.9183	DEGREES
STATE	1024	18.4485	DEGREES
STATE	1152	20.4382	DEGREES
STATE	1280	22.0242	DEGREES
STATE	1408	24.0362	DEGREES
STATE	1536	26.303	DEGREES
STATE	1664	28.7271	DEGREES
STATE	1792	32.2045	DEGREES
STATE	1920	35.5636	DEGREES
STATE	2048	38.7248	DEGREES
STATE	2176	41.8256	DEGREES
STATE	2304	44.6819	DEGREES
STATE	2432	47.8477	DEGREES
STATE	2560	48.4499	DEGREES
STATE	2688	51.9843	DEGREES
STATE	2816	56.208	DEGREES
STATE	2944	60.5585	DEGREES
STATE	3072	63.2056	DEGREES
STATE	3200	68.5922	DEGREES
STATE	3328	72.0693	DEGREES
STATE	3456	74.7204	DEGREES
STATE	3584	82.7522	DEGREES
STATE	3712	87.9708	DEGREES
STATE	3840	92.9312	DEGREES
STATE	3968	97.3436	DEGREES

FIGURE 6-23 (f)

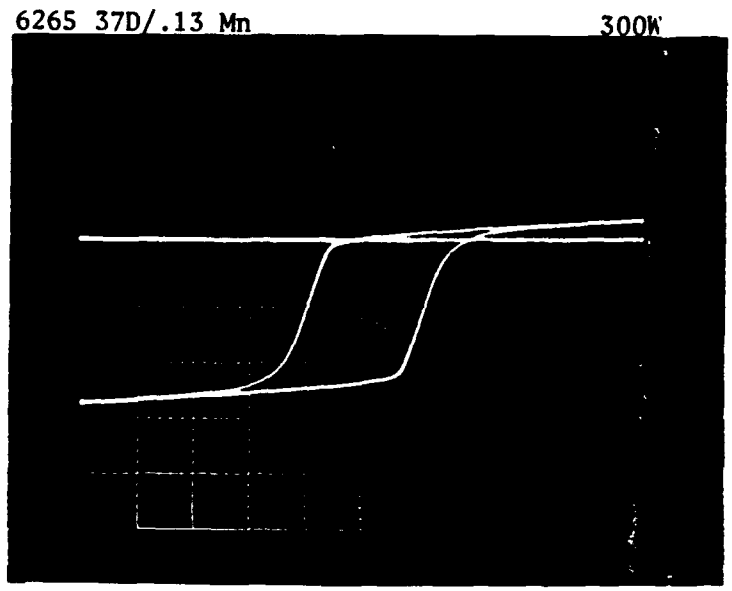

Br Avg = 1326.0

NRL MATERIAL STUDY

HIPOWER TEST RESULTS

10 Apr 1992
13:22:04

37D/.13MN

TESTED AT 198.6 WATTS

MEASURED INSERTION LOSS= .53 dB
TEMP MEASURED ON DUT= 23.1770465798
TOTAL DELTA PHASE = 98.1333
128 STATES MEASURED

STATE	0	.0619	DEGREES
STATE	128	.3231	DEGREES
STATE	256	5.3907	DEGREES
STATE	384	7.2577	DEGREES
STATE	512	8.5019	DEGREES
STATE	640	10.804	DEGREES
STATE	768	14.1839	DEGREES
STATE	896	18.4225	DEGREES
STATE	1024	20.0137	DEGREES
STATE	1152	22.329	DEGREES
STATE	1280	23.8632	DEGREES
STATE	1408	26.0969	DEGREES
STATE	1536	28.4644	DEGREES
STATE	1664	31.4083	DEGREES
STATE	1792	34.4412	DEGREES
STATE	1920	37.9527	DEGREES
STATE	2048	41.0032	DEGREES
STATE	2176	44.2042	DEGREES
STATE	2304	47.2945	DEGREES
STATE	2432	50.2227	DEGREES
STATE	2560	50.9556	DEGREES
STATE	2688	54.2471	DEGREES
STATE	2816	59.392	DEGREES
STATE	2944	59.6012	DEGREES
STATE	3072	66.4999	DEGREES
STATE	3200	70.5573	DEGREES
STATE	3328	74.2997	DEGREES
STATE	3456	78.7075	DEGREES
STATE	3584	83.2878	DEGREES
STATE	3712	89.178	DEGREES
STATE	3840	92.4178	DEGREES
STATE	3968	98.8872	DEGREES

FIGURE 6-23 (g)

6265 37D/.13 Mn 200W

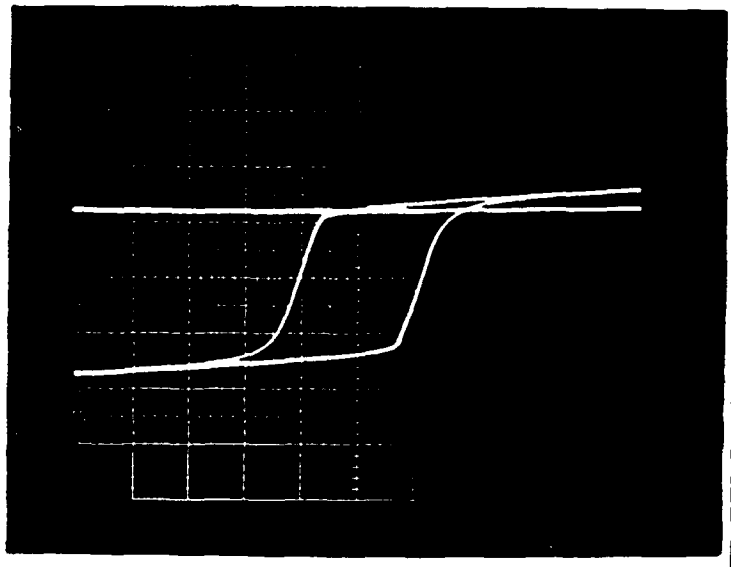

1325 10 APR 92 1334.0

Br Avg = 1334.0

NRL MATERIAL STUDY

HIPOWER TEST RESULTS

10 Apr 1992
14:04:11

37D/.13MN

TESTED AT 101.8 WATTS

MEASURED INSERTION LOSS= .53 dB
TEMP MEASURED ON OUT= 19.598300683
TOTAL DELTA PHASE = 98.8752
128 STATES MEASURED

STATE	0	.2356	DEGREES
STATE	128	2.7806	DEGREES
STATE	256	5.4168	DEGREES
STATE	384	7.7503	DEGREES
STATE	512	9.1099	DEGREES
STATE	640	12.2444	DEGREES
STATE	768	15.2726	DEGREES
STATE	896	19.5125	DEGREES
STATE	1024	21.3525	DEGREES
STATE	1152	23.5642	DEGREES
STATE	1280	25.4014	DEGREES
STATE	1408	27.4305	DEGREES
STATE	1536	29.9885	DEGREES
STATE	1664	32.9442	DEGREES
STATE	1792	36.0559	DEGREES
STATE	1920	39.3938	DEGREES
STATE	2048	42.695	DEGREES
STATE	2176	46.176	DEGREES
STATE	2304	48.9624	DEGREES
STATE	2432	51.8504	DEGREES
STATE	2560	55.2565	DEGREES
STATE	2688	59.2577	DEGREES
STATE	2816	63.5319	DEGREES
STATE	2944	67.4134	DEGREES
STATE	3072	70.8505	DEGREES
STATE	3200	74.6055	DEGREES
STATE	3328	79.1105	DEGREES
STATE	3456	83.9008	DEGREES
STATE	3584	88.6346	DEGREES
STATE	3712	93.0889	DEGREES
STATE	3840	97.6057	DEGREES
STATE	3968	102.4434	DEGREES

FIGURE 6-23 (h)

6265 37D/.13 Mn 100W

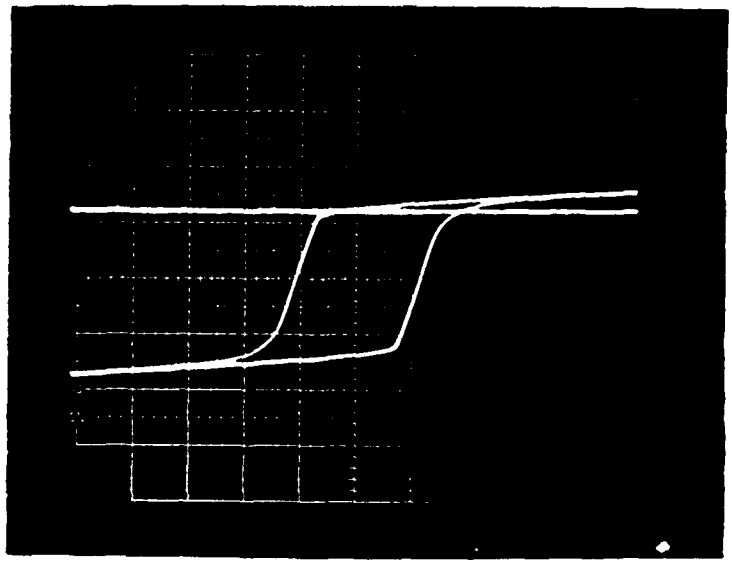

1407 10 APR 92 1342.67

Br Avg = 1342.67

NRL MATERIAL STUDY

HIPOWER TEST RESULTS

FIGURE 6-23 (i)

10 Apr 1992
14:31:00

37D/.13MN

TESTED AT 9.78 WATTS

MEASURED INSERTION LOSS= .55 dB
TEMP MEASURED ON DUT= 16.4302363404
TOTAL DELTA PHASE = 98.8742
128 STATES MEASURED

STATE	0	.5596	DEGREES
STATE	128	.4711	DEGREES
STATE	256	4.8946	DEGREES
STATE	384	8.1802	DEGREES
STATE	512	9.408	DEGREES
STATE	640	12.7564	DEGREES
STATE	768	15.8078	DEGREES
STATE	896	20.2316	DEGREES
STATE	1024	22.1845	DEGREES
STATE	1152	24.6308	DEGREES
STATE	1280	26.5123	DEGREES
STATE	1408	28.7948	DEGREES
STATE	1536	31.2353	DEGREES
STATE	1664	34.1013	DEGREES
STATE	1792	37.6405	DEGREES
STATE	1920	41.0965	DEGREES
STATE	2048	44.3423	DEGREES
STATE	2176	47.4988	DEGREES
STATE	2304	50.4951	DEGREES
STATE	2432	53.6071	DEGREES
STATE	2560	57.1218	DEGREES
STATE	2688	60.6376	DEGREES
STATE	2816	64.5867	DEGREES
STATE	2944	68.6564	DEGREES
STATE	3072	72.1749	DEGREES
STATE	3200	75.8442	DEGREES
STATE	3328	79.7041	DEGREES
STATE	3456	84.2391	DEGREES
STATE	3584	88.7195	DEGREES
STATE	3712	93.4999	DEGREES
STATE	3840	97.9788	DEGREES
STATE	3968	102.6739	DEGREES

6265 37D/.13 Mn 10W

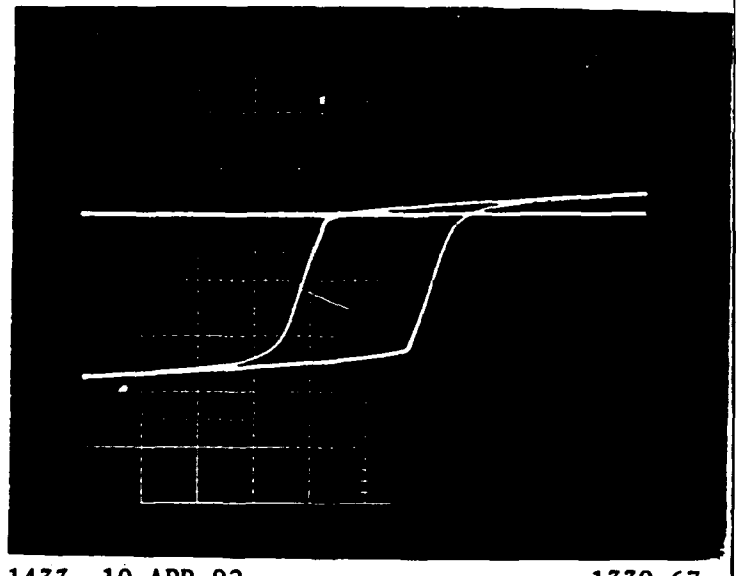

1433 10 APR 92 1339.67

Br Avg = 1339.67

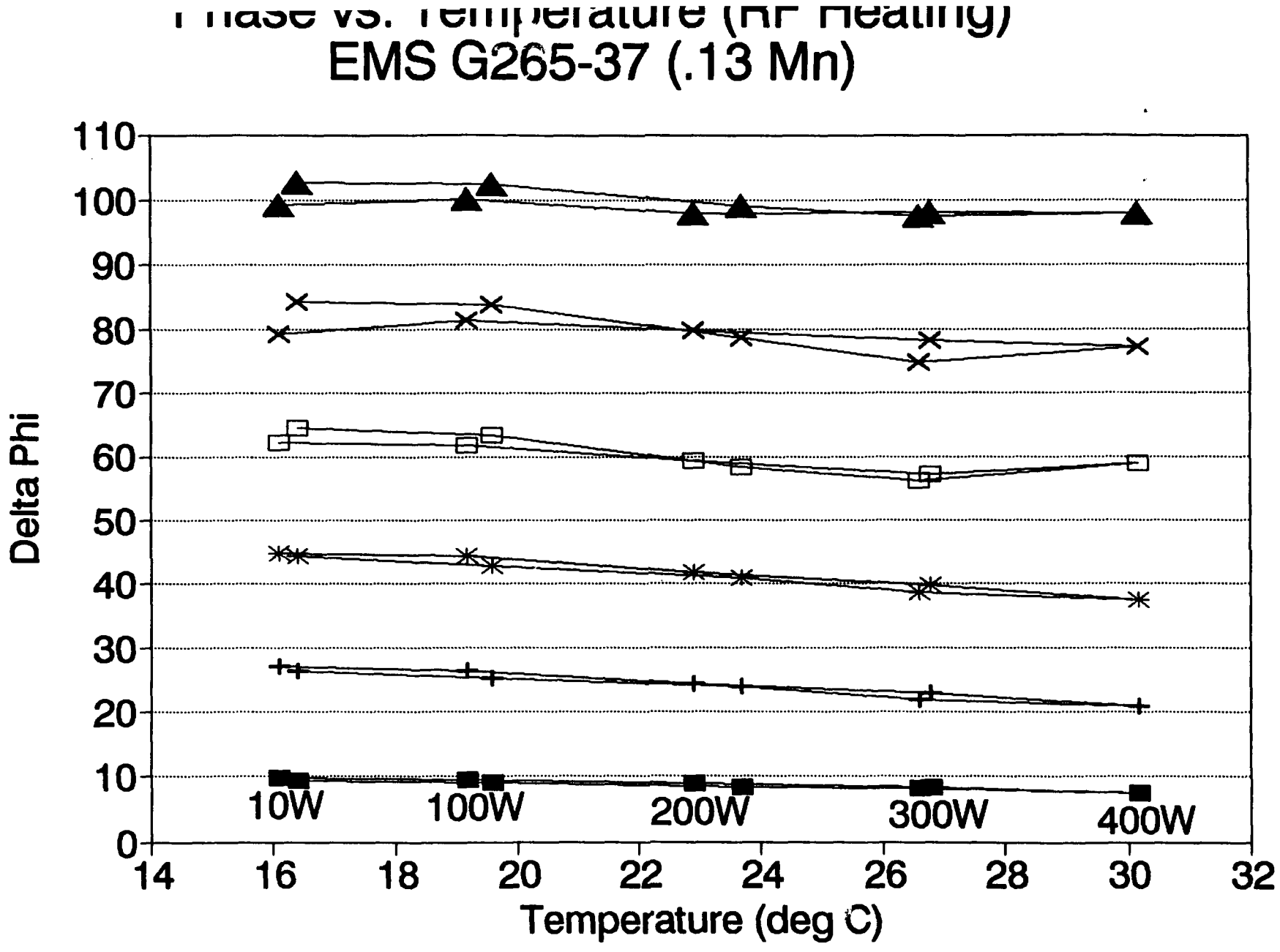
Phase vs. Temperature (RF Heating)
EMS G265-37 (.13 Mn)
Delta Phi
110
100
90
80
70
60
50
40
30
20
10
0
14
16
18
20
22
24
26
28
30
32
Temperature (deg C)
10W
100W
200W
300W
400W

FIGURE 6-24

7.0 COMPUTER AIDED ANALYTICAL STUDIES

Experimental data on remanent flux and phase shift as a function of temperature and power is being used with an EMS standard computer aided analysis program (PSAN) to develop a better understanding of the high power performance of ferrite phase shifters. Some results are shown in Table 7-1.

The following data are available and listed in numbered columns 1 through 3 of Table 7.1:

1. Br measured on round toroids in the ferrite lab.

2. Hysteresograph voltages measured on square toroids loosely positioned in the housing. (The voltages at remanence should be directly related to remanent flux. Absolute Br values will be a bit lower on the square toroids because of the corner effect, but the PSAN program includes a corner correction.)

3. Br data (again in volts) on square toroids rigidly held in the housing as a function of temperature and as a function of power.

With reference to Table 7-1, columns (1) and (2) can be used to develop a calibration value of 438 gauss/volt for the hysteresograph. By using the voltages measured on B-H loops in the housing as given in column (3), values of remanent flux (Br) in the housing at room temperature can be obtained as shown in column (4). These values are used in PSAN to calculate the phase shift listed in column (5). Corresponding experimental data is shown in column (6) for both the temperature and power test platforms.

The data shown in this table (column 6) are all taken at low power and room temperature (or 15°C for the power "P" data). The apparent discrepancy in the observed phase shift results from the fact that the temperature runs (*)

used a latch box to switch the toroid, while the power runs (**) used a standard driver. The driver does not switch the ferrite as completely as does the latch box, so less remanent magnetization results and consequently less differential phase shift. The Br data in both power and temperature sets are obtained from the same hysteresograph, and these sets of voltages (and calculated Br) all agree within measurement error.

The data of Table 7-1 is a basis for a more detailed study of temperature and power effects. It is planned in the next phase of this study to use PSAN to model temperature and power variations of phase shift.

PSAN incorporates the temperature dependence of dielectric permittivity of both ferrites and dielectrics and the temperature dependence of saturation and remanent magnetization. PSAN predictions of temperature dependence of phase shift will be compared to data taken as a function of temperature under uniform heating conditions.

PSAN predictions will also be compared to measured phase shift variations brought about by temperature changes induced by high average power. This study should permit the separation of purely temperature effects from those caused by stresses induced by thermal gradients at high average powers.

TABLE 7-1

COMPUTER AIDED MODELING OF PHASER PERFORMANCE

Mat'l.	1.Br (gauss)	2. Br(Loose) (volts)	3. Br(House) (volts)	4. Br(House) (gauss) for 438 g/v	5. PSAN (degrees)	Data (deg)
1002Mn	680	1.609	1.325 T	591 T	85.2	93*
.09			1.354 P	604 P	87.0	80**
-35D	723	1.684	1.334 T	595 T	85.7	114*
.09			1.347 P	601 P	86.6	101**
-36D	758	1.688	1.666 T	743 T	107	108*
.11			1.693 P	755 P	108.7	93**
-51						
-37B	722	1.681	1.630 T	T	85.5	112*
.13			1.627 P	P	85.9	99**
-33D	721	1.679	1.650 T	736 T	106.4	119*
.15			1.656 P	738 P	106.7	108**
-42D	601	1.350	1.315 T	586 T	84.5	103*
.17			1.327 P	592 P	85.3	88**
-41E	645	1.375	1.350 T	602 T	86.8	100*
.21			1.336 P	596 P	85.8	91**

*Toroids switched by latch box
**Toroids driven by driver

P indicates power data
T indicates temperature data

8.0 SUMMARY OF RESULTS AND SIGNIFICANT OBSERVATIONS

8.1 MATERIAL FABRICATION

No significant problems were experienced in fabricating the compounds.

Processing parameters were adjusted to achieve optimization in the ceramic, electrical, and magnetic characteristics of the compounds. A very good quality microwave polycrystalline material was achieved. In regard to stress sensitivity, none of the iterations seemed to produce any unanticipated uniqueness or significant enhancements in the properties, e.g. loss, saturation magnetization or characteristics of the final material.

Manganese (Mn) chemistry was investigated to provide assurance that Mn^{+3} was entering the garnet structure. The starting carbonate ($Mn^{+2}CO_3$) appeared to be converted to $Mn_2^{+3}O_3$ (by color and weight change) above 600°C; above 1000°C, a small hint of brown color was noted, perhaps indicating some decomposing of Mn_2O_3. Weight change suggests formation of MnO. Some additional analytical evaluation would be valuable and informative.

8.2 STATIC STRESS TESTS

Hysteresis properties of toroids appear to be very sensitive to some stress conditions such as deformation of the structure by bending or twisting or multi-mode deforming created by applying too much (or non-uniform) stress.

Longitudinal (Axial: perpendicular to M) stress tests were primarily conducted.

On the toroid structures tested, stress levels above 1000 PSI appear to begin to alter the hysteresis properties by deformation.

In stress sensitive toroidal structures, any stress supportive to reducing the remanent magnetization is readily observed; a stress supportive to

enhancing the remanent magnetization is weakly observed, most often by observing no change in the remanent states while the coercive field is observed to slightly increase.

Mn substitutions are very valuable in reducing the stress sensitivity of the compounds.

In the compounds studied, substitution of 0.09 Mn per formula unit, as used in a similar commercially available compound (Trans-Tech G-1002), does not appear to be optimized for longitudinal stress sensitivity. Our data indicate that a larger Mn substitution is significantly better (0.13 to 0.15 Mn per formula unit).

For longitudinal compressive stress, data indicate that

$\frac{B_{R(Stress)}}{B_{R(No-Stress)}} = 1$ For a Mn substitution of 0.13, for stress values up to 1000 PSI

8.3 TEMPERATURE STRESS TEST

With the materials assembled into the phase shifter structure, a hysteresis in B_r and phase shift was observed as a function of temperature.

This hysteresis changed direction from clockwise to counter-clockwise for Mn substitution below and above 0.13 respectively.

Best performance was observed for Mn substitutions in the range of 0.11 to 0.15.

These compounds exhibited very small changes in B_r due to top-to-bottom "Crush."

No hysteresis in B_R was observed for "Loose" toroids.

Data appears to be consistent with stress resulting from differences in expansion coefficients of the metallic housing and garnet material.

Hysteresis in phase shift as a function of temperature has been reduced from 10° for Trans Tech G-1002(0.09 Mn) to less than 1° for 0.13 Mn substituted G-265.

8.4 HIGH AVERAGE RF POWER TESTS

Phase shift and B_r exhibited a hysteresis with power/temperature. (Temperature variation of +15 to +32°c for power of 10 to 400 Watts CW).

Best results are obtained for Mn substitution in the range 0.11 to 0.15.

Data are consistent with that observed in temperature tests

Tests were conducted to evaluate stress resulting from differences in heating of inner and outer leg of the toroid. Data are still being fully evaluated but there appears to be only minor effects from stress resulting from differential heating.

Hysteresis with power/temperature (range noted above) was observed to be less than 0.5° for Mn substitutions of 0.11 and 0.13

8.5 STRUCTURAL CONSIDERATIONS TO REDUCE STRESS SENSITIVITY

RF structure used in these studies was a soft "drum top" housing.

To reduce stress sensitivity, RF housing should be designed to provide minimum constraint on the material. A dual toroid, plated structure with some improved mechanical packaging would appear to be a design approach possessing minimum constraint features.

8.6 WHAT IS THE IMPACT OF THE DATA COLLECTED ON ORIGINAL PLANS, EXPECTATIONS AND/OR PROJECTIONS?

All compounds evaluated to date possess $K_1<0$ and, for the most part, $\lambda_{111}<0$. (The range of Mn substitutions studied include compounds exhibiting $\lambda_{111}>0$ characteristics for $K_1<0$.)

Original plans included preparing and evaluating Mn substituted compounds to reach a composition possessing $\lambda_{111}\approx 0$ with K_1 slightly positive. Co^{+2} was to be substituted (in the amount of 0.025 Co^{+2} per formula unit) in this composition to achieve a compound with $\lambda_{111}\approx 0$ and K_1 slightly positive. Such a compound was projected to be stress insensitive.

In continuation of our original plans, the following composition would be prepared for evaluation:

Y^{+3}	Gd^{+3}	Fe^{+3}	Mn^{+3}	Co^{+2}	Si^{+4}	O_{12}
1.7	1.3	4.81	0.14	0.025	0.025	

G. Dionne, MIT(LL) has reported results of his investigations of Mn^{+3} substitutions in YIG including his measured data on magnetostrictive constants (λ_{111} and λ_{100}). His results from measurements of magnetostrictive constants indicate that Mn^{+3} substitution possesses the following characteristics:

Effect of Mn^{+3} Substitutions Per Formula Unit	λ_{100}	λ_{111}	λ_S
In YIG	$+69\times10^{-6}$	$+14\times10^{-6}$	$+36\times10^{-6}$
YIG	(-1.3×10^{-6})	(-2.8×10^{-6})	(-2.2×10^{-6})

His measured results providing stress insensitive remanence were as follows:

$\frac{\partial R_{\parallel}}{\partial \sigma} = 0$ For Mn^{+3} substitution of 0.09 and stress parallel to M

$\frac{\partial R_{\perp}}{\partial \sigma} = 0$ For M^{+3} substitution of 0.17 and stress perpendicular to M

Theory predicted 0.05 and 0.065 respectively for Mn^{+3} substitution based on measured magnetostrictive constants.

Using the measured λ_{111} values (Dionne's data) and the stress insensitive results (Dionne's data), the effects of Mn^{+3} substitution would be as follows:

$$\frac{\lambda_{100}}{+21} \qquad \frac{\lambda_{111}}{+14} \qquad \frac{\lambda_S}{+16.8} \qquad (1)$$

Our data indicate that a Mn^{+3} substitution of 0.13 appears to be the least stress sensitive. If at this substitution,

$$\frac{\partial R_{||}}{\partial \sigma} = 0$$

Then the effect of Mn^{+3} substitution on magnetostrictive constants is as follows:

$$\frac{\lambda_{100}}{+9} \qquad \frac{\lambda_{111}}{+14} \qquad \frac{\lambda_S}{+12} \qquad (2)$$

If at this substitution

$$\frac{\partial R_{\perp}}{\partial \sigma} = 0'$$

Then Mn^{+3} substitution provides

$$\frac{\lambda_{100}}{+15} \qquad \frac{\lambda_{111}}{+14} \qquad \frac{\lambda_S}{+14.4} \qquad (3)$$

Using Mn^{+3} data of (2), theory predicts the following for G-265:

$$\frac{\partial R_{||}}{\partial \sigma} \simeq 0 \quad \text{For } Mn^{+3} = 0.13$$

$$\frac{\partial R_{\perp}}{\partial \sigma} \simeq 0 \quad \text{For } Mn^{+3} = 0.16$$

Using Mn^{+3} data of (3)

$$\frac{\partial R_{||}}{\partial \sigma} \simeq 0 \quad \text{For } Mn^{+3} = 0.09$$

$$\frac{\partial R_{\perp}}{\partial \sigma} \simeq 0 \quad \text{For } Mn^{+3} = 0.13$$

Our data might more strongly support (3) but at least one additional garnet compound needs to be investigated to support this conclusion.

The results of these possibilities (1, 2, or 3) are illustrated on Dionne's data (Figure 8-1 and 8-2) and the computed curves provided as part of the initial program plans (Figure 8-3).

For Mn^{+3} data of ③

$\lambda_{100} = +15$

$\lambda_{111} = +14$

$\frac{\partial R_{11}}{\partial \sigma} = 0 \cdots\cdots \Delta$

$\frac{\partial R_1}{\partial \sigma} = 0 \cdots\cdots \nabla$

For Mn^{+3} data of ①

$\lambda_{100} = +21$

$\lambda_{111} = +14$

$\frac{\partial R_{11}}{\partial \sigma} = 0 \cdots\cdots \square$

$\frac{\partial R_1}{\partial \sigma} = 0 \cdots\cdots \diamond$

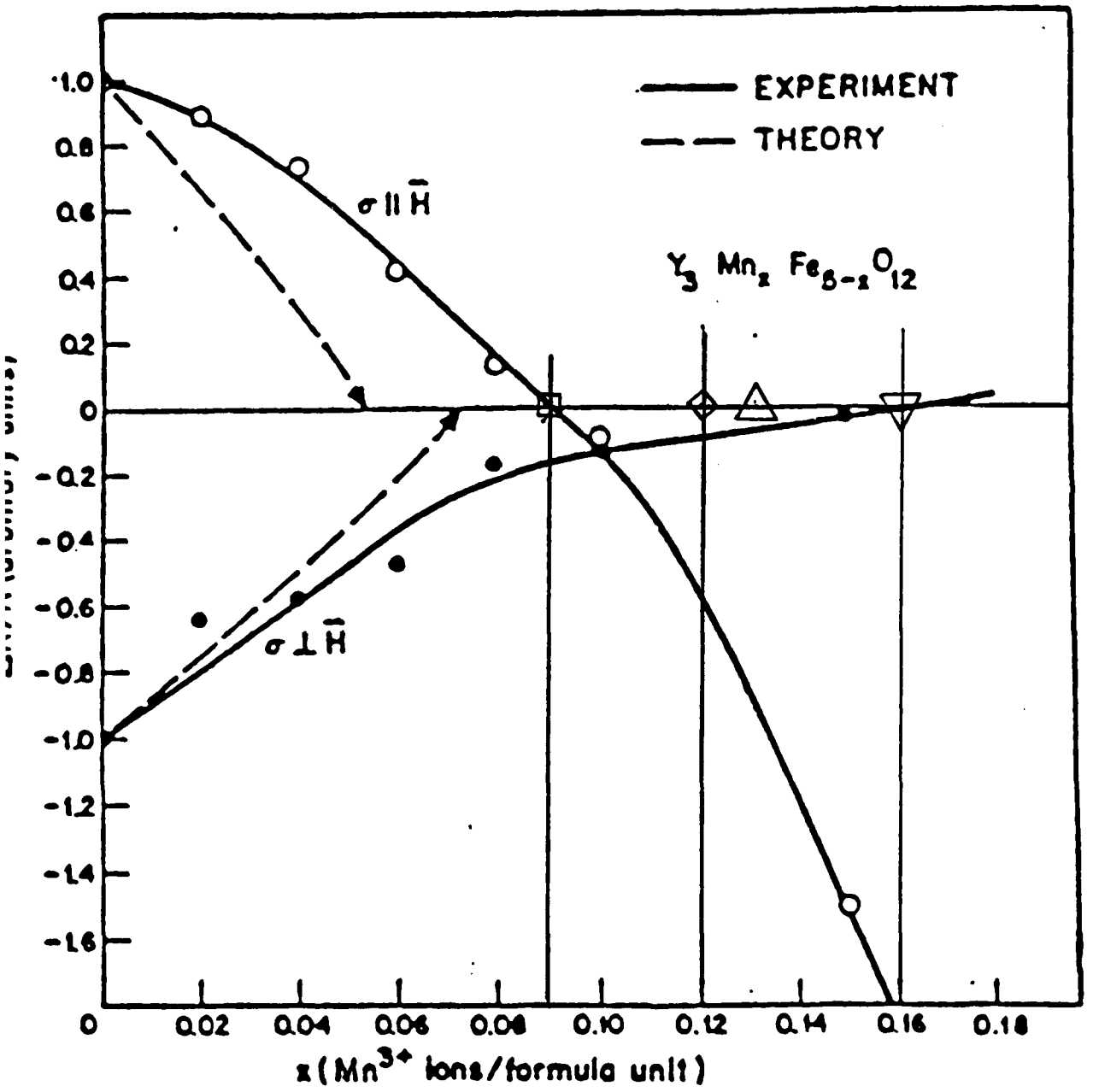

FIGURE 8-1

Fractional change in remanence ratio as a function of Mn^{3+} content for compressive stress both parallel and perpendicular to magnetic field. (After Dionne) (Data points resulting from discussion in Section 8.6 are indicated).

For Mn^{+3} λ_{100} = +21; Data from 1

For Mn^{+3} λ_{100} = +15; Data from 3

For Mn^{+3} λ_{100} = +9; Data from 2

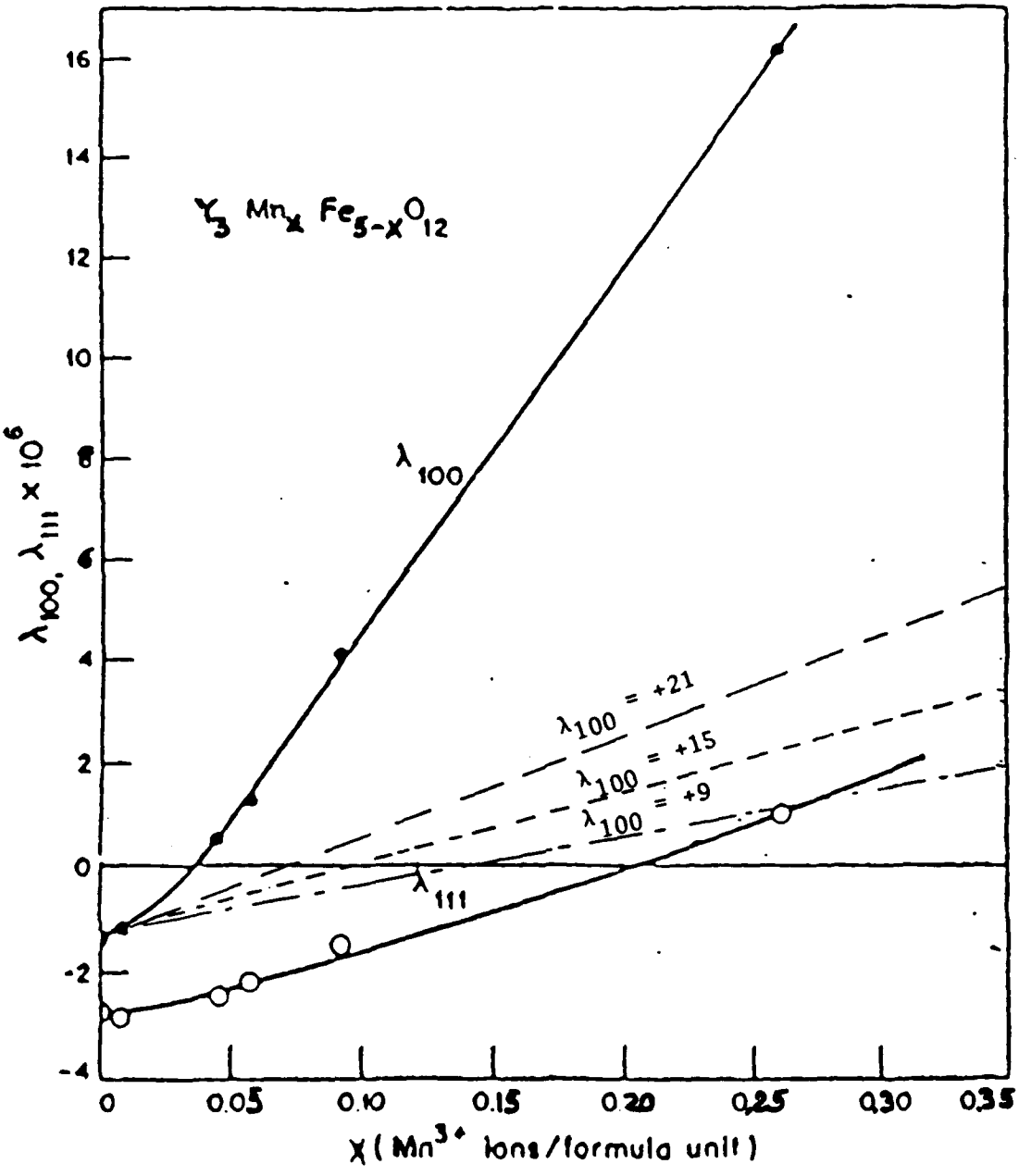

FIGURE 8-2

Room temperature magnetostriction constants λ_{100} and λ_{111} for family $Y_3Mn_xFe_{5-x}O_{12}$. (After Dionne) (Different values of λ_{100} are shown as discussed in Section 8.6).

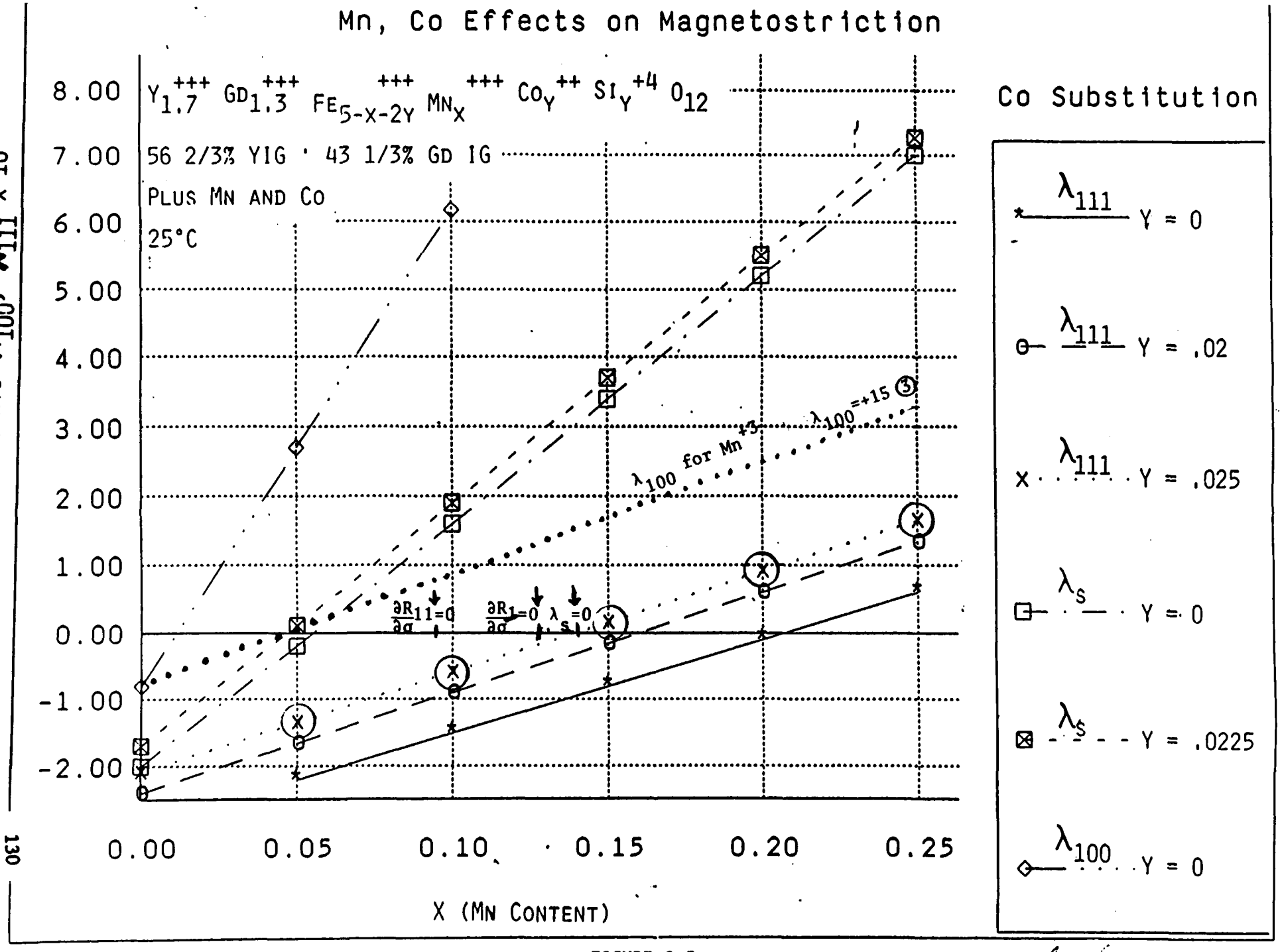
Mn, Co Effects on Magnetostriction
$Y_{1.7}^{+++}\ GD_{1.3}^{+++}\ FE_{5-X-2Y}^{+++}\ MN_X^{+++}\ Co_Y^{++}\ SI_Y^{+4}\ O_{12}$
56 2/3% YIG · 43 1/3% GD IG
PLUS MN AND Co
25°C
MAGNETOSTRICTIVE CONSTANTS λ_{100}, $\lambda_{111} \times 10^6$
8.00
7.00
6.00
5.00
4.00
3.00
2.00
1.00
0.00
-1.00
-2.00
0.00
0.05
0.10
0.15
0.20
0.25
X (MN CONTENT)
λ_{100} for Mn^{+3}
$\lambda_{100}=+15$ ③
$\frac{\partial R_{111}}{\partial \sigma}=0$
$\frac{\partial R_{1}}{\partial \sigma}=0$ $\lambda_s=0$
Co Substitution
λ_{111} Y = 0
λ_{111} Y = .02
λ_{111} Y = .025
λ_s Y = 0
λ_s Y = .0225
λ_{100} Y = 0

FIGURE 8-3

9.0 PROPOSED TASKS FOR 2ND YEAR

9.1 PHASE II TASKS FROM SOW

ANALYTICAL PHASER MODEL

The phaser model will be used to predict performance of promising structural/material combinations

MATERIAL PREPARATION AND CHARACTERIZATION

Improved stress insensitive materials will be prepared and characterized as in Phase I. If the COTR determines that the analysis indicates substantial performance advantages, composite structures will be fabricated and characterized.

RF EVALUATION

The most promising phaser toroidal corporations and geometries will be selected, fabricated and characterized in a waveguide structure. One will be selected for a final demonstration vehicle. Performance will be compared to the baseline vehicle and Phase 1 demonstration vehicles.

9.2 PROPOSED SPECIFIC TASKS FOR PHASE II

Complete analysis of data from Phase I studies.

Select one Mn substituted compound for more detailed x-ray and SEM evaluation to document microstructure characteristics (analytical support from NRL is requested)

Complete fabrication of CO^{+2} substituted compound. Characterize the magnetic, microwave, and stress properties of this compound

Prepare and evaluate at least one additional microwave garnet compound with Mn^{+3} substitutions to verify ability to predict and compensate magnetostrictive (stress) sensitivity

Study a Li-Zn-Ti ferrite compound with Mn^{+3} substitutions to achieve low stress sensitivity ($4\pi Ms \approx 1700$ Gauss)

Analytically evaluate composite toroid structure. With COTR approval, fabricate one structure for demonstration evaluation.

The most promising phaser toroidal configurations and geometries will be selected, fabricated and characterized in a waveguide structure to demonstrate improved performance.